# FDR4ALT

# Uncertainties Characterization Document

Public

## AUTHORS TABLE

| Object | Name |
|---|---|
| Authors | Emma Woolliams, Sajedeh Behnia (NPL) Fanny Piras, Jean-Alexis Daguzé, Marie-Laure Fréry, Hélène Roinard, Annabelle Ollivier, Victor Quet, Beatriz Calmettes (CLS), Malcolm McMillan (Lancaster Univ.), Bruno Picard (FLUCTUS), Frank Fell, Ralf Bennartz (INFORMUS), Sara Fleury, Fernando Nino, Marion Bocquet, Camille Boulard (LEGOS), Heidi Salila (FMI), Angelica Tarpanelli (IRPI) |
| Checked by | Gabriele Brizzi (SERCO) and Pierre Féménias (ESA) |
| Accepted by | Pierre Féménias (ESA) |

## CHRONOLOGY ISSUES

| Issue | Date | Object |
|---|---|---|
| 1.0 | 02/12/22 | Intermediate version for Phase 2 PM#2 |
| 2.0 | 02/05/23 | Final version for Final Review |
| 3.0 | 23/05/23 | Final version for Final Review with ESA RIDs implemented |
| 3.1 | 04/07/23 | Minor corrections |

## Table of content

# 1  Introduction

This document has been written in the frame of the FDR4ALT project, ESA contract N°4000128220/19/I-BG.  It is a deliverable of task 4 of the project and identified as [D-5-02].

## 1.1  The FDR4ALT Project

In the framework of the European Long Term Data Preservation Program (LTDP+) which aims at generating innovative Earth system data records named Fundamental Data Records (basically level 1 altimeter and radiometer data) and Thematic Data Records (basically level 2+ geophysical products), ESA/ESRIN has launched a reprocessing activity of ERS-1, ERS-2 and ENVISAT altimeter and radiometer dataset, called the FDR4ALT project (Fundamental Data Records for Altimetry). A large consortium of thematic experts has been formed to perform these activities which are:

1) To define products including the long, harmonized record of uncertainty-quantified observations.

2) To define the most appropriate level 1 and level 2 processing.

3) To reprocess the whole times series according to the predefined processing.

4) To validate the different products and provide them to large communities of users focused on the observation of the atmosphere, ocean topography, ocean waves, coastal, hydrology, sea ice, ice sheet regions.

## 1.2  Purpose and scope of this document

This Uncertainties Characterization Report aims at documenting the uncertainty information provided in the FDR4ALT products. For each Fundamental Data Record (FDR) and each Thematic Data Product (TDP), it details how the uncertainty was evaluated, how it is provided in the product and how it should be used. Finally, this report will indicate how the uncertainty information could be improved in the future.

Please note that a larger reflexion on the dominant sources of uncertainties have been performed in the frame of this project, and it is documented in the Uncertainty Characterization Definition Document [D-5-01]. This document gives more details about the rationale behind all uncertainties described here.

# 2  Terminology

This section aims at defining clearly the terminology used in the FDR4ALT deliverables.

- **Product** refers to a specific type of file, defined and described by a dedicated handbook, and designed for a clear purpose (the FDR4ALT project, the REAPER project, …). It is a "container". One product refers to one file. The use of plural is designed to refer to a group of files, for instance the Thematic Data Products. "FDR4ALT products" will usually refer to all TDPs and FDRs, i.e., the outputs of the whole project. Note that the word "product" does not imply any notion of start date or end date, whereas "dataset" does.
- **File** can be used to refer to one single product or any other file that is not a product.
- **Parameter or variable** refers to a product's field, i.e., the content of the product. For instance, the sea level anomaly is a parameter of the Ocean & Coastal Thematic Data Products.
- **Dataset** can be used to refer to any group of data, not necessarily products. However, in the context of this project, it will often be used to refer to a sub-ensemble of products, on a specific period of

time or a specific geographic area. For instance, the TDS (test dataset) refers to a <u>dataset</u> of 3 years of test <u>products</u>.

# 3   Fundamental Data Records

## 3.1   ALT Fundamental Data Records

### 3.1.1 Overview of the uncertainty analysis

The ALT FDR addresses level-0 and level-1 altimeter-related variables which mainly consists of providing waveforms and all the instrumental parameters describing the altimeter operating status and configuration through the satellite lifetime. It aims at giving an exhaustive list of Level-0 and Level-1 parameters.

A "bottom-up" approach for the altimetric measurement is extremely challenging. Therefore, in the frame of this project, the only uncertainty provided in the ALT FDR is the one associated with the waveform classification based on the probability of each class. It will be briefly discussed in this section. Other uncertainties are treated collectively at the TDP levels, as discussed in subsequent sections below.

In the ALT FDR, waveform classification for both ENVISAT (RD 1) and ERS missions is available (see [D-1-02] [D-2-01]). This algorithm gives a class number corresponding to a certain waveform shape (see Figure 3-1) and a probability score. The waveform classification is performed using a neural network. The specific implementation and parameterization of the neural network are critical steps, which determine the classification performance. Several network design parameters have been defined to ensure the best learning and predictions. These include the network size (the number of inputs, output, and hidden neurons), the input feature variables, the transfer function (also called the activation function), and the training database definition. Finally, a single hidden layer neural network using a sigmoidal function is used. Outputs of the neural network are a class number associated to a probability. The higher the probability, the better is the prediction of the neural network. From the output tuple (class number, score) for a given waveform, one can derive a kind of quantitative or qualitative uncertainties at waveform level that maybe linked to Level-2 quantitative uncertainties since waveform shape quality is crucial for modelling and retracking geophysical parameters as surface height.
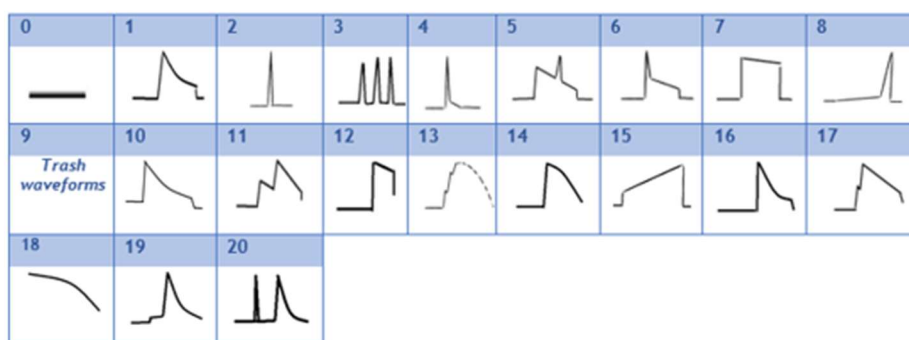


*Figure 3-1 : Correspondence between class number and waveform shape*

Please note that the Uncertainty Characterization Definition Document [D-5-01] contains a lot of information about the altimetric measurements and has been written as an attempt to summarize all effects that could be source of uncertainties in the waveform.

## 3.1.2 Uncertainty evaluation

Figure 3-2 shows the gridded mean probability of the most likely class whatever the predicted class. This illustrate well that the neural network can predict a class number with a confidence greater than 80% over open-ocean, coastal and some land regions. Greenish regions are for prediction either ambiguous or wrong due to very complex terrains (topography, inland water, ice) as seen over Greenland and Antarctica.

### Mean probability of the most likely class [ERS1]
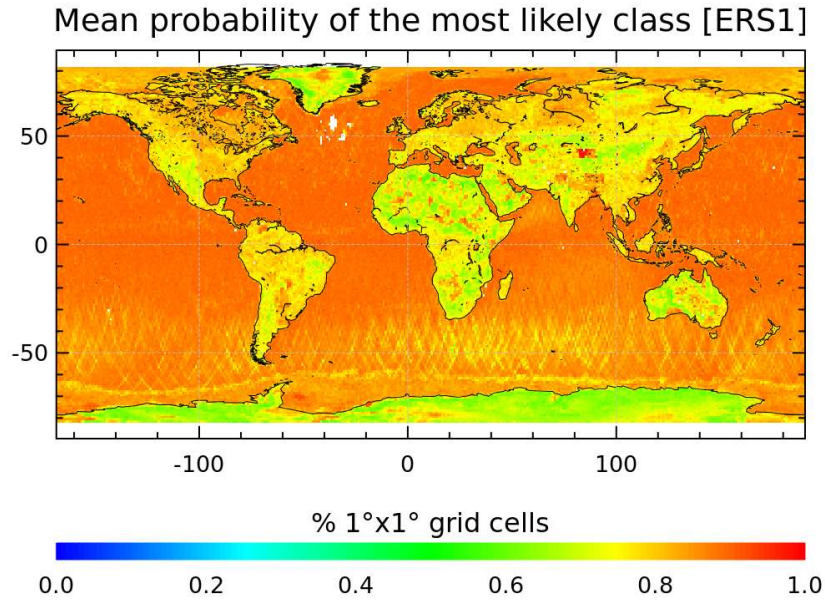


*Figure 3-2: Mean probability of the most likely class over one cycle of data.*

Figure 3-3 (right) shows the location of the first most likely probability when class N°1 is predicted over one cycle of data. Class 1 is the oceanic class and corresponds to most of the data as illustrated by the global coverage. Also, we can note that score (left) is very good (around 90%) indicating a very good confidence in the prediction. That is not always the case for more complex waveforms or when the prediction is ambiguous between two classes. Here we conclude that the neural network performs very well on this class over open ocean.
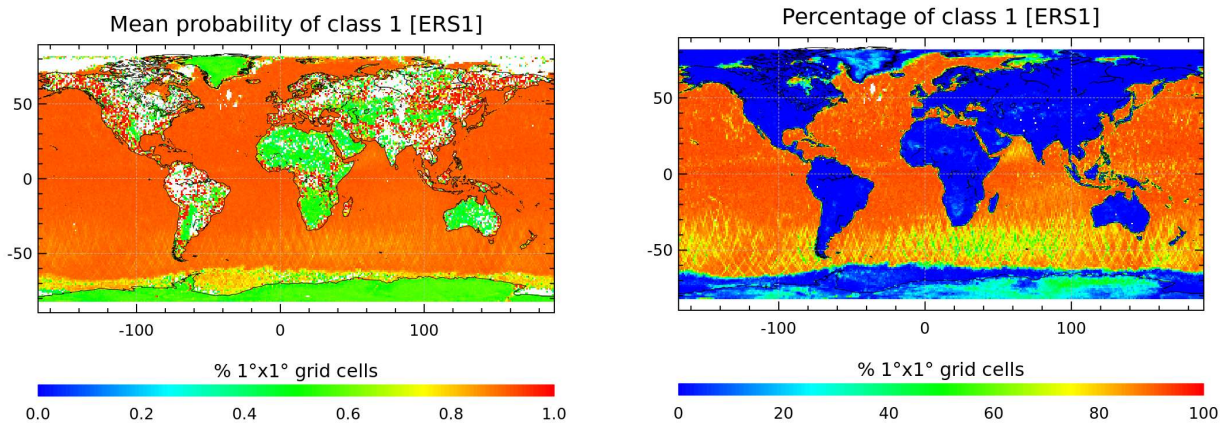


*Figure 3-3 : Example of gridded maps of the probability associated to predicted class N°1 for ERS-1 (left) and its geographical distribution and density over cycle 147 (right).*

### 3.1.3 Uncertainty provided

#### 3.1.3.1 How uncertainty information is provided in the product

For each 20 Hz waveform, the outputs of the waveform classification are available for the 3 missions:

| Variable | NetCDF field name |
|---|---|
| Most probable class | *waveform_main_class (/)* |
| Second most probable class | *waveform_second_class(/)* |
| Probability of being the most probable class | *waveform_main_class_score(%)* |
| Probability of being the second most probable class | *waveform_second_class_score(%)* |

#### 3.1.3.2 How the uncertainty information should be used

The waveform class probability reflects the uncertainty in associating the waveform shape to one or more of the reference classes. The information may also be used to discriminate surfaces. For instance, it can be used in sea-ice to discriminate leads and floes.

The higher the class probability is, the lower is the uncertainty associated with the waveform classification. This can be used to quantify uncertainties at level of the waveform and may be linked to the uncertainties at level-2 and retracking estimates.

#### 3.1.3.3 Roadmap for further uncertainty analysis

This project has not yet propagated uncertainties from the waveform (and the altimeter) to the TDP. This is not a trivial task, particularly through the different waveforms seen over these scenes. Work in the ESA ASELSU project has identified instrumental and processing uncertainties for Sentinel 6 Michael Freilich over the ocean and started the process of propagating those uncertainties to sea level anomaly and global mean sea level. Monte Carlo Uncertainty Analysis methods were used to propagate instrumental noise to the retracked parameters. It is likely, that a similar bottom-up approach could be applied to the ERS and ENVISAT data in later projects and that such analysis could be propagated through the different retracking algorithms used for some of the project's TDPs.

This FDR4ALT project has provided probabilities of a surface being a particular type in the classification algorithm. Another valuable extension would be to identify the impact of misclassification on the subsequent retracking (for now, only the Adaptive retracker uses the waveform classification as input) so that uncertainties associated with the classification process can be propagated.

### 3.1.4 Reference documents

| RD 1 | J. Poisson, G. D. Quartly, A. A. Kurekin, P. Thibaut, D. Hoang and F. Nencioli, "Development of an ENVISAT Altimetry Processor Providing Sea Level Continuity Between Open Ocean and Arctic Leads," in IEEE Transactions on Geoscience and Remote Sensing, vol. 56, no. 9, pp. 5299-5319, Sept. 2018, doi: 10.1109/TGRS.2018.2813061. |
|---|---|

## 3.2 MWR Fundamental Data Records

### 3.2.1 Overview of the uncertainty analysis

The MWR FDR uncertainty analysis is performed using a bottom-up approach. The microwave forward model has been analysed and sources of uncertainties were identified.
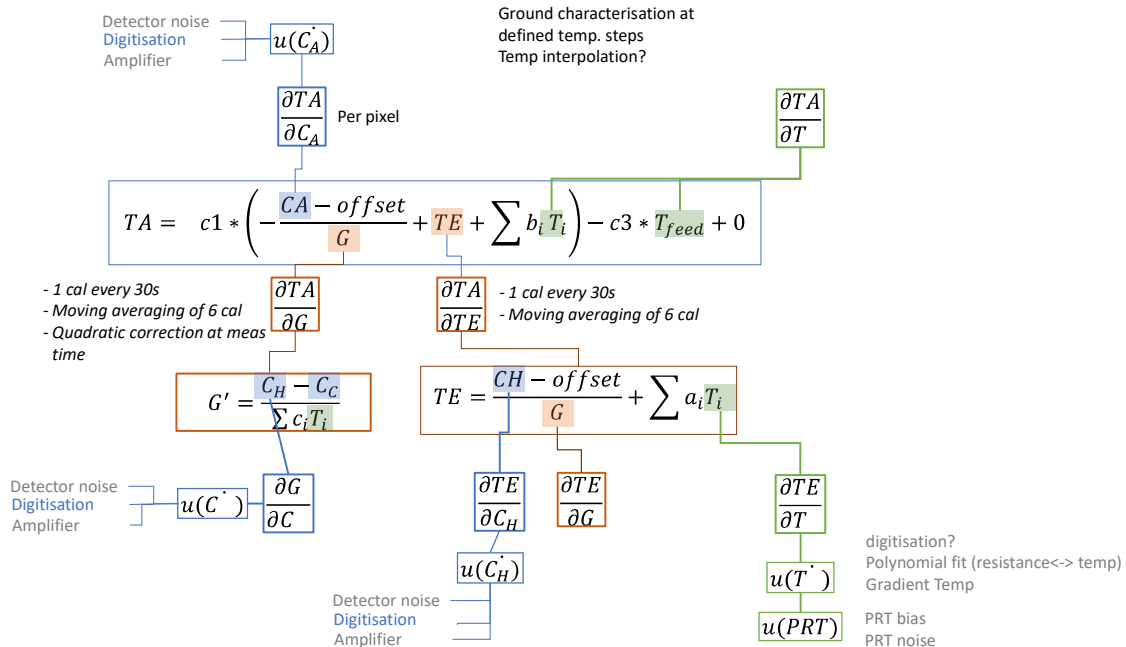


*Figure 3-4: Uncertainty tree of antenna temperature estimation*
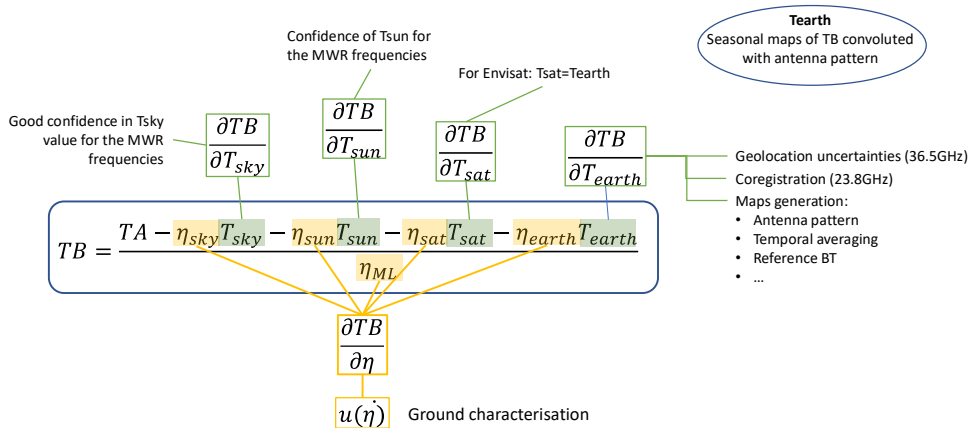


*Figure 3-5: Uncertainty tree of brightness temperature estimation*

The sources of uncertainty identified for the Microwave radiometer are the following:

- Noise Equivalent Delta Temperature (C)
- Internal temperature sensors noise and stability (C)
- Antenna pattern correction (PC)
- Temperature gradients along waveguides (NC)
- Temperature dependency of characterisation parameters (NC)

- Reference temperatures (Hot load for calibration, Dicke load) (NC)

Some of these sources are considered in the assessment proposed for this project (C), or partially considered (PC). Others are not considered here. It could be explained by lack on information the technical documentation available, or the difficulty of assessment.

## 3.2.2 Uncertainty evaluation

### 3.2.2.1 Noise Equivalent Delta Temperature

The radiometer output fluctuates because of the inherent stochastic properties of receiver electronics. Random noise is introduced in the radiometer observations by thermal emissions from every component of the receiver and antenna system.

The Radiometer Noise Equivalent Delta Temperature (NeDT), also called sensitivity, is defined as the smallest change in scene brightness temperature that can be resolved at the output of the radiometer. It depends on the system noise temperature $T$sys, the pre-detection bandwidth $B$, the integration time $\tau$ and the gain fluctuations. We also must consider the fluctuations in the gain on short timescales. The system noise temperature is the sum of the receiver noise temperature $T_{REC}$ and the observed antenna temperature $TA$.

For a Dicke radiometer such as ENVISAT, ERS-1 and ERS-2, the theoretical value of NeDT is written as:

$$\Delta T = \sqrt{\frac{2 * (T_{\mathrm{REC}} + TA) + 2 * (T_{\mathrm{REC}} + T_{\mathrm{ref}})}{B\tau} + (T_{\mathrm{ref}} - TA) * \left(\frac{\Delta G}{G}\right)^2} \qquad (3.1)$$

NeDT was estimated from analysis of cold and hot calibration counts. Allan standard deviation is estimated for both calibrations over a one-day time period. This period was chosen to reduce the noise in the estimation NeDT, and to account for missing files. Figure 3-6 shows the time-series over one cycle of the NeDT for both channels of ENVISAT. Cold and Hot estimated NedT are close to each other and close the NeDT retrieved by spectral analysis of brightness temperature over one cycle. These are the values used to compute dynamically the NeDT for each count of Earth measurements.
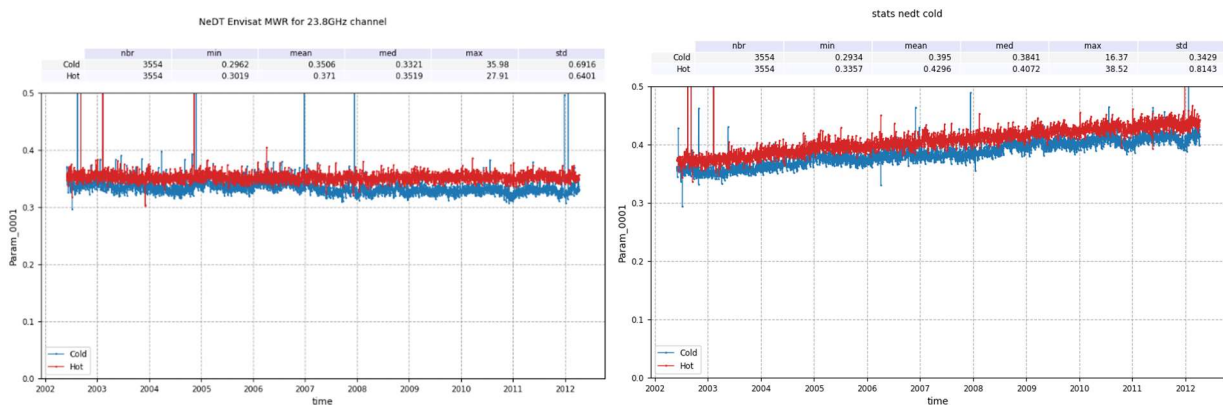


*Figure 3-6: Noise Equivalent Delta Temperature for both channels of ENVISAT MWR : left) 23.8 Ghz; right) 36.5 GHz*
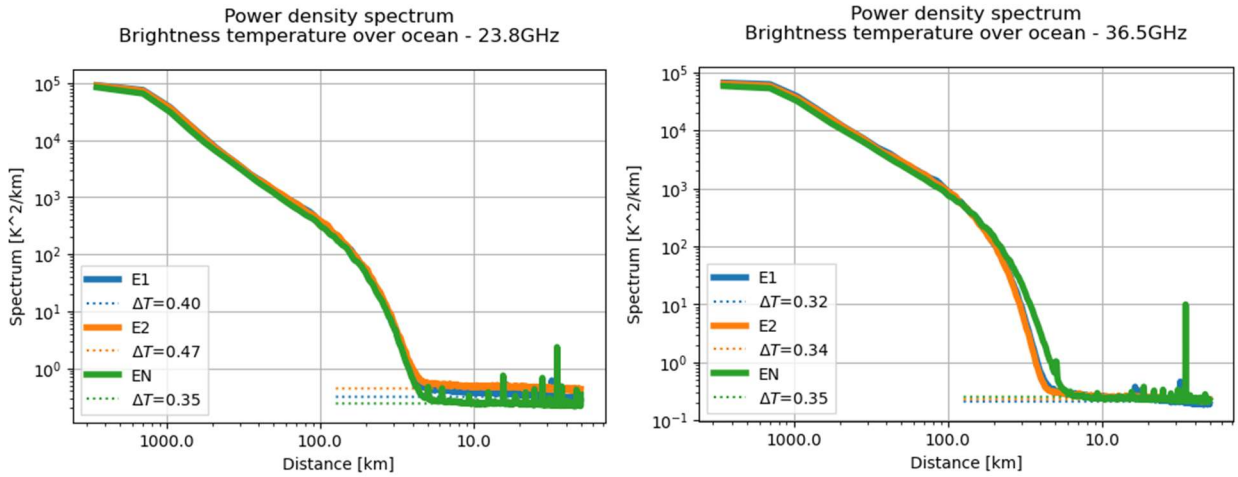
*Figure 3-7: Noise Equivalent Delta Temperature for both channels of ENVISAT, ERS2- and ERS-1 MWR estimated by spectra analysis over ocean : left) 23.8 Ghz; right) 36.5 GHz*

Figure 3-8 and Figure 3-9 show the timeseries of estimated NeDT for ERS2 and ERS1 respectively, using the same method as ENVISAT. The results are completely different from ENVISAT ones. Cold and Hot NeDT are very different, and Hot NeDTs present very high variances, with strong seasonal variations. These values are quite different from the values retrieved with spectral analysis presented in Figure 3-7. We did not have the time to investigate if this issue comes from our processing for estimation of the NeDT or represents the reality, thus we choose a safe solution by using a constant value for NeDT for all the timeseries:

- ERS1: 0.40K @ 23.8GHz, 0.32K @ 36.5GHz,
- ERS2: 0.47K @ 23.8GHz, 0.34 @ 36.5GHz.
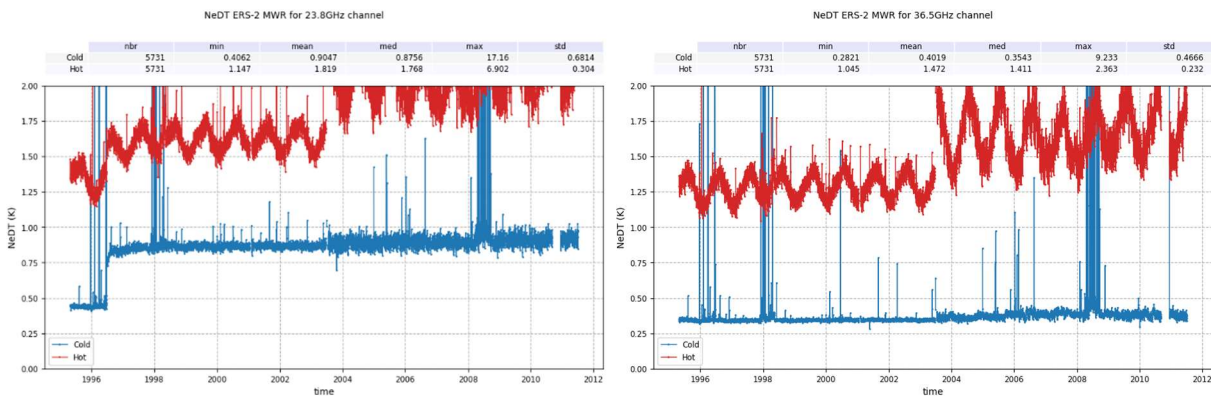


*Figure 3-8: Noise Equivalent Delta Temperature for both channels of ERS-2 MWR : left) 23.8 Ghz; right) 36.5 GHz*
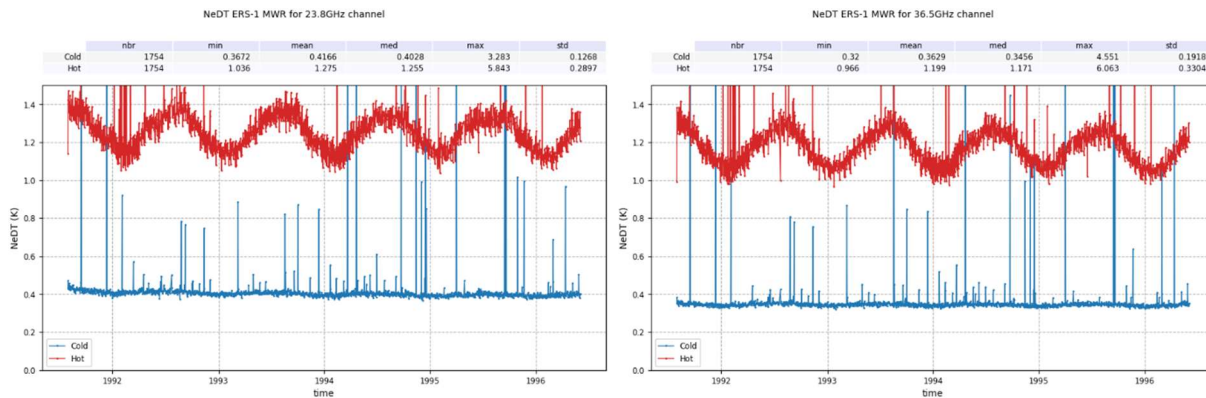
*Figure 3-9: Noise Equivalent Delta Temperature for both channels of ERS-1 MWR : left) 23.8 Ghz; right) 36.5 GHz*

## 3.2.2.2 PRT measurements, noise and uncertainties

PRTs are used to measure the temperature of the different parts of the instrument and satellite and these temperatures are used in the radiometer transfer model (as the $T_i$ quantities in the expressions for $TE$ the residual temperature; and $TA$ the antenna temperature). A set 18 over 32 available temperatures are needed in the transfer model, but only one physical temperature is transmitted along with each acquisition by the radiometer (Figure 3-10). The processing will be performed only with a full window of 32 temperatures. That means that it takes a window of 32 acquisitions to obtain the full information needed for the model, which creates an error correlation between the different acquisitions within that window.
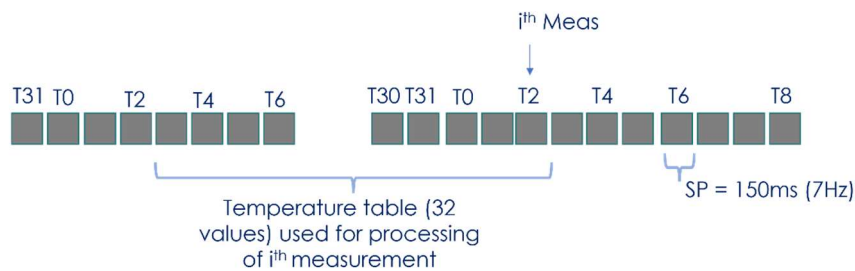


*Figure 3-10: ENVISAT and ERS internal temperatures availability in telemetry*

There is noise in the PRT temperature measurements. The standard deviations were estimated from the PRT measurements directly. The Allan deviation is used for the estimation of the standard deviation in the measurements for each PRT used in the radiometer transfer model. A window of about 25 passes (about one day) is used for the estimation of the uncertainty. This uncertainty leads to an error that is correlated between the measurements, as described above.

We considered here only the random part of the uncertainties that could be generated by the sensors. Systematic part such as long-term drift are still to be assessed.

Figure 3-11 presents the timeseries for two temperature sensors of ENVISAT. Figure 3-12 and Figure 3-13 presents ERS-2 and ERS-1 timeseries respectively. ERS-2 timeseries is much noisier than ERS-1; but the amplitude is still small (lower than 0.05K most of the time).
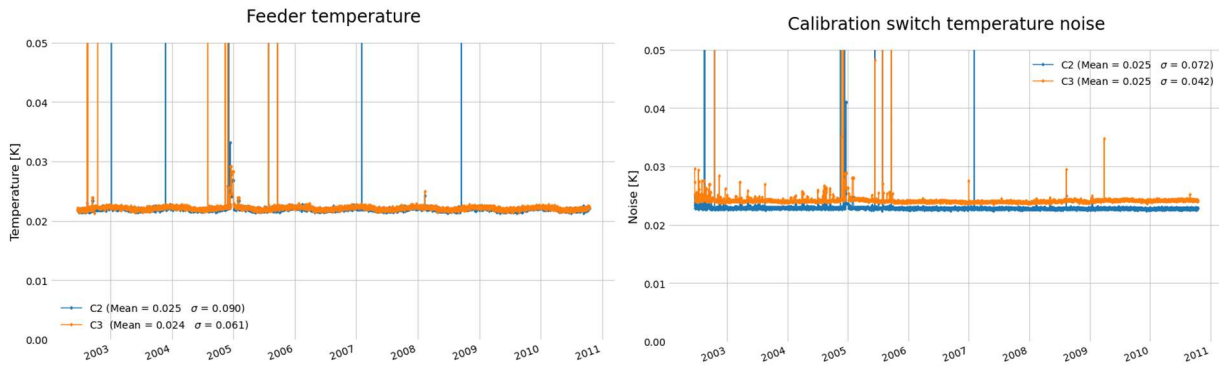
*Figure 3-11: Noise on ENVISAT internal temperature sensors: example for feeder temperature (left) and calibration switch temperature (right)*
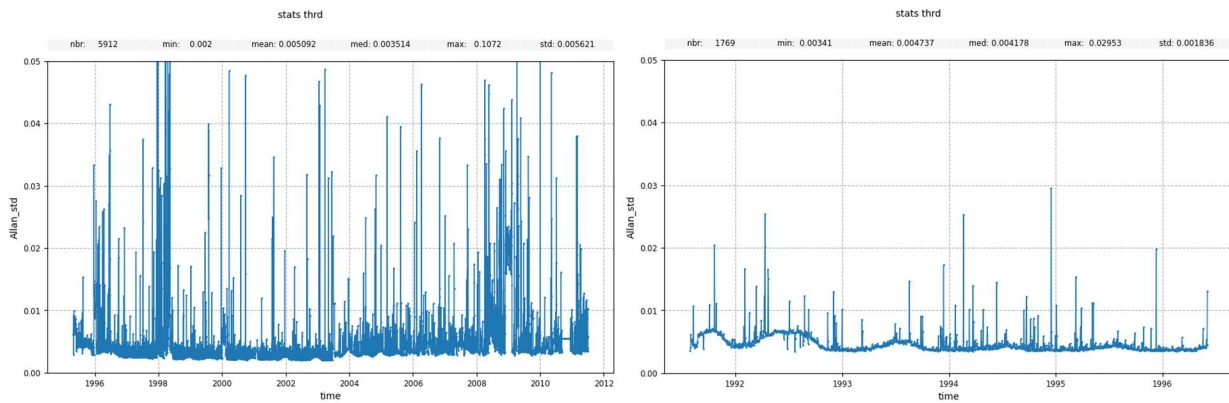


*Figure 3-12: Noise on ERS-2 internal temperature sensors: example for hot load temperature (23.8 GHz) (left) and hot/cold calibration switch temperature for 23.8GHz channel (right)*
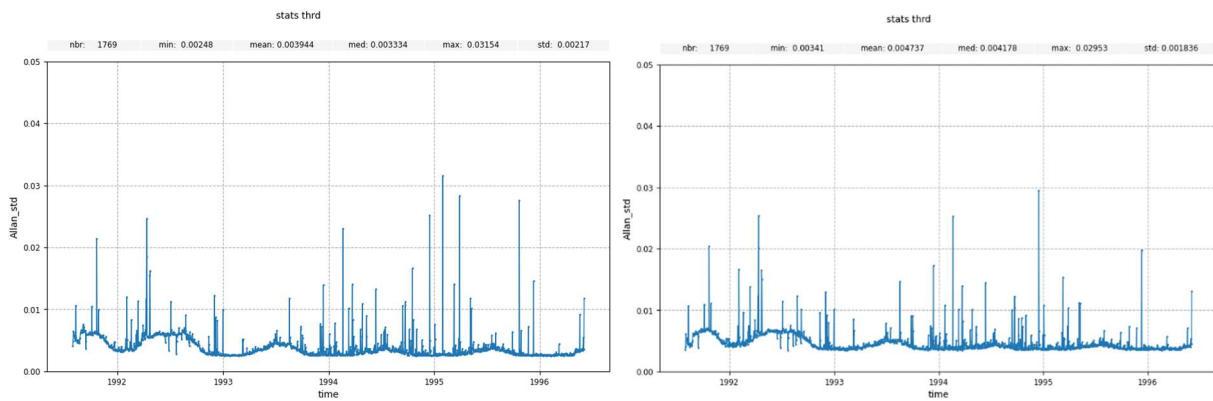


*Figure 3-13: Noise on ERS-1 internal temperature sensors: example for hot load temperature (23.8GHz) (left) and hot/cold calibration switch temperature for 23.8GHz channel (right)*

Uncertainties Characterization Document
CLS-ENV-NT-22-0667 - Issue 3.1 – 05/07/2023

### 3.2.2.3 Antenna pattern correction uncertainties

The brightness temperatures are estimated by correcting the antenna temperatures for the sidelobe contributions. However, the correction is not perfect because the real contamination is difficult to quantify.

$$TB = \frac{TA_{\mathrm{r}} - \eta_{\mathrm{earth}}Tsl_{\mathrm{earth}} - \eta_{\mathrm{sat}}Tsl_{\mathrm{sat}} - \eta_{\mathrm{sky}}Tsl_{\mathrm{sky}}}{\eta_{\mathrm{ml}}} + 0 \qquad (3.2)$$

**On-Earth sidelobe temperature** is provided by seasonal maps, one set of 4 maps for each channel. These sidelobe maps are computed from maps of brightness temperatures convoluted with the radiometer antenna pattern when available. The value for the correction is evaluated at each measurement position by bilinear interpolation within the map of the corresponding season.

The **satellite temperature** is poorly known. In the previous reprocessing, the platform was considered to be so highly reflective that the Earth radiance is a good approximation of its radiance. This approximation is probably incorrect. Given our lack of knowledge of the satellite radiance, we will use the satellite temperature as an adjustment parameter for intercalibration if the hottest temperatures have too high values.

The uncertainty from this contribution comes from the residual error due to the no-perfect correction.

Due to the correction process and the equation of retrieval of the brightness temperature, we identified three contributions:

1. Maps: Seasonal maps which provide the temperature as seen by the sidelobe
2. Pointing uncertainties: uncertainties in the pointing will lead to uncertainties in the geolocation of MWR pixels and thus in the estimation of the correction inside the map by bilinear interpolation.
3. Efficiencies uncertainties: the values provided by the manufacturer were estimated on-ground after measurement of the antenna pattern. They are provided with an uncertainty.

The first part of the uncertainty coming from the on-Earth sidelobe correction is very difficult to estimate. It would require knowing the reality of the observation by the sidelobes and compare it to the seasonal maps used as a correction.

Here, Numerical Weather Prediction (NWP) model could be useful as they can provide daily global information. NWP analyses and a Radiative Transfer Model could be used to compute maps of simulated brightness temperatures. These maps can then be convoluted with the antenna pattern over the range of the sidelobe at the geolocation of the satellite. This analysis would be very time-consuming. A simplification could be considered by performing box averaging of brightness temperatures over one month. These maps can then be convolved with the antenna pattern. This solution would require less effort than the initial solution but is still time-consuming.

A last solution is to use the difference between the antenna temperature as observed by the microwave radiometer and the temperature used for the sidelobe correction. The main assumption is that the uncertainty will come from the difference between the reality and the correction, in areas such as high latitudes where ice extent is varying very quickly. We are aware of the limitations of this solution.

The uncertainties associated to the on-Earth sidelobe correction were estimated using the latest method. Figure 3-14, Figure 3-15, Figure 3-16 illustrates the results for ENVISAT, ERS-2 and ERS-1 respectively. Four months are presented for both channels, one for each season.

| ENVISAT | 23.8GHz | 36.5GHz |
|---------|---------|---------|
| Feb 2003 | | |
| May 2003 | | |
| August 2003 | | |
| Nov 2003 | | |
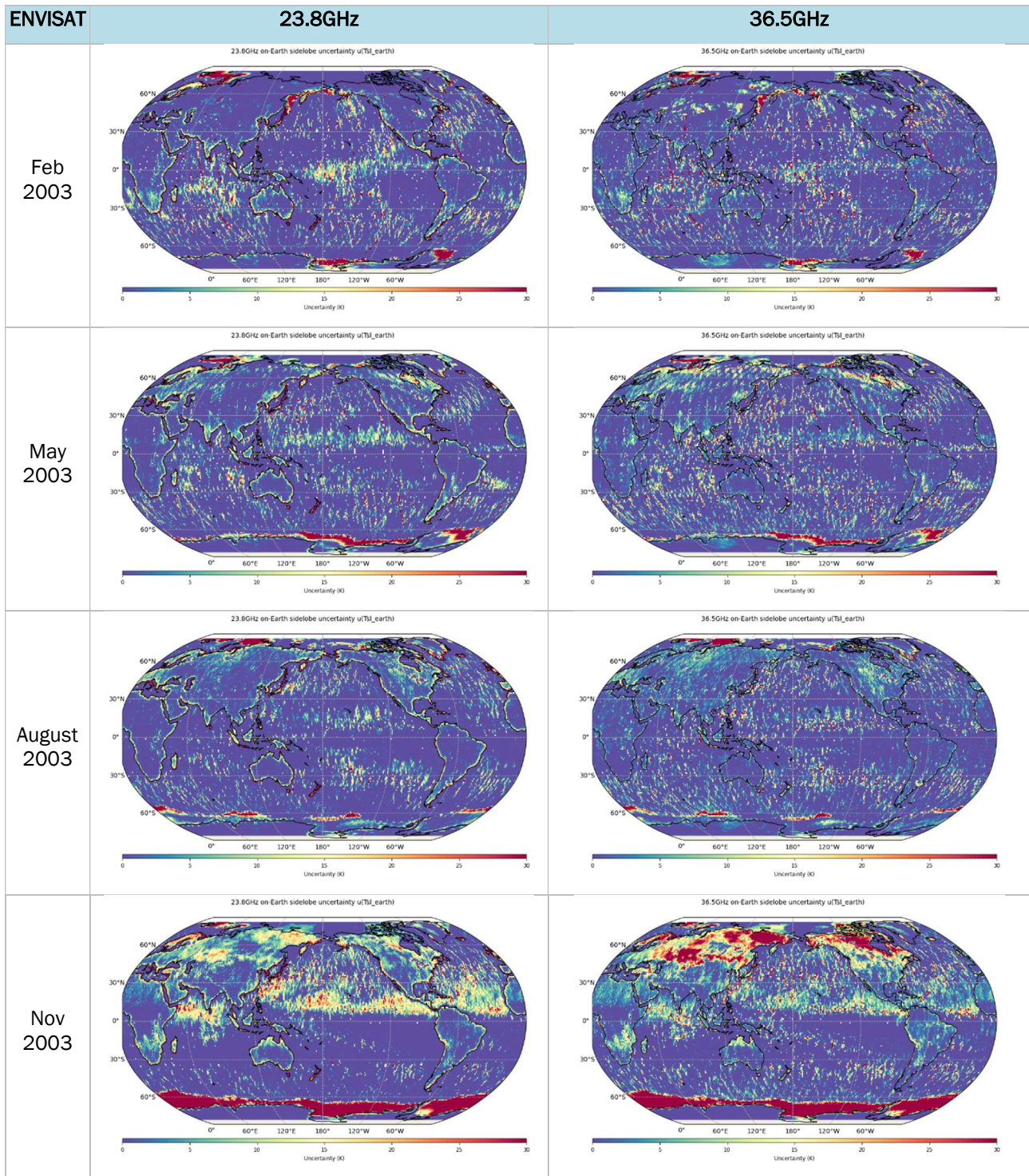
*Figure 3-14: uncertainties on ENVISAT on-Earth sidelobe correction map February, May, August, November 2003*
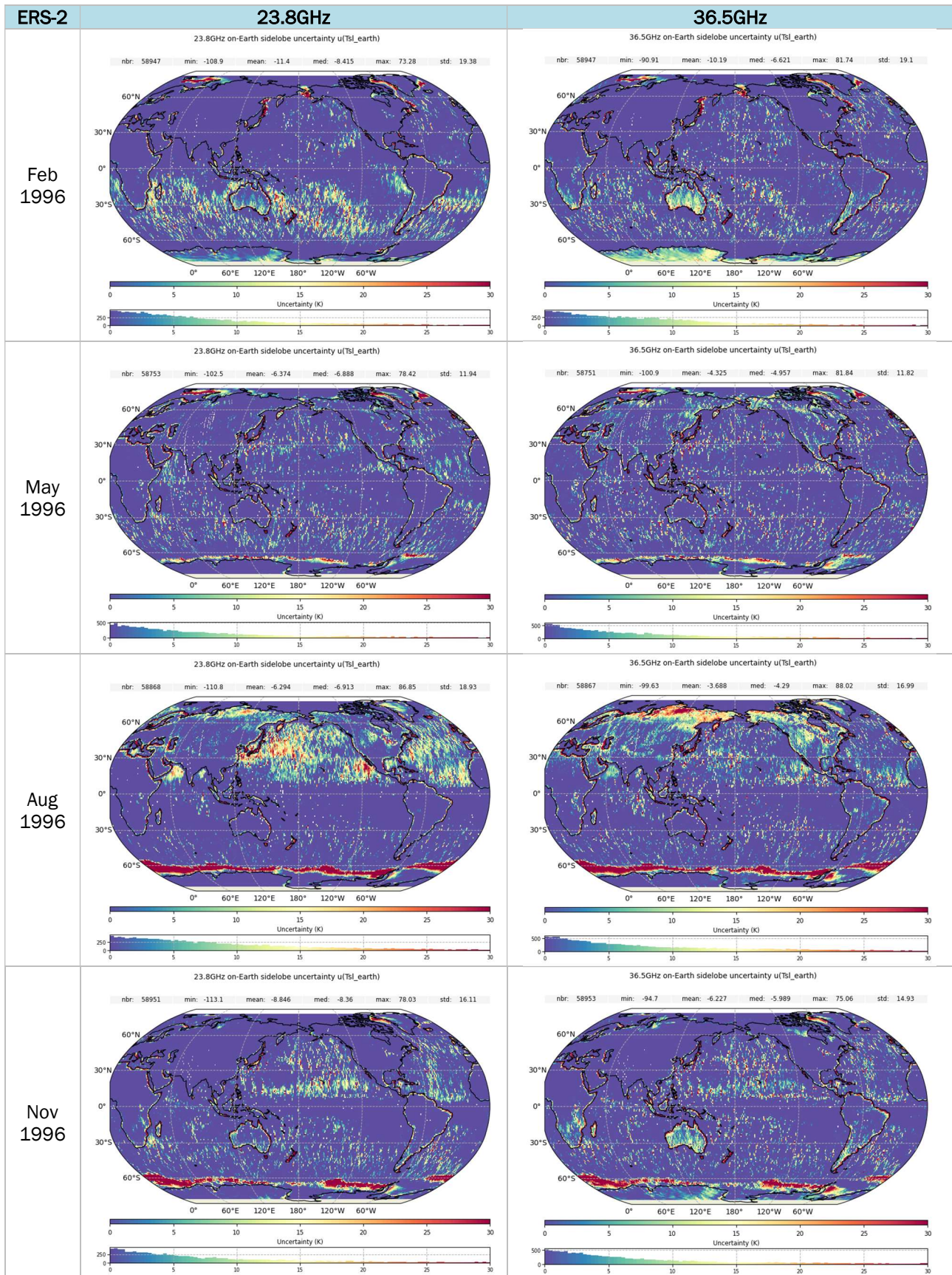
*Figure 3-15: uncertainties on ERS-2 on-Earth sidelobe correction map February, May, August, November 1996*

| ERS-1 | 23.8GHz | 36.5GHz |
|---|---|---|
| **Feb 1993** | 23.8GHz on-Earth sidelobe uncertainty u(Tsl_earth) | 36.5GHz on-Earth sidelobe uncertainty u(Tsl_earth) |
| **May 1993** | 23.8GHz on-Earth sidelobe uncertainty u(Tsl_earth) | 36.5GHz on-Earth sidelobe uncertainty u(Tsl_earth) |
| **Aug 1993** | 23.8GHz on-Earth sidelobe uncertainty u(Tsl_earth) | 36.5GHz on-Earth sidelobe uncertainty u(Tsl_earth) |
| **Nov 1993** | 23.8GHz on-Earth sidelobe uncertainty u(Tsl_earth) | 36.5GHz on-Earth sidelobe uncertainty u(Tsl_earth) |

*Figure 3-16: uncertainties on ERS-1 on-Earth sidelobe correction map for February, May, August, November 1993*

## 3.2.2.4 Brightness temperature uncertainties

The uncertainties on the brightness temperatures are estimated using the different contributions selected during this study: NEDT, temperature sensor noise, antenna pattern correction. The propagation of the uncertainties is performed by the law of propagations of uncertainties through the transfer model. Details can be found in the document "Uncertainty Characterization Definition Document" ([D-5-01]).

The floor level of the uncertainties is provided by the NeDT, and some geographical patches can be observed which comes from the on-Earth sidelobe correction. Most patches with small amplitudes are observed over ocean. Some patches with higher uncertainties are observed in the high latitude areas where the most difference between the correction and the reality can be found. ENVISAT, and ERS1 and ES2 with smaller values, in winter period presents patches in the high latitudes with much higher amplitudes than the other seasons. This would require more analysis, as the same behaviour was observed for Sentinel-3 during a study about MWR brightness temperatures uncertainties funded by ESA/ESTEC.
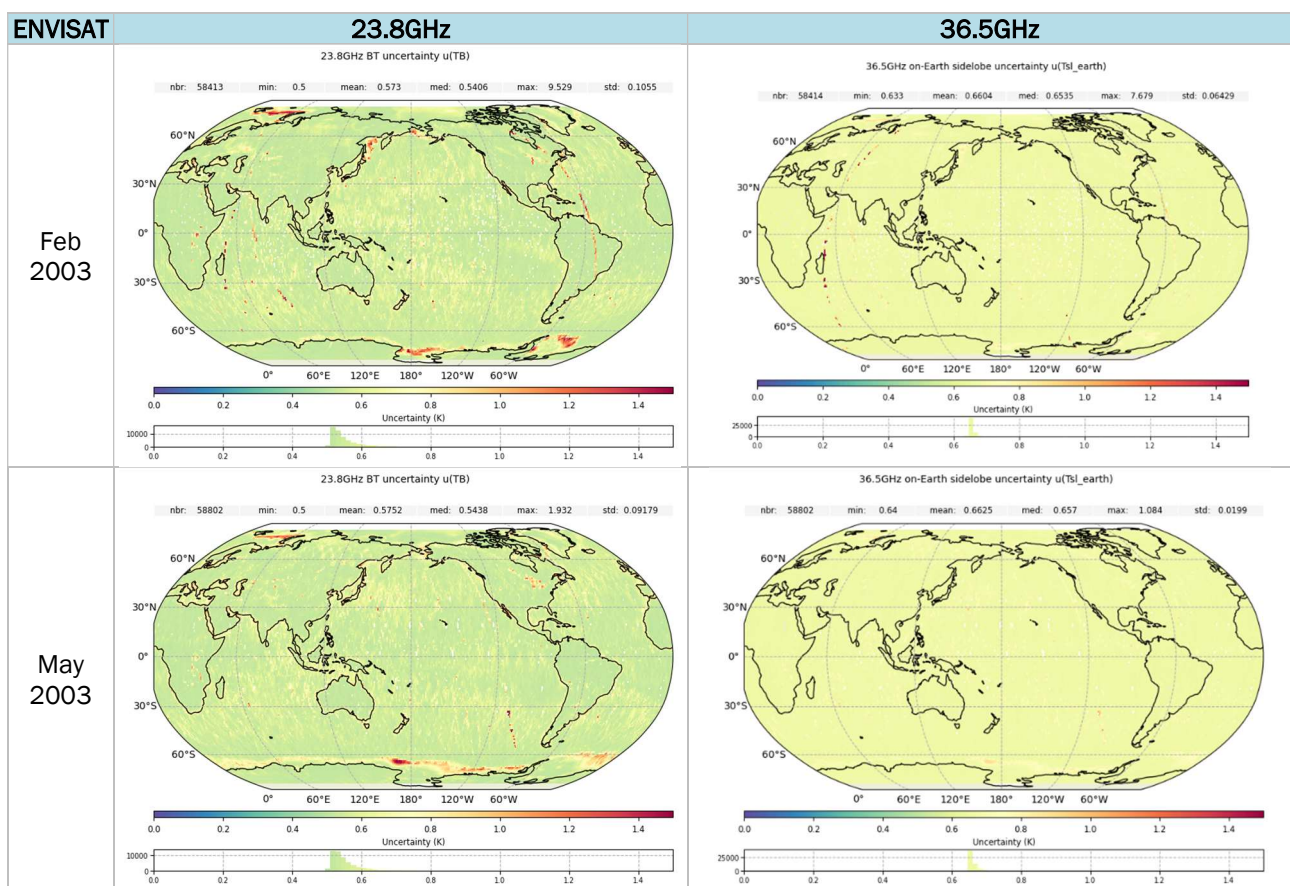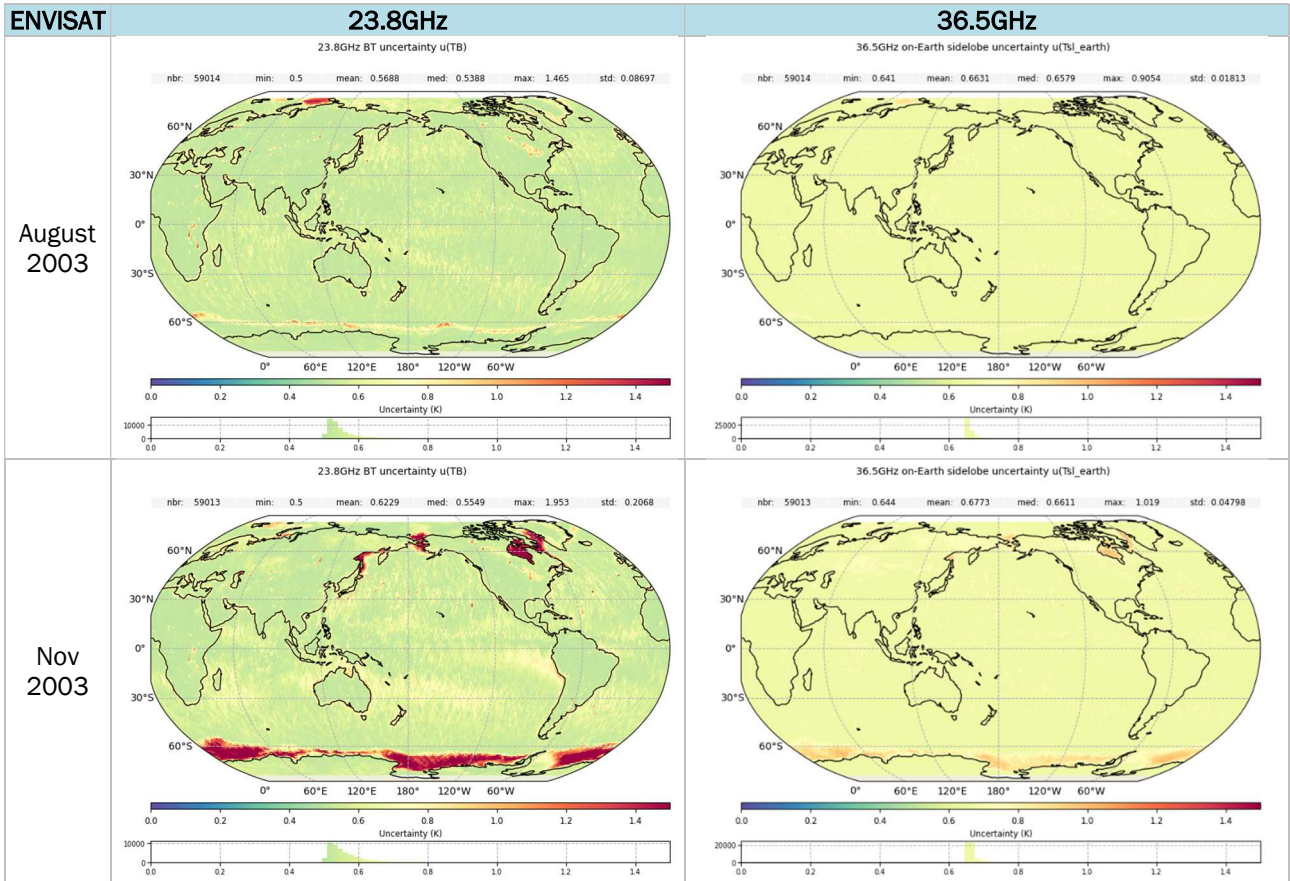
*Figure 3-17: ENVISAT Brightness temperatures uncertainties for February, May, August, November 2003 for 36.5GHz*

| ERS-2 | 23.8GHz | 36.5GHz |
|---|---|---|
| Aug 1996 |  |  |
| Nov 1996 |  |  |
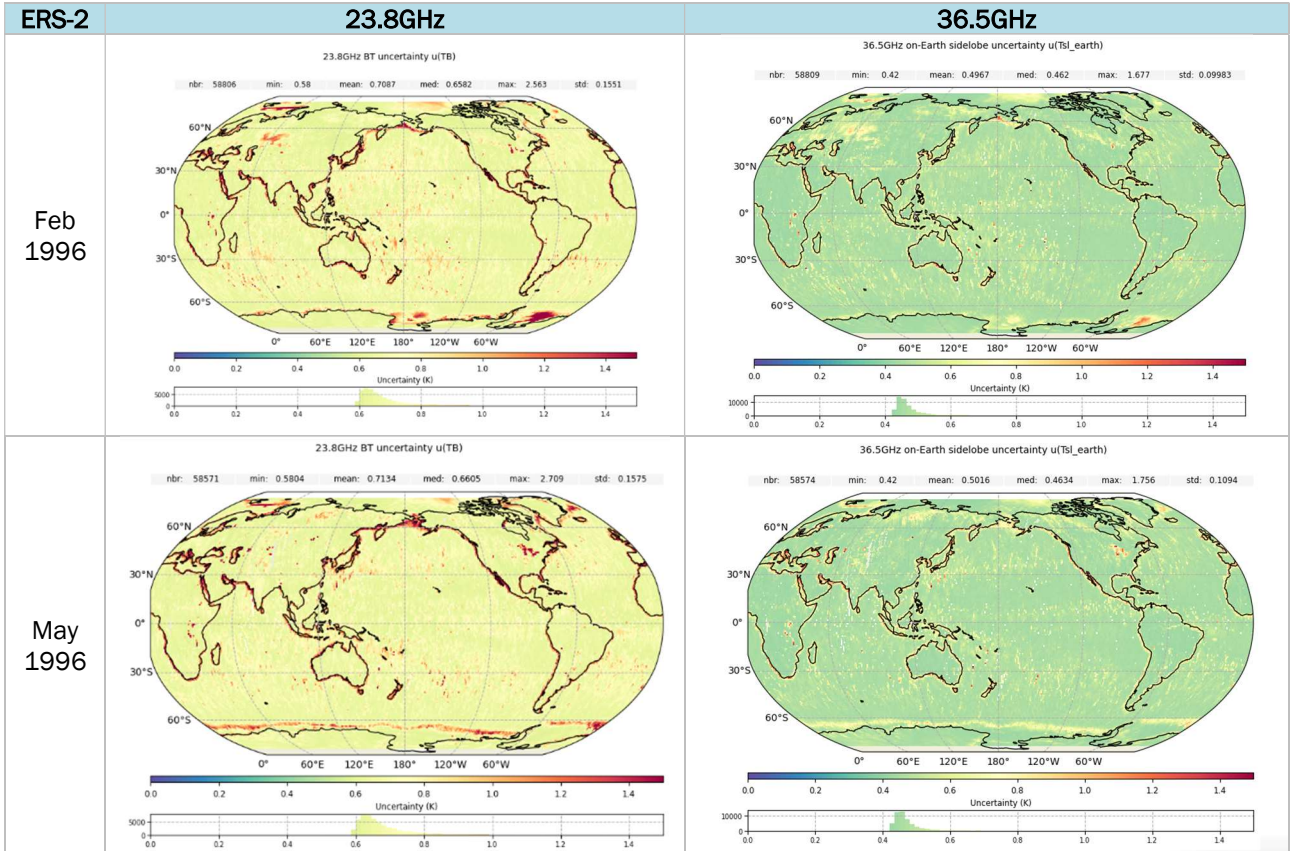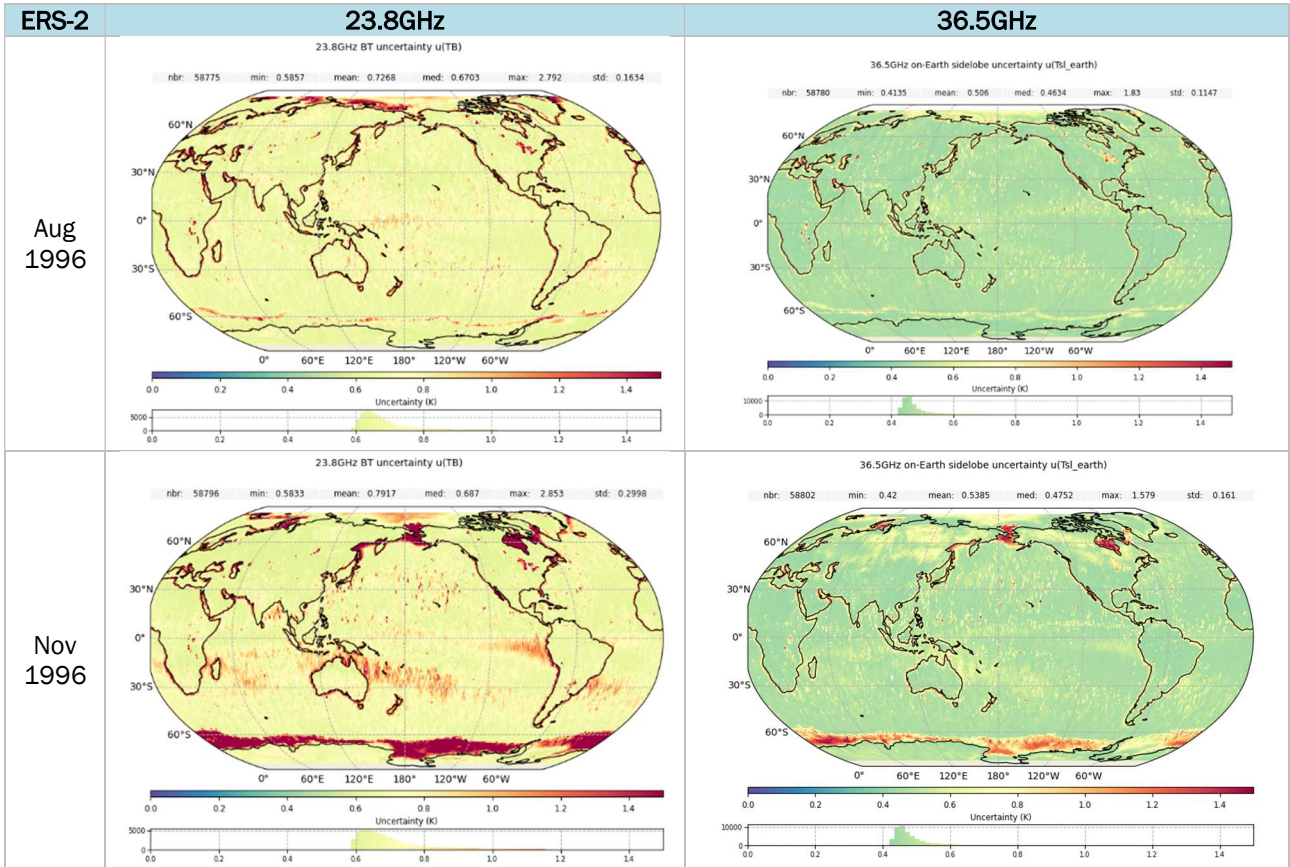
*Figure 3-18: ERS-2 Brightness temperatures uncertainties for February, May, August, November 1996*

| ERS-1 | 23.8GHz | 36.5GHz |
|---|---|---|
| Feb 1993 |  |  |

Uncertainties Characterization Document
CLS-ENV-NT-22-0667 - Issue 3.1 – 05/07/2023

| ERS-1 | 23.8GHz | 36.5GHz |
|---|---|---|
| May 1993 | 23.8GHz BT uncertainty u(TB)<br>nbr: 58525  min: 0.5  mean: 0.6428  med: 0.5854  max: 2.913  std: 0.1699 | 36.5GHz on-Earth sidelobe uncertainty u(Tsl_earth)<br>nbr: 58525  min: 0.44  mean: 0.5194  med: 0.4815  max: 1.871  std: 0.1061 |
| Aug 1993 | 23.8GHz BT uncertainty u(TB)<br>nbr: 58733  min: 0.5  mean: 0.651  med: 0.5912  max: 2.736  std: 0.1748 | 36.5GHz on-Earth sidelobe uncertainty u(Tsl_earth)<br>nbr: 58734  min: 0.44  mean: 0.5232  med: 0.4822  max: 1.974  std: 0.1125 |
| Nov 1993 | 23.8GHz BT uncertainty u(TB)<br>nbr: 58775  min: 0.5  mean: 0.7135  med: 0.6079  max: 2.91  std: 0.311 | 36.5GHz on-Earth sidelobe uncertainty u(Tsl_earth)<br>nbr: 58777  min: 0.44  mean: 0.5508  med: 0.4908  max: 1.572  std: 0.1571 |

*Figure 3-19: ERS-1 Brightness temperatures uncertainties for February, May, August, November 2003*

## 3.2.3 Uncertainty provided

### 3.2.3.1 How uncertainty information is provided in the product

The uncertainty is provided per brightness temperature as a single value.

### 3.2.3.2 How the uncertainty information should be used

These uncertainties should be used as an uncertainty bar on the brightness temperatures.

### 3.2.3.3 Roadmap for further uncertainty analysis

The roadmap for further analysis would be to see if it is possible to go further about sources not assessed in the first stage of the project:

- Temperature gradients along waveguides (NC)
- Temperature dependency of characterisation parameters (NC)
- Reference temperatures (Hot load for calibration, Dicke load) (NC)

These contributions are very linked to the design and ideally should have been characterized during on-ground characterisation. The temperature gradients can be analyzed with the internal temperature available, if the position of the temperatures can be found in the available documentation. The two latest seems difficult to achieve.

We would look for improvement and/or completion of the estimation for the sources considered here:

- Drift of PRT measurements
- Antenna pattern correction: better assessment of uncertainty from correction maps, pointing uncertainty, efficiency uncertainty

Further work is also needed on the propagation of uncertainties from these individual components to the TDP, and to consider the analysis of error correlation structures between the spectral channels and between different individual observations (time and/or space correlation) so that this information can be used in subsequent uncertainty analysis.

# 4 Thematic Data Products Validation Report

## 4.1 Land-Ice Thematic Data Products

### 4.1.1 Overview of the uncertainty analysis

The uncertainty for the Land Ice Thematic Data product is computed using a top-down approach, based upon an empirical parameterisation of elevation differences relative to airborne reference data. Specifically, uncertainty is parameterised as a function of surface slope. This is motivated by the knowledge that measurement accuracy degrades as a function of ice sheet surface slope, due to the challenges of retracking waveforms and identifying the correct echoing point over increasingly complex ice sheet terrain. The empirical relationship used to compute the TDP uncertainty parameter is computed through comparison to cotemporaneous Operation IceBridge (OIB) and pre-IceBridge airborne laser altimeter reference data.

A top-down approach to uncertainty estimation is implemented because a bottom-up formal propagation of uncertainties from Level-0 to Level-2 has not yet been achieved over the complex topography of ice sheet surfaces. Instead, we implement an approach that characterises the uncertainty implicitly, using the distribution of differences computed with respect to independent reference data. These reference data are acquired from airborne platforms and utilise a laser altimeter, meaning that they offer higher accuracy and precision when measuring the air-snow interface than the radar altimetry data, and better constrained uncertainties. Specifically, Operation IceBridge data have been shown to provide a vertical accuracy of 7 cm and a vertical precision of 3 cm [**RD** 3], and pre-IceBridge data to have a vertical accuracy of 20 cm [**RD** 2]. This approach aims to implicitly characterise the dominant sources of uncertainty associated with deriving measurements of ice sheet surface elevation from altimetry echoes; namely due to (1) retracking (i.e. the retrieval of range from the altimeter waveform), (2) radar wave penetration into the snowpack, (3) the echo relocation (commonly termed the slope correction; which accounts for the fact that over ice sheets the target

surface is not orthogonal to the radar boresight vector, thereby meaning that the point of closest approach is upslope of nadir), and (4) geophysical corrections. Each of these factors is summarised briefly in turn.

**Retracking.** Uncertainty resulting from imperfections in the retracking is a common issue across all domains. Over ice sheets, specifically, retracking is challenging, and is particularly prone to uncertainty in coastal regions where complex topography can lead to multiple distinct surface reflections within the receive window and, as a consequence, noisy or multi-peak waveforms.

**Snowpack Penetration.** Over ice sheets, microwave energy at Ku-band frequencies can penetrate several metres into the snowpack. The degree of penetration of the radar wave into the snowpack is spatially and temporally variable, meaning that derived elevations do not always correspond to the true air-snow interface. This can complicate the interpretation of Ku-band altimeter elevation measurements, and lead to uncertainties with respect to measurements of the true surface and its evolution.

**Echo Relocation.** Over ice sheets, the sloping and undulating nature of their surface means that the point of closest approach to the satellite is not at nadir, but rather is situated upslope. Therefore, in conventional, Low Resolution Mode (LRM) altimeters, the 'angle of arrival' between the satellite boresight and the surface reflection point (usually assumed to be the Point of Closest Approach) is not known directly, and instead must be approximated based upon an auxiliary slope model, derived from a Digital Elevation Model. Uncertainties associated with the DEM, or in identifying the Point of Closest Approach corresponding to the retracking point, can therefore lead to uncertainties associated with the derived elevation. Formally constraining the uncertainties on the DEM over the range of topographic surface encountered on an ice sheet remains a challenge.

**Geophysical Corrections.** As is common with Level-2 altimetry processing over most surfaces, a range of geophysical corrections must be applied to account for atmospheric path delays and shorter-period fluctuations in Earth's surface. These include dry and wet tropospheric corrections, a correction for ionospheric path delays, and tidal corrections, and are commonly derived from physical models that each have their own uncertainties.

## 4.1.2 Uncertainty evaluation

The Land Ice TDP uncertainty parameter is computed by firstly deriving an empirical relationship between surface slope and the observed differences between reference and satellite measurements bring uncertainty to each along-track TDP measurement, based upon the magnitude of the surface slope at that location and a look up table generated from the empirical values. The method is described below. In practice, for each mission, the airborne data archive was searched to identify the cycle which coincides with the greatest volume of validation data. The cycles selected were ENVISAT cycle 78 (April-May 2009), ERS-2 cycle 84 (April-June 2003) and ERS-1 cycle 140 (May-September 1994). The associated airborne reference data are shown in Figure 4-1. This analysis was performed over the Greenland Ice Sheet because airborne data coverage is much more extensive over Greenland than Antarctica.
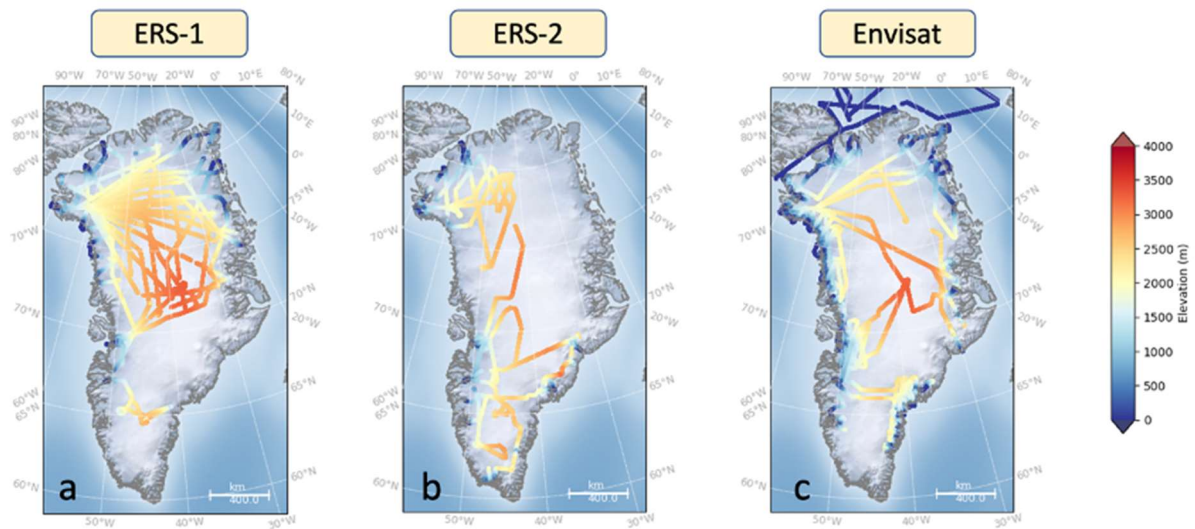
*Figure 4-1 : The airborne reference data acquired over Greenland that is used to constrain the Land Ice TDP uncertainty model for ERS-1 (a), ERS-2 (b) and ENVISAT (c).*

Uncertainty was computed by the following steps:

1. Identify pairs of near co-located (within 500 metres; i.e. less than the altimeter pulse limited footprint), near co-incident (within 30 days) airborne and satellite data.

2. Correct the elevation of the reference data for surface slope. This accounts for the fact that the satellite-airborne pairs are not exactly co-located, and that for non-flat surfaces there will consequently be an elevation difference purely due to the difference in the sampling position within the 500 m search radius.

3. Compute satellite-minus-airborne elevation differences at each comparison point.

4. Derive an estimate of the magnitude of the surface slope at each comparison point, based upon measurements from an auxiliary Digital Elevation Model.

5. Define the look up table. Collate individual satellite-minus-airborne elevation differences within 0.1° slope bands. Compute the median of the absolute elevation differences within each slope band. These median values typically lie in the range 0-10 m, depending upon the magnitude of the slope and the satellite mission. Define a look up table for the current mission, which relates the median absolute elevation difference of each band to all slopes within that band.

6. Use the look up table. For each altimetry measurement, estimate the surface slope at its echoing location based upon its geographical coordinates and the slope map derived in step 4. Then, use the mission-specific look up table defined in step 5 to assign an associated uncertainty to that altimetry measurement based upon the surface slope at its location. At high slopes (> 1.3°) the number of comparison points becomes small (< 100 measurements per slope bin, on average; compared to $10^2$-$10^3$ measurements per bin at lower slopes). As a result, the statistics for higher slope bins computed in step 5 are relatively unstable (standard deviation 2-4 times higher above 1.2 degrees than below 1.2 degrees). For slopes greater than 1.3 degrees, we therefore assign uncertainties based upon a linear regression of uncertainty against slope with 0 intercept, which is fitted to the uncertainties of the lower slopes (< 1.3 degrees).

7. Repeat steps 1-6 for each mission.

Figure 4-2 provides the spatial distribution of uncertainties across Greenland, for each mission. Within the interior of the ice sheet, uncertainties are typically sub-metre. Moving towards the coast, as the topography becomes more complex, uncertainties grow to the order of 10 meters close to the ice sheet margin.
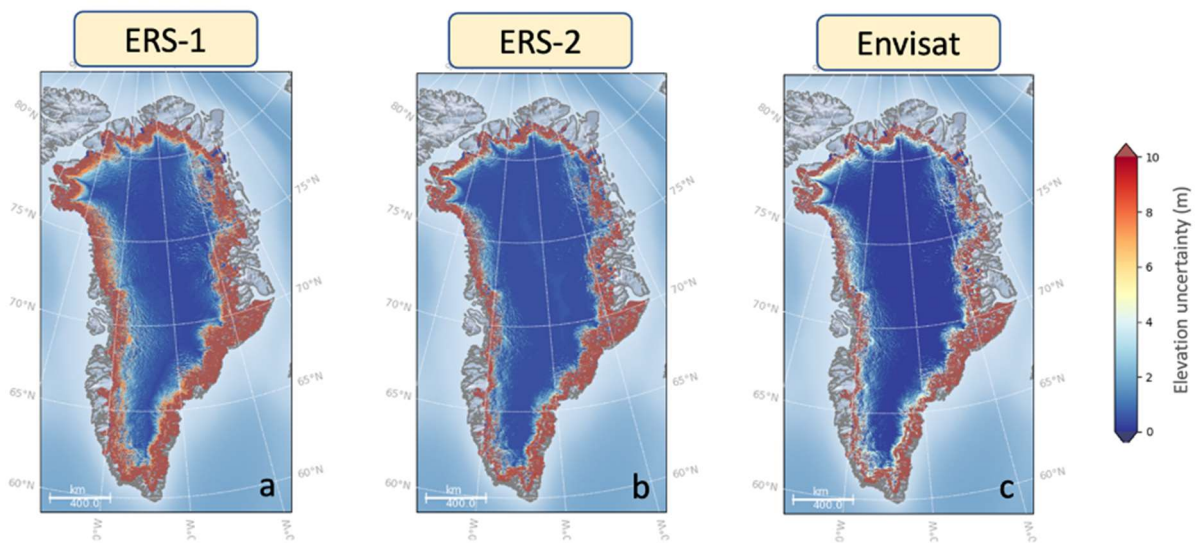


*Figure 4-2 : Per-mission uncertainty across the Greenland Ice Sheet; a. ERS-1; b. ERS-2; c. ENVISAT.*

## 4.1.3 Uncertainty provided

### 4.1.3.1 How uncertainty information is provided in the product

Uncertainty is provided as a single value for each TDP record within the NetCDF 'main' group of the product. The variable is named "surface_elevation_uncertainty" where the unit is metres. This uncertainty parameter provides an estimate of the overall uncertainty associated with each given elevation measurement.

### 4.1.3.2 How the uncertainty information should be used

The uncertainty associated with each TDP measurement represents the average deviation that TDP measurements acquired over surfaces with that given slope exhibit from co-located, cotemporaneous reference elevation measurements. This information can therefore be used by the user to assess the typical deviation that might be expected between each measurement and the true surface. The information is provided along-track, and therefore spatially variable, to allow the user maximum flexibility to utilise this information for their specific applications.

### 4.1.3.3 Roadmap for further uncertainty analysis

Here, we evaluate uncertainty using a top-down approach using airborne laser altimetry as a reference dataset. In the future, further methodological development of the uncertainty analysis should focus upon developing bottom-up approaches that systematically consider all sources of uncertainty throughout the Level-1 and Level-2 processing chains and propagating these uncertainties through to the TDP product. It is important to note that the formal propagation of uncertainties over highly complex ice sheet surfaces is a non-trivial challenge and would require a substantial body of work.

## 4.1.4 Reference documents

| RD 2 | Krabill, W. & Thomas, R. & Martin, C. & Swift, R. & Frederick, E. (1995). Accuracy of Airborne Laser Altimetry Over the Greenland Ice Sheet. International Journal of Remote Sensing - INT J REMOTE SENS. 16. 1211-1222. 10.1080/01431169508954472. |
|---|---|
| RD 3 | Martin, C. F., Krabill, W. B., Manizade, S. S., Russell, R. L., Sonntag, J. G., Swift, R. N., & Yungel, J. K.: Airborne Topographic Mapper Calibration Procedures and Accuracy Assessment. NASA Techni NASA/TM\u20132012-215891, Goddard Space Flight Center, Greenbelt, Maryland 20771. Available Online at: https://ntrs.nasa.gov/api/citations/20120008479/downloads/20120008479.pdf, 2012. |

## 4.2  Sea-Ice Thematic Data Products

### 4.2.1 Overview of the uncertainty analysis

The methodology used for sea ice thickness estimation is a bottom-up approach based on the dominant sources of uncertainty. For a single observation, the current method of providing uncertainties is through error propagation of the contributing parameters.  In order to estimate the propagation of uncertainties during the calibration, the uncertainty budget has been split in two main parts, before and after the calibration procedure.

The uncertainty budget methodology concerning the first part is taken from Ricker et al. [**RD 4**]. We assume that for this part there are 3 sources of uncertainty: the speckle noise, largely discussed in Wingham et al. [**RD 5**], the accuracy of the sea surface anomaly (SLA) measurement (both are random uncertainties), and finally a bias that corresponds to retracker threshold choice, surface roughness and snow radar signal penetration [**RD-7**].

**Uncertainties associated with random effects in the retracker.**

According to Wingham et al. [**RD 5**], where they summarised the results of a Monte Carlo simulation, speckle noise generates an uncertainty from 7 cm to 14 cm (depending on the acquisition mode) on the range measurement. This uncertainty depends on the number of individual echoes used to compute the averaged echoes (for LRM sensors The uncertainty associated with SLA will also depend on the surface type (leads or floes). We consider that the errors associated with each surface, are not correlated, and can be combined to give the random part of radar freeboard uncertainties: $\sigma^2_{FB} = \sigma^2_{SLA} + \sigma^2_{speckle}$, with $\sigma_{SLA}$ = std(SLA) along 25 km sliding windows, and $\sigma_{speckle}$ = 0.07m for ERS-1&2 and $\sigma_{speckle}$ = 0.10m for ENVISAT.

**Uncertainties associated with the snow radar penetration and surface roughness.**

The major sources of uncertainty come from the knowledge of the properties of the surfaces encountered by the signal or its behaviour with respect to these surfaces. In particular, there remains a large source of uncertainty about the actual level of penetration of radar waves into the snow or about where the signal is really reflected (ice/snow interface or not). On top of that, there is uncertainty about the choice of the threshold of the retracker due to the surface roughness's. The estimation of these uncertainties has been taken from a more recent study Landy et al 2020 **[RD 6].** More details can also be found in Bocquet et al. **[RD 7].**

During the calibration procedure, uncertainties on the radar freeboard and on the involved parameters are propagated by using a Monte Carlo methodology.

These FBr uncertainties are finally propagated to SIT uncertainties by taking into account the snow, ice, water densities uncertainties as well as the snow depth uncertainty. There are all assume to be uncorrelated and

combined using the sum squared partial derivative equation to derive SIT uncertainties. Radar freeboard, Snow depth and ice densities uncertainties are the most predominant in the SIT uncertainties budget.

## 4.2.2 Uncertainty evaluation

Methodologies to evaluate the uncertainty of the radar freeboard have been already proposed in previous studies. The one used in the context of this project for the raw radar freeboard is presented in Ricker et al. [**RD 4**] and in Landy et al 2020 [**RD 6**]. But as explained above the main challenge was to find out a way to propagate the uncertainties among the Neural Network (NN) calibration step. For that purpose we have developed and original methodology which combine NN and Monte Carlos. The approach is fully described in Bocquet et al. [**RD 7**].

The interest of this NN + Montecarlo approach is the fact that it is generic and can be applied for all missions and all processing options. However, the NN correction and its Montecarlo distribution must be recomputed for each case (mission, product, retracker, corrections, hemisphere, ...).

This radar freeboard uncertainty computation is summarized in Figure 4-3, from along track estimation then through the calibration procedure associated with a Monte Carlo simulation for the estimation of the uncertainties.

The top section of the diagram shows the determination of the uncertainty in the gridded freeboard product from the along-track uncertainties using Monte Carlo simulations.

These distributions are then used to build 100 neural networks, which themselves processed 100 sets of sampling. We finally obtain 10000 corrected data sets which distribution represent the final uncertainty.
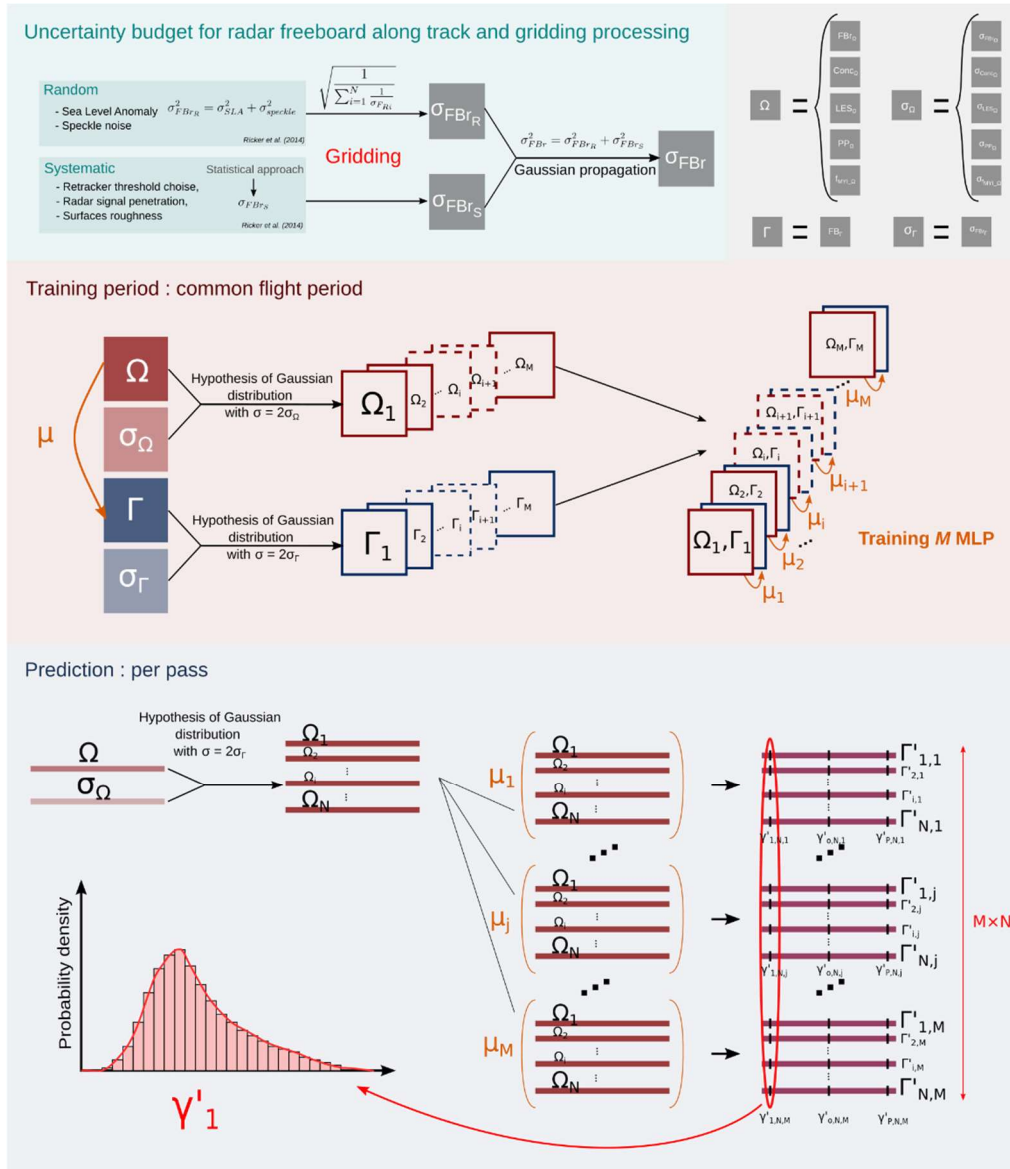
*Figure 4-3 : Summary of the FBr uncertainty evaluation. Top panel characterize the along track uncertainty budget, middle panel the training period of the calibration and the bottom panel the along track prediction step. Ω represents the inputs of the calibration and Γ the target FBr, sigma σ their related uncertainties.*

The equilibrium equation of the ice in the water and combined with the speed propagation reduction of the radar wave in the snow aims to the following equation, where $FB_{Ku}$ is the measured freeboard, SD the snow depth, c and $c_s$ the wave speed into vacuum and snow, and $\rho_s$, $\rho_i$, and $\rho_w$ the densities of the snow, the ice and the water.

$$SIT = \frac{\rho_w}{\rho_w - \rho_i} FB_{Ku} + \frac{(c/c_s - 1)\rho_w + \rho_s}{\rho_w - \rho_i} SD$$

Using the radar speed propagation into snow equation suggested by Ulaby et al. 1996 [**RD 8**]: $c/c_s = (1 + T \rho_s)^{1.5}$ with $T = 0.00051$, we obtain:

$$SIT = \frac{\rho_w}{\rho_w - \rho_i} FB_{Ku} + \frac{\rho_w \delta_p (1 + T\rho_s)^{1.5} - \rho_w + \rho_s}{\rho_w - \rho_i} SD$$

From the hypothesis that the five involved parameters FB$_{Ku}$, SD, $\rho_s$, $\rho_i$, and $\rho_w$ are un-correlated we can estimate the SIT uncertainty as the square root of the sum of the square of each parameter uncertainty multiplied by the SIT partial derivative relatively to this parameter, which aims to the following equation:

$$
\begin{aligned}
u^2_{SIT} = \ & u^2_{FBku}\left[\frac{\rho_w}{\rho_w-\rho_i}\right]^2 + \\
& u^2_{SD}\left[\frac{\rho_w(1+T\rho_s)^{1.5}-\rho_w+\rho_s}{\rho_w-\rho_i}\right]^2 + \\
& u^2_{\rho s}\left[\frac{1+1.5\,T\rho_w(1+T\rho_s)^{0.5}}{\rho_w-\rho_i}\,SD\right]^2 + \\
& u^2_{\rho w}\left[-\frac{\rho_i\,FB_{Ku}+SD\,(\rho_s-\rho_i+\rho_i(1+T\rho_s)^{1.5})}{(\rho_w-\rho_i)^2}\right]^2 + \\
& u^2_{\rho i}\left[\frac{\rho_w\,FB_{Ku}+SD\,(\rho_s-\rho_w+\rho_w(1+T\rho_s)^{1.5})}{(\rho_w-\rho_i)^2}\right]^2 + 0
\end{aligned}
$$

Some typical values are presented in Table 4-1 .

The densities and their uncertainties values used to process the sea ice thickness within the distributed products are the following:

<div align="center">

water=0.5 [Wadhams et al. 1992] [RD 9]

snow=3.2 [Warren 1999 [RD 10]

on MYI=23 ; on FYI=36 [Alexandrov et al. 2010] [RD 11]

</div>

*Table 4-1 : Typical examples for First Year Ice and Multi Year Ice values with the corresponding sensitivity coefficient c² and uncertainty c²u² Estimation of sea ice thickness uncertainty, based on the current methods. Because of their low uncertainty or low sensitivity coefficient, the snow and water densities have little impact on the SIT uncertainty (green values). On the other hand, the radar freeboard, the snow depth and the ice densities have non-negligible impacts. The results in green have little impact on the total uncertainty and in red have a non-negligible impact on the total uncertainty.*

| | FYI (FBi=0.10m) | | | | MYI (FBi=0.20m) | | | | Ref |
|---|---|---|---|---|---|---|---|---|---|
| | mean | u | c² | c²u² | mean | u | c² | c²u² | |
| FBku (m) | 0.07 | 0.10 | 91.59 | 0.92 | 0.12 | 0.10 | 52.0 | 0.52 | variable (just an example here) |
| SD (m) | 0.15 | 0.15 | 24.11 | 0.54 | 0.35 | 0.15 | 13.7 | 0.31 | Warren 1999 [RD 10] |
| $\rho_i$ (kg/m³) | 917 | 36.0 | 16.2 10⁻⁵ | 0.21 | 882 | 23.0 | 23.1 10⁻⁵ | 0.12 | Alexandrov et al. 2010 [RD 11] |
| $\rho_s$ (kg/m³) | 290 | 3.2 | 6.65 10⁻⁶ | 0.00 | 290 | 3.2 | 2.05 10⁻⁵ | 0.00 | Warren 1999 [RD 10] |
| $\rho_w$ (kg/m³) | 1024 | 0.5 | 13.9 10⁻⁵ | 0.00 | 1024 | 0.5 | 19.0 10⁻⁵ | 0.00 | Wadhams et al. 1992 [RD 9] |
| SIT | 1.36 | 1.29 | | | 2.16 | 0.97 | | | |

Figure 4-4 represents sea level anomaly (SLA), sea ice thickness (SIT) and radar freeboard (FBr) along two tracks for NH and SH with their related uncertainties.
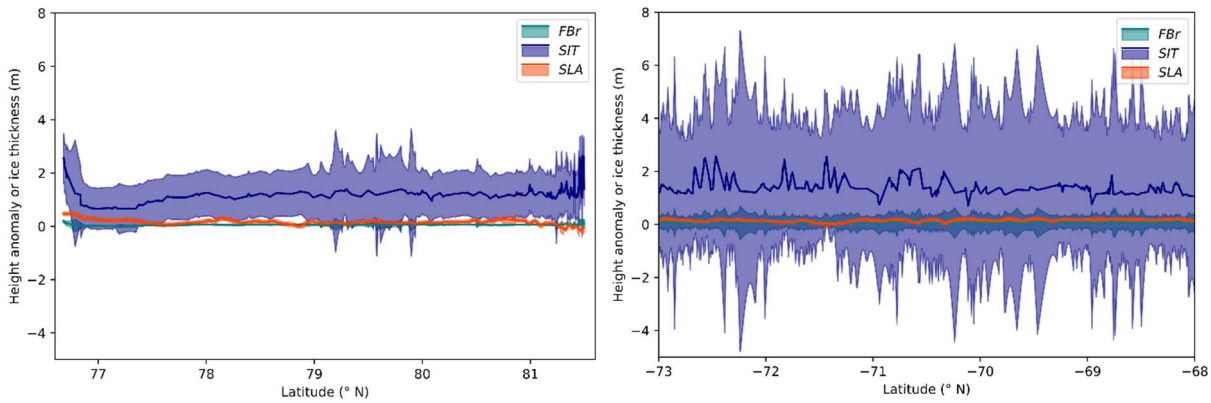
*Figure 4-4: Sample of along track FBr, SIT and SLA values +/- uncertainties (for NH on the left, c86 t10 and SH, c90 t26 on the right).*

Uncertainties on SIT are in average larger for Antarctic Sea-Ice than for Arctic sea ice. For the SIT uncertainty budget, the three components that impact the more the SIT uncertainty are the one from FBr, snow depth and sea ice density uncertainty (cf Table 4-1).

## 4.2.3 Uncertainty provided

### 4.2.3.1 How uncertainty information is provided in the product

Uncertainties are provided for each value of the along track data in the main group of the NetCDF. The name of uncertainty variables end with "_uncertainty" and each single values the uncertainty in meter: "sea_ice_thickness_uncertainty", "radar_freeboard_uncertainty", "sea_ice_freeboard_uncertainty" and "sea_level_anomaly_uncertainty".

### 4.2.3.2 How the uncertainty information should be used

**Limitation of the uncertainty budget:**

1. Systematic uncertainty budget comes from Landy et al [**RD 6**]. Their study computed uncertainties for gridded product purposes and suggested that uncertainties can be larger for along-track data. Uncertainties may be underestimated for along-track data.
2. According to Landy et al [**RD 6**].], one of the main sources of uncertainties on sea ice thickness retrieval is the surface roughness, the second one is the radar partial snow penetration. Here we decided only to consider the surface roughness as it is not as simple to distinguish the contribution of the two sources especially considering the methodology that has led to this budget (retracker algorithm comparison). A part of the snow penetration issue can be missed here, the uncertainties can be underestimated also for that reason.
3. Everything is assumed to be uncorrelated, that can lead to an under- or overestimation of the total uncertainties while propagating the uncertainties with a sum squared equation if there are significant correlations, but it should not be the case.
4. The noise in Monte Carlo simulation has been computed considering the distribution of the several variables to follow a gaussian distribution, while the distributions could be skewed, this could also impact the uncertainties results.
5. SLA calibration is not taken into account, again, an underestimation of the SLA and FB and SIT can be observed.
6. Only dominant sources of uncertainty have been considered. A complete metrological approach would consider all sources of uncertainty.
7. Each observation is considered independently. So, error correlation structures between observations have not been evaluated.

### 4.2.3.3 Roadmap for further uncertainty analysis

Two points could be studied in more details. The SLA calibration uncertainty should be taken into account. A prospective for the uncertainty budget would be to propagate uncertainty using a MC approach from the beginning of the processing chain. It would also be interesting to generate the samples for the MC simulation randomly but spatially correlated.

## 4.2.4 Reference documents

| RD 4 | Ricker, R., Hendricks, S., Helm, V., Skourup, H., and Davidson, M.: Sensitivity of CryoSat-2 Arctic sea-ice freeboard and thickness on radar-waveform interpretation, The Cryosphere, 8, 1607–1622, https://doi.org/10.5194/tc-8-1607-2014, 2014. |
|---|---|
| RD 5 | Wingham, D., Francis, C., Baker, S., Bouzinac, C., Brockley, D., Cullen, R., de Chateau-Thierry, P., Laxon, S., Mallow, U., Mavrocordatos, C., Phalippou, L., Ratier, G., Rey, L., Rostan, F., Viau, P., and Wallis, D.: CryoSat: A mission to determine the fluctuations in Earth's land and marine ice fields, Advances in Space Research, 37, 841 – 871, doi: 10.1016/j.asr.2005.07.027, 2006. |
| RD 6 | Landy, J. C., Petty, A. A., Tsamados, M., & Stroeve, J. C. (2020). Sea ice roughness overlooked as a key source of uncertainty in CryoSat-2 ice freeboard retrievals. *Journal of Geophysical Research: Oceans*, 125, e2019JC015820. https://doi.org/10.1029/2019JC015820 |
| RD 7 | Bocquet, M., Fleury, S., Piras, F., Rinne, E., Sallila, H., Garnier, F., and Rémy, F.: Arctic sea ice radar freeboard retrieval from ERS-2 using altimetry: Toward sea ice thickness observation from 1995 to 2021, EGUsphere [preprint], https://doi.org/10.5194/egusphere-2022-214, 2022. |
| RD 8 | Ulaby, F. T., Moore, R. K., and Fung, A. K.: Microwave remote sensing: Active and passive, Volume 3-From theory to applications, vol. 3, 1996. |
| RD 9 | Wadhams, Peter, et al. "Relationship between sea ice freeboard and draft in the Arctic Basin, and implications for ice thickness monitoring." Journal of Geophysical Research: Oceans 97.C12 (1992): 20325-20334. |
| RD 10 | Warren, S. G., Rigor, I. G., Untersteiner, N., Radionov, V. F., Bryazgin, N. N., Aleksandrov, Y. I., and Colony, R.: Snow Depth on Arctic Sea Ice, Journal of Climate, 12, 1814–1829, https://doi.org/10.1175/1520-0442(1999)012<1814:SDOASI>2.0.CO;2, 1999. |
| RD 11 | Alexandrov, V., Sandven, S., Wahlin, J., and Johannessen, O. M.: The relation between sea ice thickness and freeboard in the Arctic, The Cryosphere, 4, 373–380, https://doi.org/10.5194/tc-4-373-2010, 2010. |

## 4.3  Ocean & Coastal Thematic Data Products

## 4.3.1 Overview of the uncertainty analysis

### 4.3.1.1 Context

A bottom-up approach for the SLA (Sea Level Anomaly) would require defining all the uncertainty terms and combining them in a way that is consistent with the real correlations that affect all these terms. As discussed in [D-5-01], **it is extremely hard to implement a bottom-up uncertainty characterisation method** and **we have decided in this project to use**, for the ocean uncertainty characterization, **a top-down approach**. It consists in characterizing the different uncertainties in terms of amplitude but also in term of space and temporal correlations. These are then combined using a spectral approach accounting for their relative contributions at the different space and time scales. The approach has been presented by Thibaut & al at the Chicago OSTST in 2019 [**RD 12**].

A new method, based on Power Spectral Density (PSD) has been developed at CLS in the frame of the CRISTAL Phase A/B1 study with ESTEC [**RD 14**] accounting for spatial and temporal correlated errors, combining them

and finally providing graphs mapping the uncertainties for different spatial and temporal scales. It gives the capability to describe the uncertainty variance of each source of error for all frequencies in the spatial and temporal dimensions. A mission performance simulation tool (MPS) has been specifically developed in the frame of the CRISTAL study for deriving these "maps" of error that represent the 2D error in spatial and temporal dimension [**RD 14**]. An example of the output "error map" is available down below (Figure 4-6) We used this approach in the FDR4ALT context and to provide in the along-track product uncertainties corresponding to different wavelengths that will be described later.

The uncertainty of each source of error can be described by its variance and the correlation of the signal error in space and time.

To calculate the combined uncertainty budget for the SLA, that accounts for all terms present in the SLA equation, we consider first that each individual uncertainty describes an effect that follows a normal distribution law (true most of the time). The distribution is thus described by its variance at $1s$ (the standard uncertainty, which has a confidence level of ~68%), its spatial correlation length ($x$) and its temporal correlation length ($t$).

The auto-correlation function can be modelled by classical exponential functions for both time and space:

$$R(x,t) = \sigma^2\, e^{-\frac{1}{2}\left(\frac{x}{\lambda_x}\right)^2}\, e^{-\frac{1}{2}\left(\frac{t}{\lambda_t}\right)^2} \tag{4.1}$$

where $\lambda_t$ is the temporal correlation length and $\lambda_x$ is the spatial correlation length. The Power Spectral Density is then computed as the Fourier Transform of the autocorrelation function (correlogram method).

$$\mathcal{F}\left(e^{-ax^2}\right)(\xi) = \sqrt{\frac{\pi}{a}}\exp\left[-\frac{\xi^2}{4a}\right] \tag{4.2}$$

The combined uncertainty is then the combination of the different sources of uncertainties integrated for the correct application target/scale. The computation can be divided in three main steps:

- ✓ Computation of the individual 2D PSD of each source of uncertainty
- ✓ Combination of all individual 2D PSD to compute the total 2D PSD
- ✓ Computation of the 2D STD maps (in space and time) obtained by integration of the total 2D PSD

This method can be extended to as many sources of uncertainty as necessary, always considering spatial and temporal correlation of the errors.

## 4.3.1.2 FDR4ALT strategy

We can describe the uncertainty sources with the following table that includes all the main contributors to the final SLA uncertainty budget. All the values that have been considered in this table have been taken from the literature that is referenced in the right column of the table. Some of them could be clearly further investigated and refined, but this table is proposed as a first attempt to describe all sources of uncertainties.

For the FDR4ALT project, it has been decided to compute these error maps for different SWH values. Indeed, the SSH random error (white noise) vary significantly depending on the SWH values. Therefore, a spectral analysis of the Sea Level Anomaly has been performed for different classes of SWH (Figure 4-5). The value of the noise plateau (i.e, the random noise) is considered as the SSH random error of Table 4-2 (ENVISAT) and Table 4-3 (ERS). Note that the SLA used to perform this analysis is the final SLA provided to the users in the TDP.

*Table 4-2 : Sources of uncertainty and their spatial and temporal correlation length scales (For ENVISAT)*

| Error Source | Values (cm) | | Spatial correlation length | Temporal correlation length | References |
|---|---|---|---|---|---|
| SSH Random error | 0m>swh>1m | 3,5 | 0 km | 0 day | Spectral analysis performed on real data |
| | 1m>swh>2m | 3,3 | | | |
| | 2m>swh>3m | 3,8 | | | |
| | 3m>swh>4m | 4,5 | | | |
| | 4m>swh>5m | 5,7 | | | |
| | swh>5m | 9,6 | | | |
| SSB Large scale error | 0.3 | | 300 km | Inf | Tran et al., 2019 |
| Sea State correlated | 1 | | 10 km | Inf | Tran et al., 2019 |
| Ionosphere | 0,15 | | 600 km | 0 days | Imel et al., 1995 |
| WTC | 1 | | 80 km | 1 hour | Brown et. al, 2015 ; |
| Dry troposphere | 0,2 | | 600 km | 2 days | J3 performance doc (CLS) |
| MSS | 0,55 | | 1 km | Inf | Pujol et al., 2018 |
| Ocean Tides | 1 | | 1000 km | < 1 day | Lyard et al., 2018 |
| Orbit solution | 1,5 | | > 10 000 km | < 1 day | Ollivier et al., 2018; Couhert et al, 2015 |

*Table 4-3 : Sources of uncertainty and their spatial and temporal correlation length scales (For ERS)*

| Error Source | Values (cm) | | Spatial correlation length | Temporal correlation length | References |
|---|---|---|---|---|---|
| SSH Random error | 0m>swh>1m | 8,9 | 0 km | 0 day | Spectral analysis performed on real data |
| | 1m>swh>2m | 9,93 | | | |
| | 2m>swh>3m | 12,3 | | | |
| | 3m>swh>4m | 14,4 | | | |
| | 4m>swh>5m | 16,6 | | | |
| | swh>5m | 20,7 | | | |
| SSB Large scale error | 0.3 | | 300 km | Inf | Tran et al., 2019 |
| Sea State correlated | 1 | | 10 km | Inf | Tran et al., 2019 |
| Ionosphere | 0,15 | | 600 km | 0 days | Imel et al., 1995 |
| WTC | 1 | | 80 km | 1 hour | Brown et. al, 2015 ; |
| Dry troposphere | 0,2 | | 600 km | 2 days | J3 performance doc (CLS) |
| MSS | 0,55 | | 1 km | Inf | Pujol et al., 2018 |
| Ocean Tides | 1 | | 1000 km | < 1 day | Lyard et al., 2018 |
| Orbit solution | 1,5 | | > 10 000 km | < 1 day | Ollivier et al., 2018; Couhert et al, 2015 |



*Figure 4-5 : Spectral Analysis of the provided SLA performed for different SWH values : ENVISAT (left) and ERS-2 (right). Here for ENVISAT, the SLA includes the HFA (High Frequency Adjustment)*

For more details, please refer to [D-5-01].

An error map (or error matrix) has been computed for each of the SSH random error (so 6 maps in total for each mission). Figure 4-6 shows an example of an error map obtained for ENVISAT. We used 0.1 day for the temporal resolution and 350 meters for the spatial resolution, which corresponds to the spatial resolution on-ground between each of the 20Hz measurements.
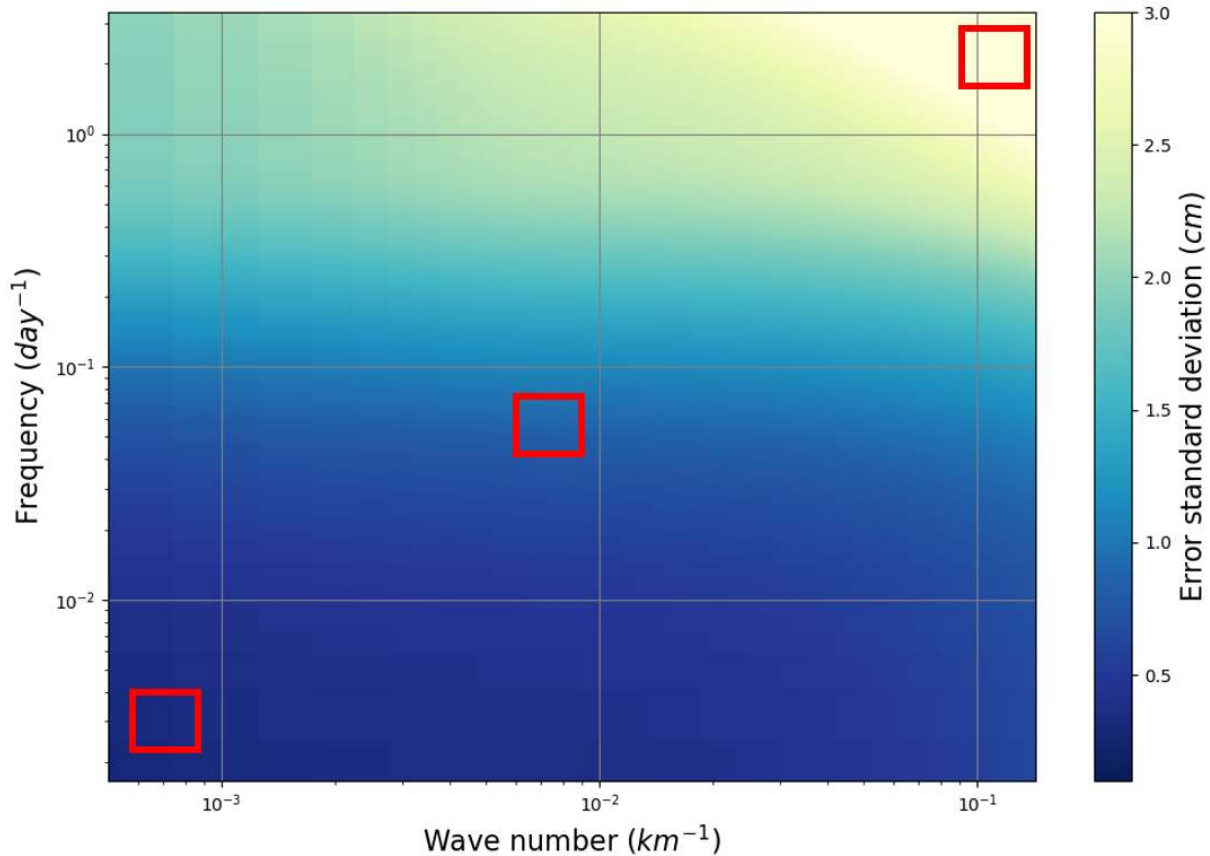


*Figure 4-6 : Error matrix for ENVISAT, 2m<SWH<3m. The red boxes represent the areas chosen to be averaged as uncertainties for 3 different scales.*

To obtain an along-track uncertainty estimation and as illustrated in Figure 4-6 with the red boxes, it has been decided to average this matrix over different time and space frequencies, in order to provide 3 different uncertainties for 3 different scales, corresponding to different fields of application for the users. Table 4-4 summarized the boundaries used for each of the scales. Note that these boundaries have been chosen by discussing internally with different experts and are consistent with Fig.4 of [**RD 14**]. They are nonetheless open for discussion and could be modified if users find it necessary.

| NetCDF field name | Time min (days) | Time max (days) | Dist min (km) | Dist max (km) |
|---|---|---|---|---|
| *short_scale_uncertainty* | 0 | 0.30 | 0 | 0.350 |
| *meso_scale_uncertainty* | 15 | 20 | 150 | 300 |
| *large_scale_uncertainty* | 300 | 600 | 200 | 2000 |

*Table 4-4 : Time and space boundaries used to average the matrix for each of the uncertainties.*
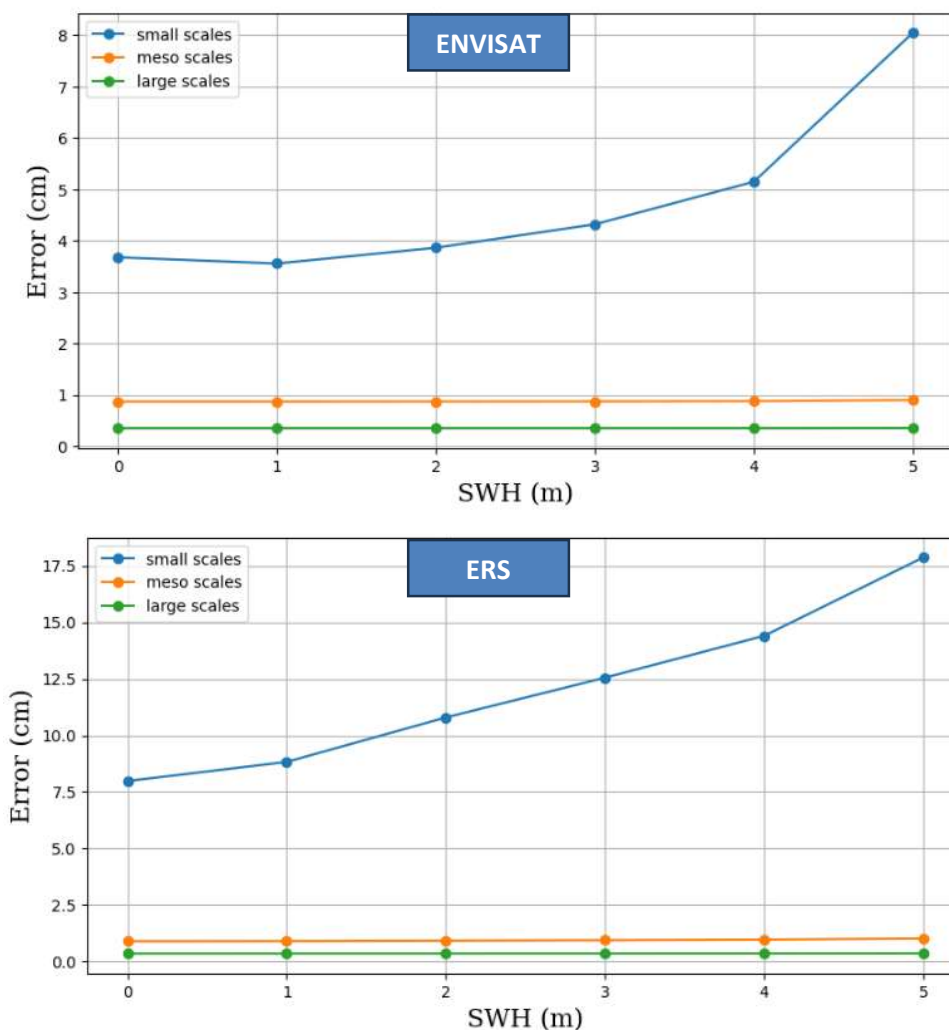
*Figure 4-7 : Outcome of the uncertainty analysis using the simulation tool for ENVISAT (top) and ERS 1/2 (bottom): uncertainties computed for 3 different scales, for different SWH values.*

Figure 4-7 displays the final outcome of the uncertainty computation before interpolation to real data: 3 arrays (one for each scale) varying along the SWH value. One can observe that the small scales uncertainty varies significantly depending on the SWH as expected. The meso-scale uncertainty displays a very small variation depending on the SWH (almost not visible here). The climate uncertainty, as expected, is static for any given SWH.

Once the 3 arrays have been computed using the simulation tool, the uncertainty values can finally be interpolated **along-track** using the real SWH value, i.e., the Adaptive for ENVISAT and the MLE3 for ERS.

One can note that the uncertainty for ERS is significantly larger than for ENVISAT: this is mainly because the Adaptive Retracker, combined with a HFA adjustment, has been applied to ENVISAT and not ERS. Furthermore, the ERS white noise is naturally larger because only 50 pulses are averaged to obtain the 20Hz waveform, versus 100 for ENVISAT.

## 4.3.2 Uncertainty evaluation

### 4.3.2.1 Along-track example

The uncertainty provided in the TDP can be used as error bars or error envelops. Figure 4-8 shows an example of the SLA along-track 20Hz associated with its small-scale uncertainty.
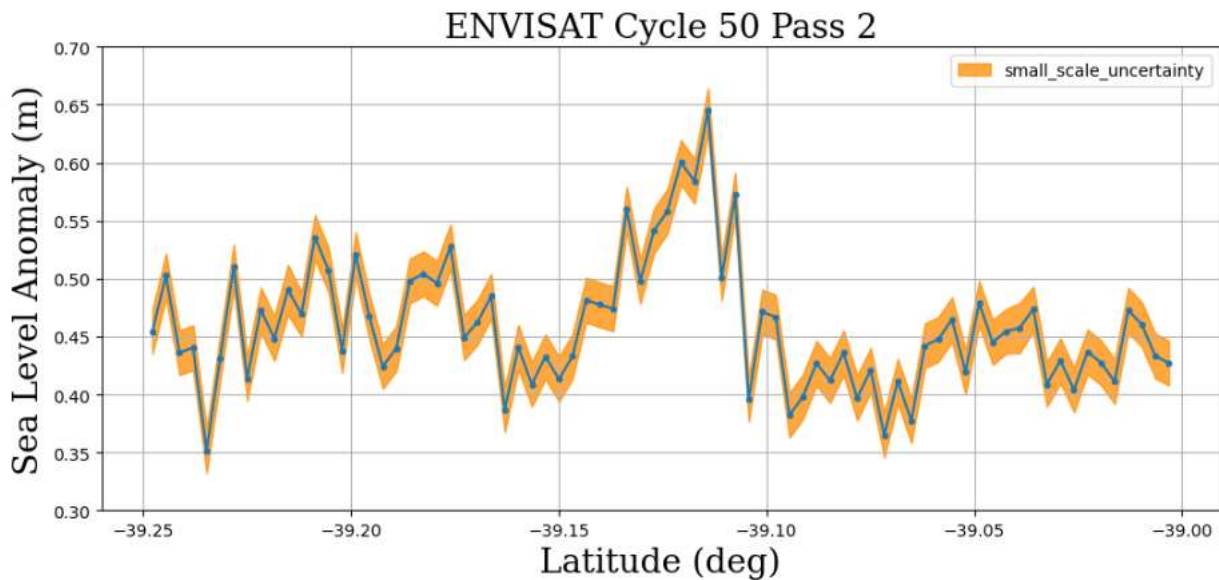
*Figure 4-8 : Example of the small-scale uncertainty used as an envelope for the sla along-track (20Hz). The blue line is the sea level anomaly, and the orange envelope corresponds to the small_scale_uncertainty*

## 4.3.2.2 Gridded maps over one cycle

Here the uncertainties are assessed over one 1Hz ENVISAT cycle. As expected, Figure 4-9 shows that the small-scale error is correlated to the sea-state: the error is higher for high SWH values. Figure 4-10 shows that the meso-scale error is slightly correlated to the sea-state.

Finally, and as expected, the large-scale error is the same regardless of the sea-state conditions, as showed in Figure 4-11.
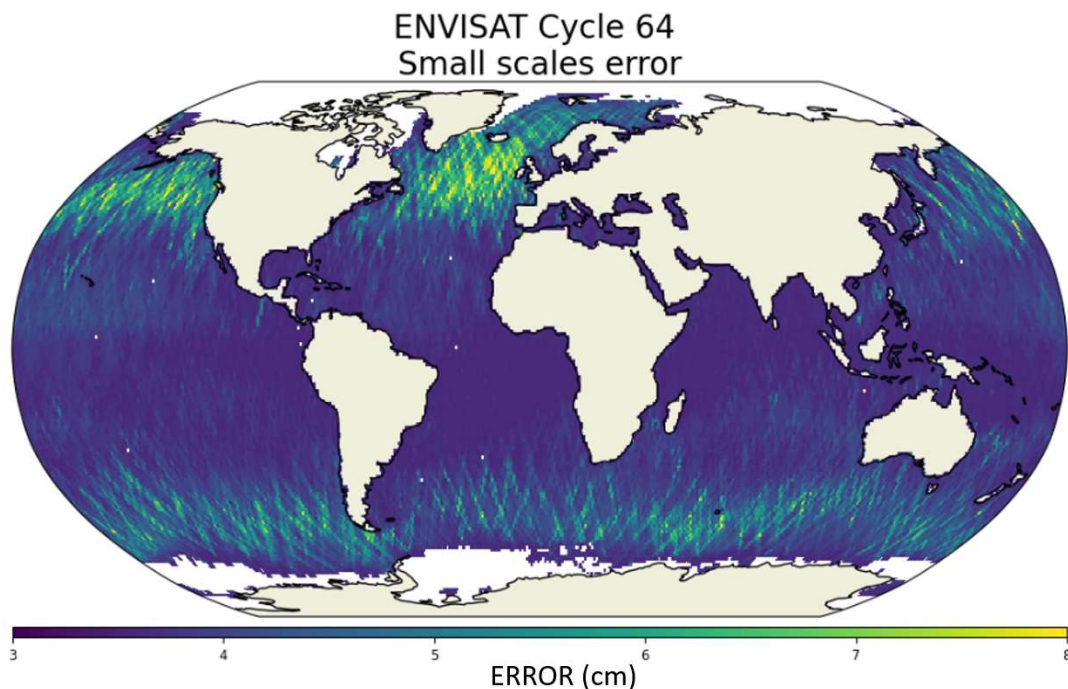


*Figure 4-9 : Gridded map of the small scales error for one ENVISAT cycle (1Hz)*
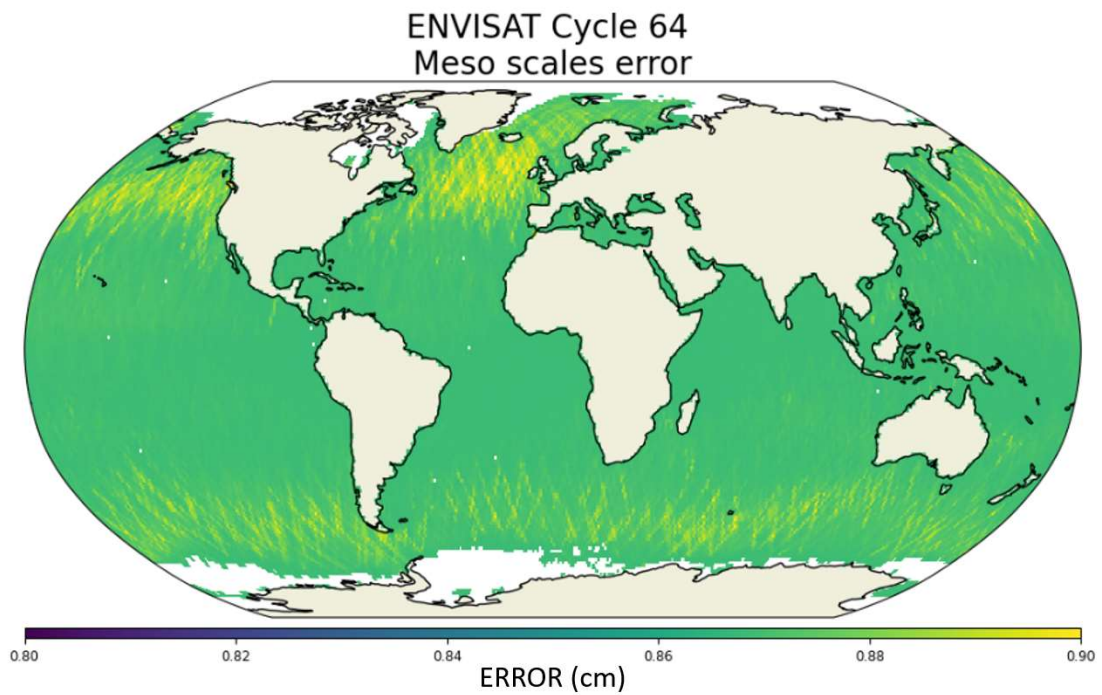
*Figure 4-10 : Gridded map of the meso scales error for one ENVISAT cycle (1Hz)*
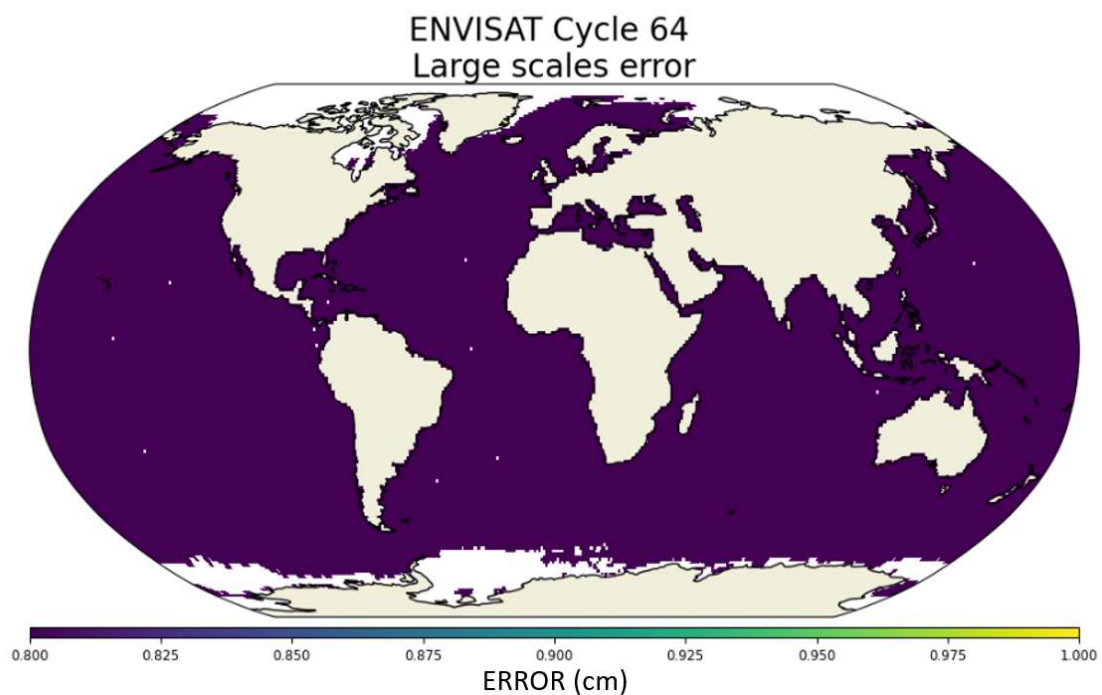


*Figure 4-11 : Gridded map of the large scales error for one ENVISAT cycle (1Hz)*

## 4.3.3 Uncertainty provided

### 4.3.3.1 How uncertainty information is provided in the product

In the FDR4ALT Ocean and Coastal TDP, we propose to provide, for all points along the track, the uncertainty at different scales at very short scales and at meso-scales. As seen in Figure 4-7, they will vary depending on the SWH value, especially the short scale uncertainty. The value of error at large scales will only be provided once in the global attributes of the product, as we consider that they will not vary along the orbit.

| NetCDF field name | Availability |
|---|---|
| *short_scale_uncertainty* | Dynamic value provided along-track |
| *meso_scale_uncertainty* | Dynamic value provided along-track |
| *large_scale_uncertainty* | Static value (one per file, given in the global attributes) |

Note that these 3 fields are available at 20Hz and at 1Hz.

Note that no uncertainty is provided close to the coast (<50km) due to the complexity of estimating it. More information about the uncertainty in the coastal areas is available is the Uncertainty Characterization Definition Document [D-6-01]

### 4.3.3.2 How the uncertainty information should be used

The user must use one of the 3 uncertainties values depending on their need: for example, a user interested in GMSL (Global Mean Sea Level) shall use the "*large_scale_uncertainty*", whereas a user interested looking directly at the 20Hz locally shall use the "*short_scale_uncertainty*".

The short scale uncertainty can be directly used as an error bar on the 20Hz or 1Hz SLA measurements.

Users must be aware that the uncertainty field must be associated to the field "*sea_level_anomaly*" in the product (main group). If a user computes another sea level anomaly (using the expert group for example), the uncertainty provided in this TDP will not be applicable anymore.

The along track uncertainties for the short scales and meso-scales can be combined with the uncertainties associated with the large scales to propagate uncertainties to individual applications. Alternatively, the figures above can be used to identify typical uncertainties for a given spatial and temporal scale.

### 4.3.3.3 Roadmap for further uncertainty analysis

The values from Table 4-2 could be further investigated and improved. For instance, the value of the SSB large scale errors could be considered as variable for different SWH, which would induce a stronger dependency of the meso-scale uncertainty to the sea-state. This analysis must be seen as a first attempt to consider the time/spatial correlations of the uncertainties for the ocean.

More generally, although estimating the uncertainty in the waveform and propagating it to ocean products is challenging, the ESA ASELSU project has been working towards this aim. In the first phase of the ASELSU project it has detailed each source of uncertainty from the altimeter to the GMSL using a bottom-up approach, by detailing each, from the altimeter to the GMSL (instrumental effects, calibrations, retracker, sea-state-bias, …). The second phase of the project, expected to start in early 2023, will extend this work and begin to quantify and propagate those uncertainties. As with the ALT FDR, one could take advantage of the outputs of ASELSU and apply it on the ERS and ENVISAT data, to compute the uncertainty on the Sea Level Anomaly. It would be beneficial to both projects to compare those results to the results obtained with the power spectral density method.

### 4.3.4 Reference documents

| RD 12 | Thibaut P., J.C.Poisson, M.Lievin, L.Amarouche, M.Ablain, M.Tsamados and R.Cullen : "A new way to assess and represent the error budget for any altimeter mission", Chicago OSTST, 2019 |
|---|---|
| RD 13 | Raynal and Labroue (2021) provide a detailed assessment of global uncertainties as part of the Sentinel-3 Mission Performance Centre (MPC) activities |
| RD 14 | Meghan F. Cronin, Robert A. Weller, Richard S. Lampitt and Uwe Send :Ocean Reference Stations', Earth Observation. InTech, Jan. 27, 2012. doi: 10.5772/27423. |

## 4.4 Ocean Waves Thematic Data Products

### 4.4.1 Overview of the uncertainty analysis

The analysis of high frequency component of SWH showed that depending on the sea state conditions, a bump of energy appears (or not) around 10km. This bump, also studied in De Carlo et al. 2023 [RD 16] was shown to be the signature of the so-called wave groups. This physical phenomenon corresponds to the envelope of the directional waves when they have a small frequential spreading (long swell period). Observed by the nadir ground track this signal their signature on the along track spectra is an additional plateau that collapses around the efficient ground track frequency (around 10km for ENVISAT). This over energy has a sinusoidal signature well observable with 5Hz data that can efficiently be removed by a EMD filter (sum of harmonics described in [RD 19]).

Once filtered, the SWH signal delivered in the FDR4ALT products is no longer sensitive to the wave's period. On the other hand, the residual SWH – SWH_filtered contains this correlated signal information related to the observation system. This was defined as the uncertainty on the signal.

### 4.4.2 Uncertainty evaluation

The evaluation of SWH uncertainty is based on the difference between filtered and non-filtered data. Here is a spectral analysis of SWH data from cycle 25 of ENVISAT. The idea is to use the variability removed by the EMD filter to compute the uncertainty. The EMD filtering method is described in [RD 19] and does not imply any frequency limit.

Yet when plotting the filtered and non-filtered signals, it is visible that both signals split at around 50km.

In order to get all the additional energy caused by wave groups it was chosen to integrate the residual over sliding windows over 50km.
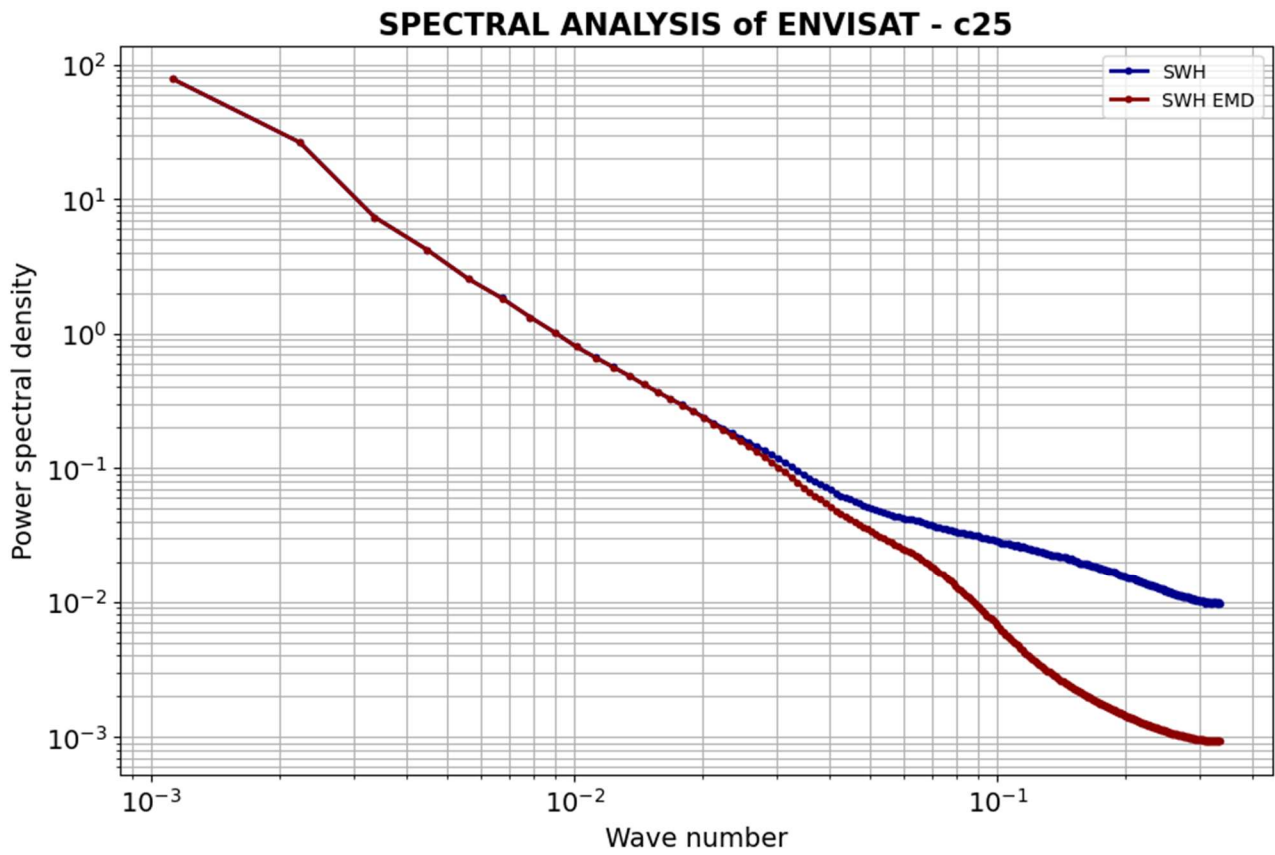
*Figure 4-12 : Spectral analysis of ENVISAT 5 Hz data from cycle 25 with and without EMD filtering*

➔ **ENVISAT**
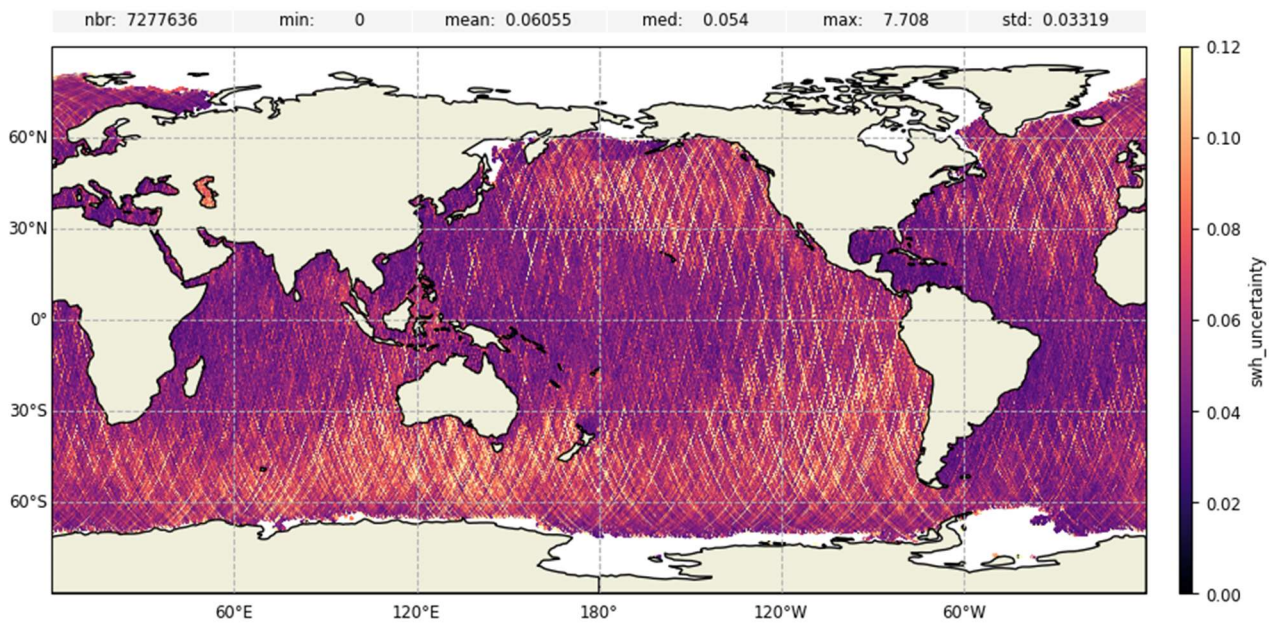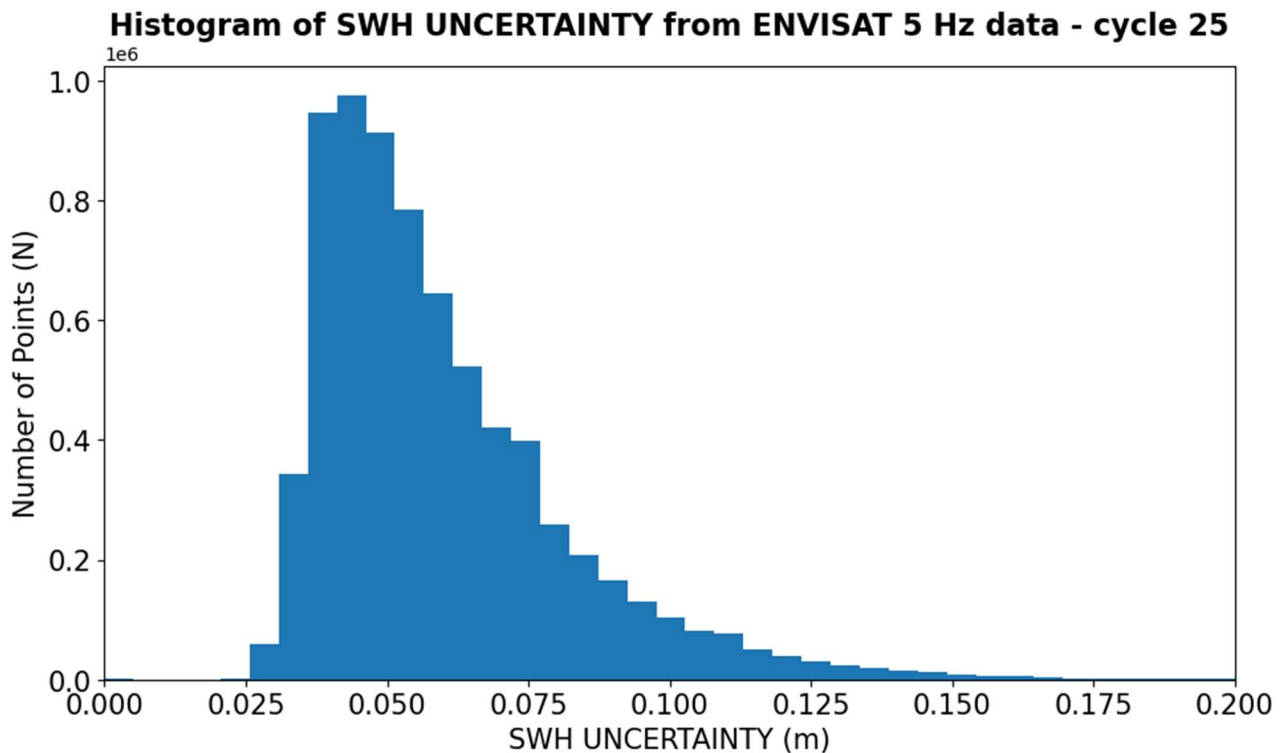
*Figure 4-14 : Histogram of SWH Uncertainty from 5 Hz ENVISAT data from cycle 25 (raw data)*

Figure 4-13 and Figure 4-14 are representing values (cartography and histogram) of this uncertainty provided in the Ocean Waves TDP from one cycle (cycle 25).

It can be observed that the uncertainty presents some geographical structures correlated with the sea state and the mean wave period of waves as intended (see Figure 4-15). It was the expected result because the EMD filtering is supposed to remove the 10 km oscillation caused by wave groups in the along track SWH signal in areas where the sea state is composed by well-structured swells and high wavelength/wave period.

MEAN WAVE PERIOD from ERA5 data - cycle 25

| nbr: 29113644 | min: 1.412 | mean: 6.408 | med: 6.33 | max: 13.58 | std: 1.385 |
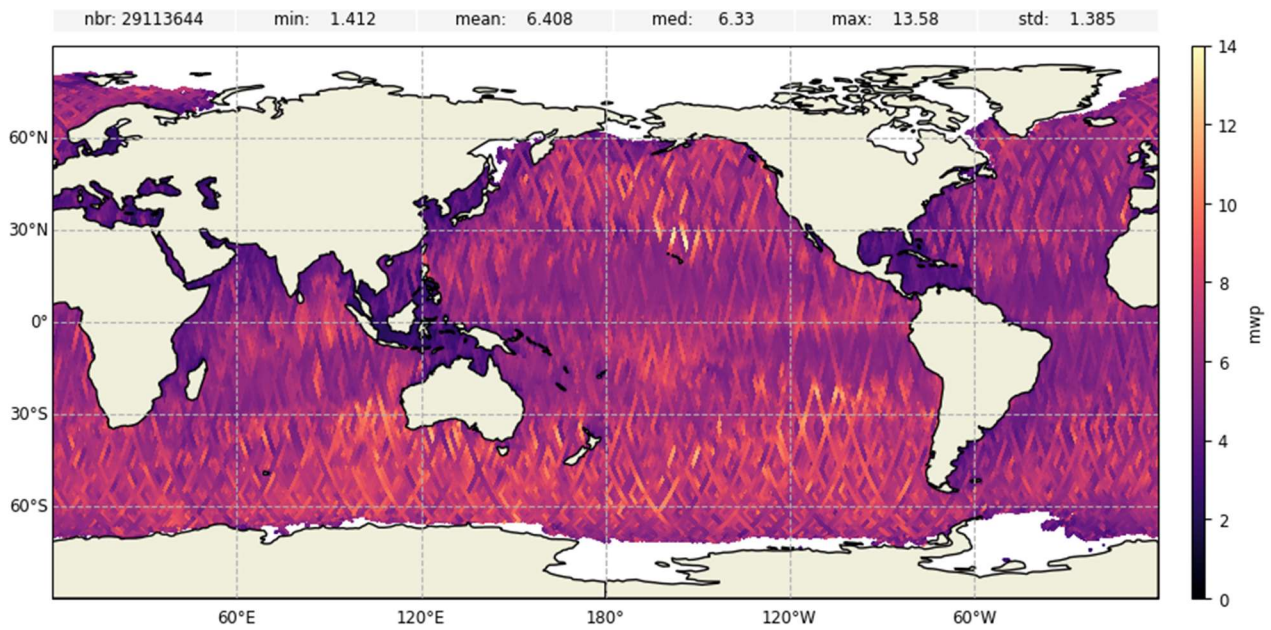
*Figure 4-15 : Mean wave period from ERA5 model data*

Values taken by this uncertainty are between 3 and 12 cm which is consistent with results obtained by Marine De Carlo in [**RD 16**].

Long term monitoring:

MEAN of SWH UNCERTAINTY from ENVISAT 5 Hz data - cycle 6 to 113 (m)
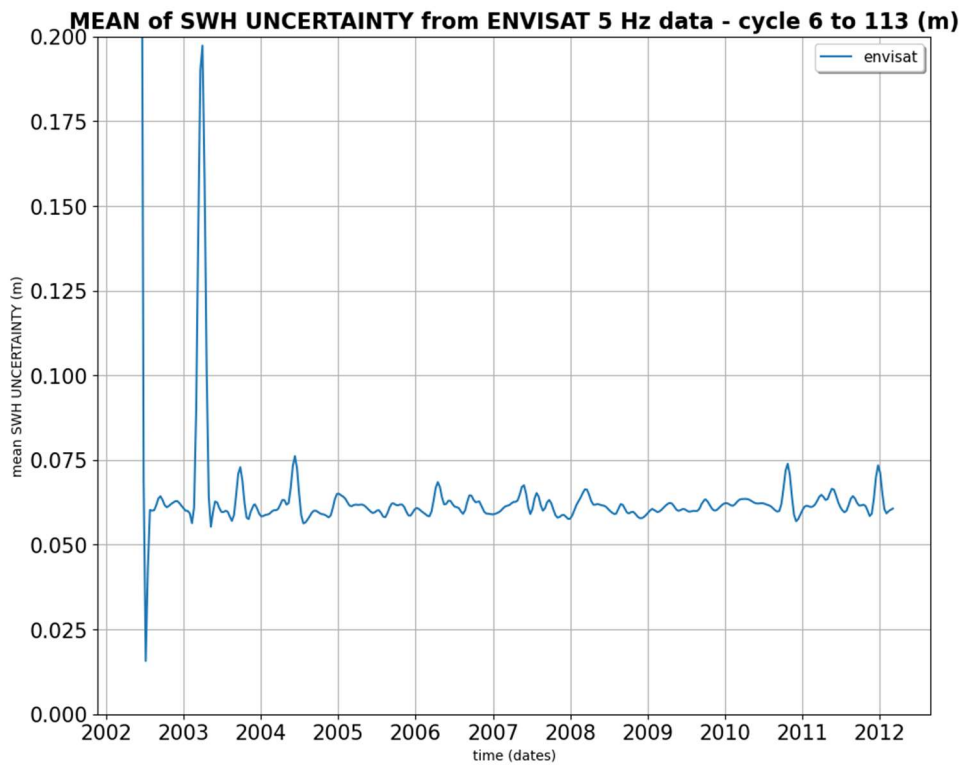
*Figure 4-16 : Long term monitoring of the SWH Uncertainty from ENVISAT 5 Hz data (cycles 6 to 113)*

This long-term global monitoring of the uncertainty shows a stability in the variability removed by the EMD filtering. There are 3 exceptions during cycles 6, 14 and 15. Those cycles presents anomalies in SWH values too (see FDR4ALT Product Validation Report Document [D-4-02]) and so such anomalies in uncertainties are not unexpected.

Unlikely, the uncertainty related to the wave period varies in time geographically (see Figure 4-17). This is consistent with the literature showing a slight increasing of swell period in the eastern Pacific when observed by models.
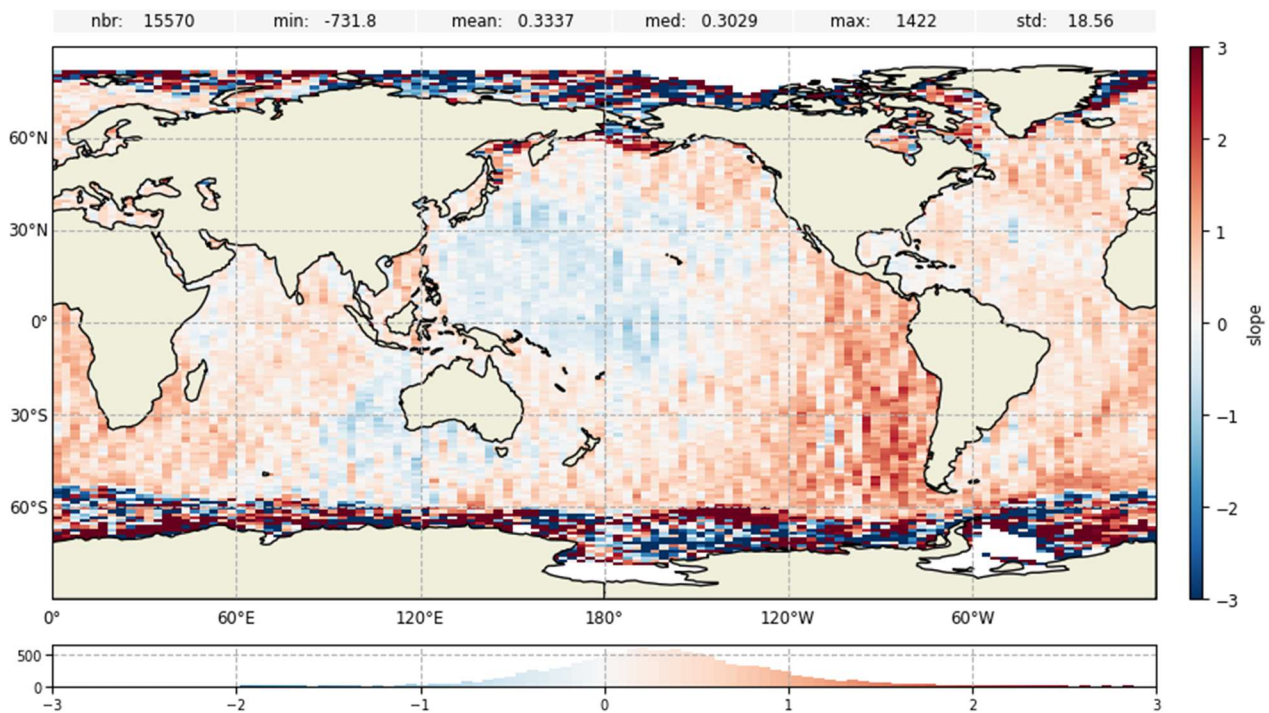


*Figure 4-17 : Regional trend of the evolution of uncertainties of ENVISAT data per geographical boxes (1°x3°) from cycle 22 to 113*

➔ **ERS-2**

## SWH UNCERTAINTY from ERS-2 5 Hz data - cycle 40

| nbr: 8100101 | min: 0 | mean: 0.3662 | med: 0.355 | max: 2.633 | std: 0.07489 |
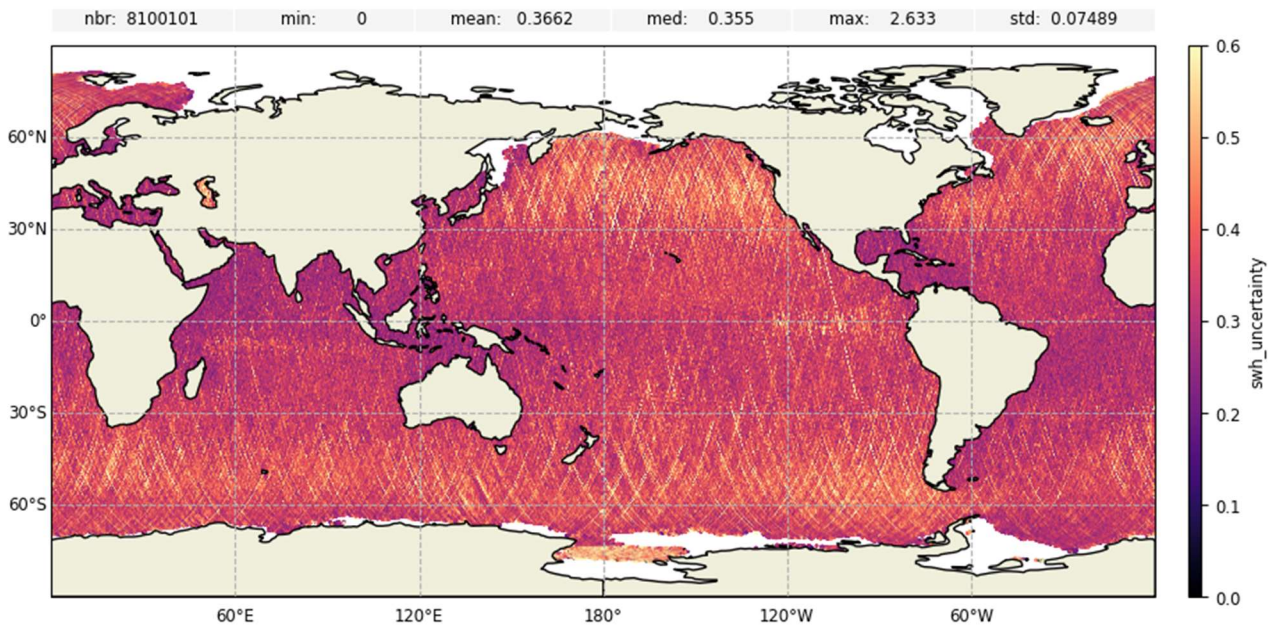


*Figure 4-18 : SWH Uncertainty field of 5 Hz ERS-2 data over cycle 40 (raw data)*

## Histogram of SWH UNCERTAINTY from ERS-2 5 Hz data - cycle 40
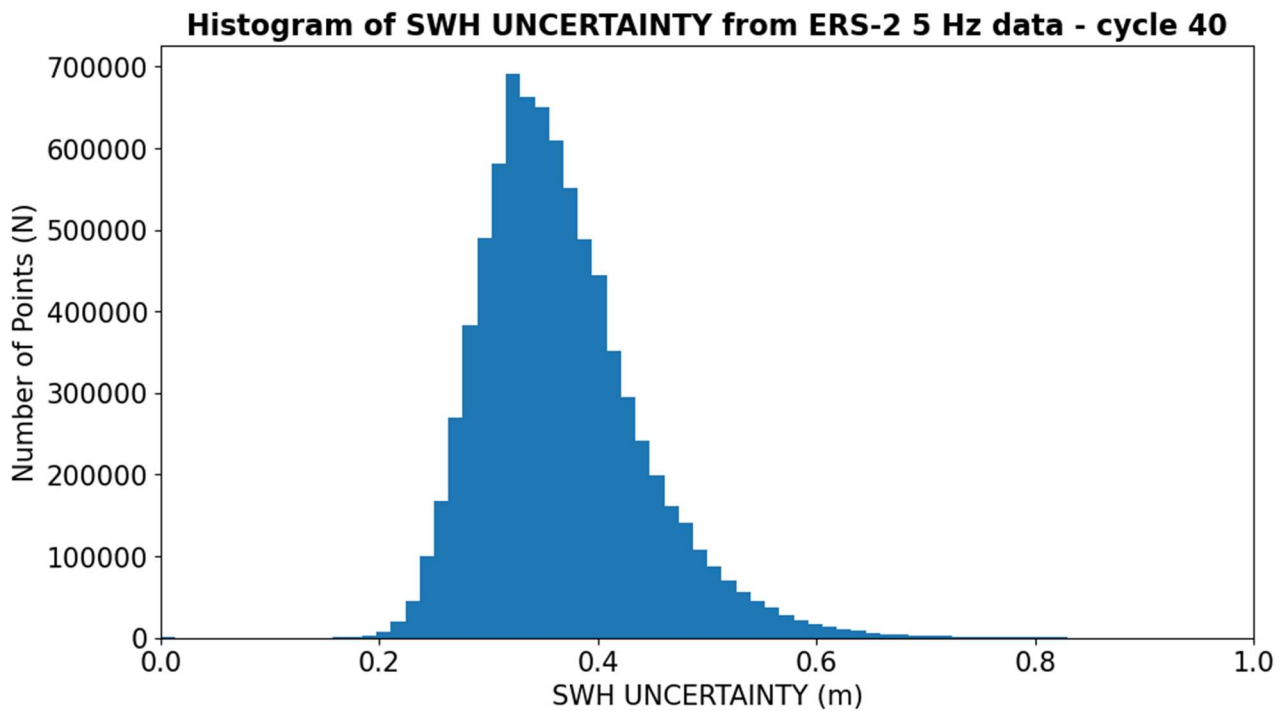


*Figure 4-19 : Histogram of SWH Uncertainty from 5 Hz ERS-2 data from cycle 40 (raw data)*

## MEAN OF SWH UNCERTAINTY from ERS-2 5 Hz data - cycle 1 to 85 (m)
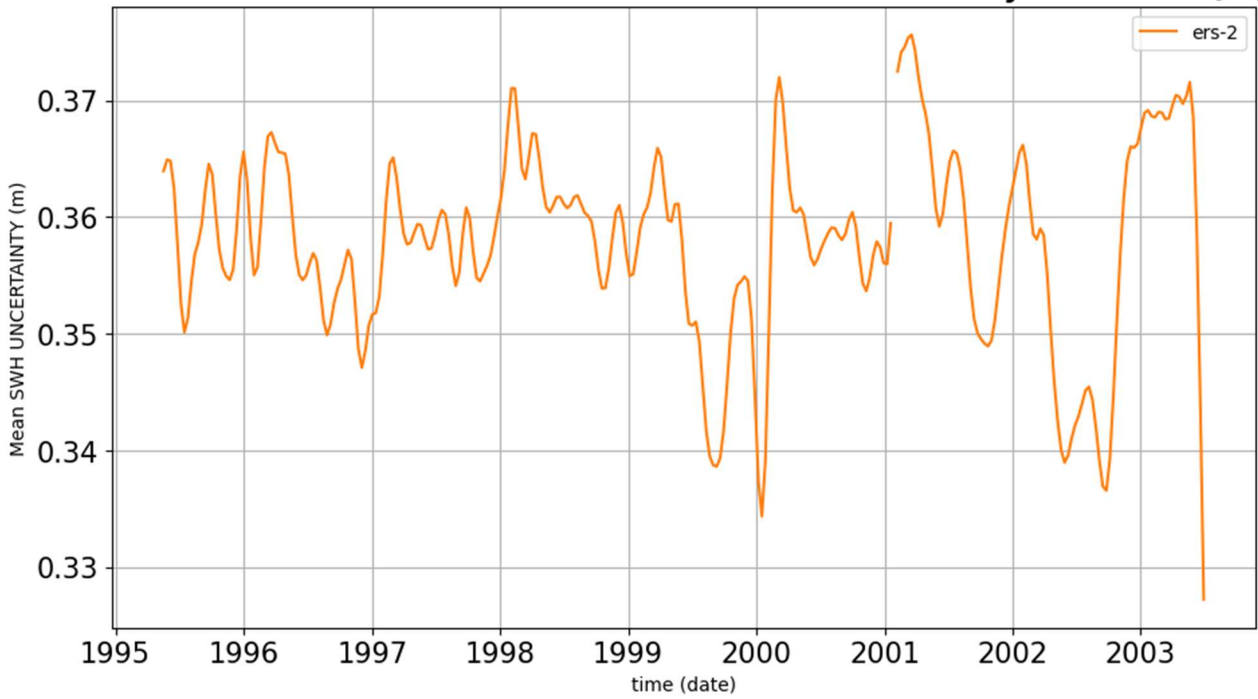


*Figure 4-20 : Long term monitoring of the SWH Uncertainty from ERS-2 5 Hz data (cycles 1 to 85)*

➔ **ERS-1**

## SWH UNCERTAINTY from ERS-1 5 Hz data - cycle 153
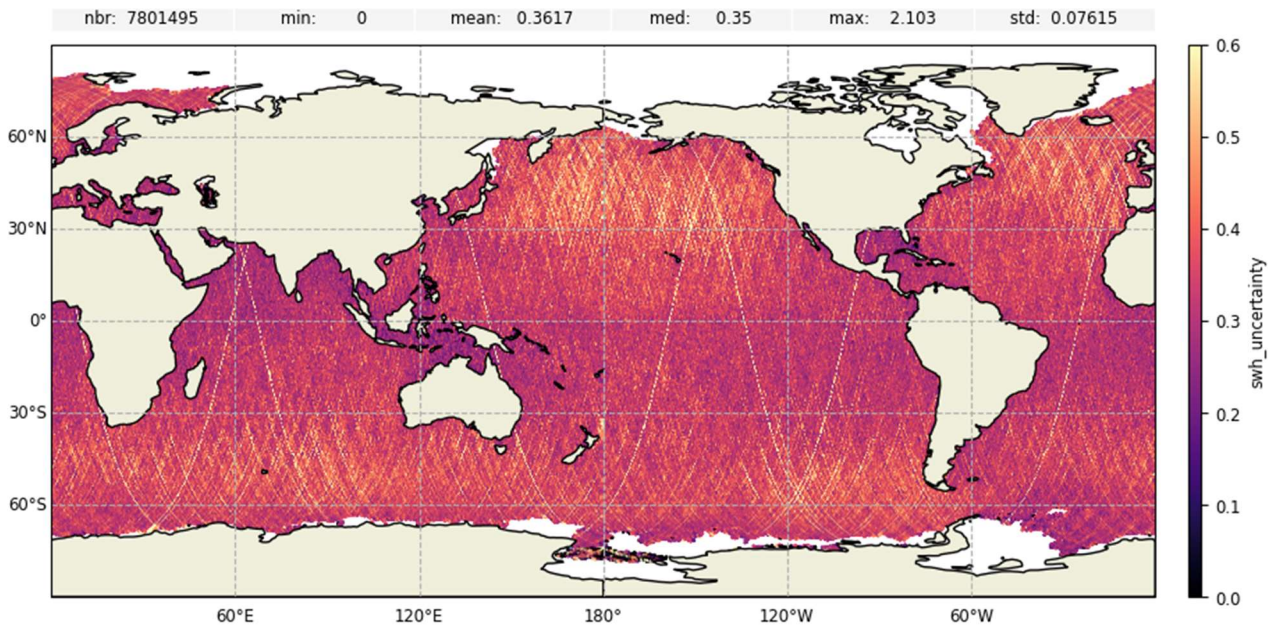


*Figure 4-21 : SWH Uncertainty field of 5 Hz ERS-1 data over cycle 153 (raw data)*
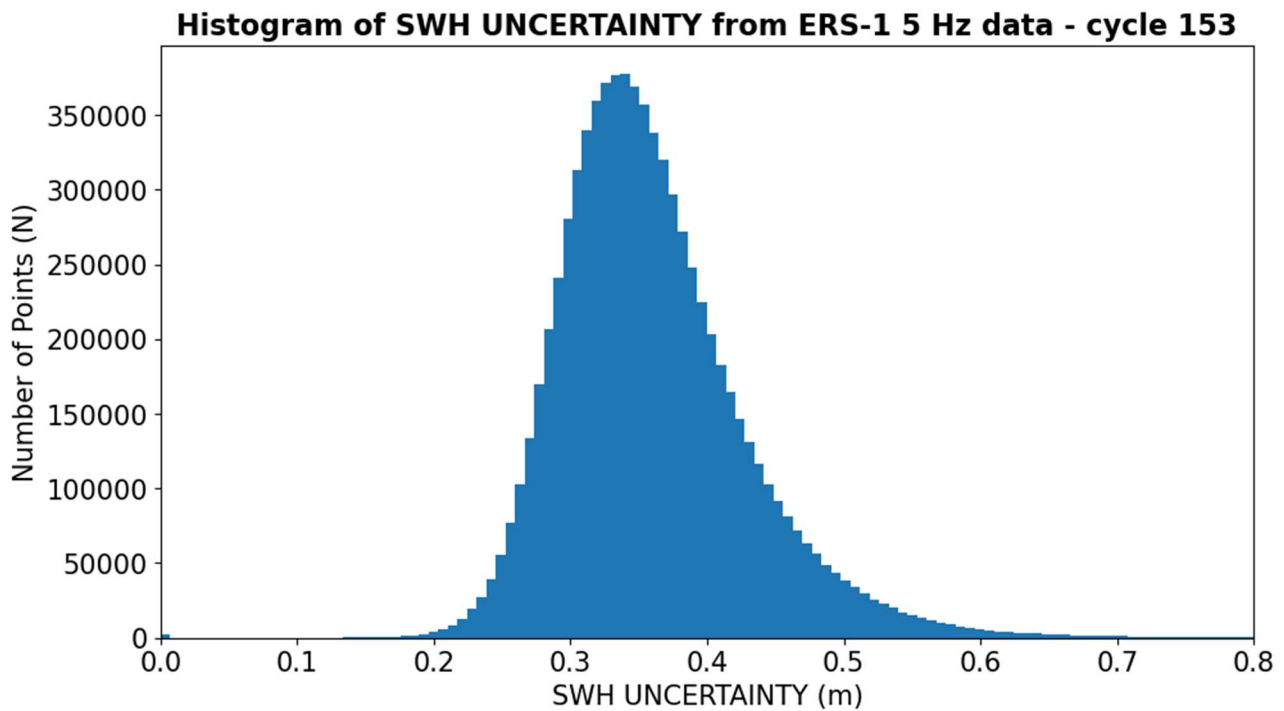
*Figure 4-22 : Histogram of SWH Uncertainty from 5 Hz ERS-1 data from cycle 153 (raw data)*
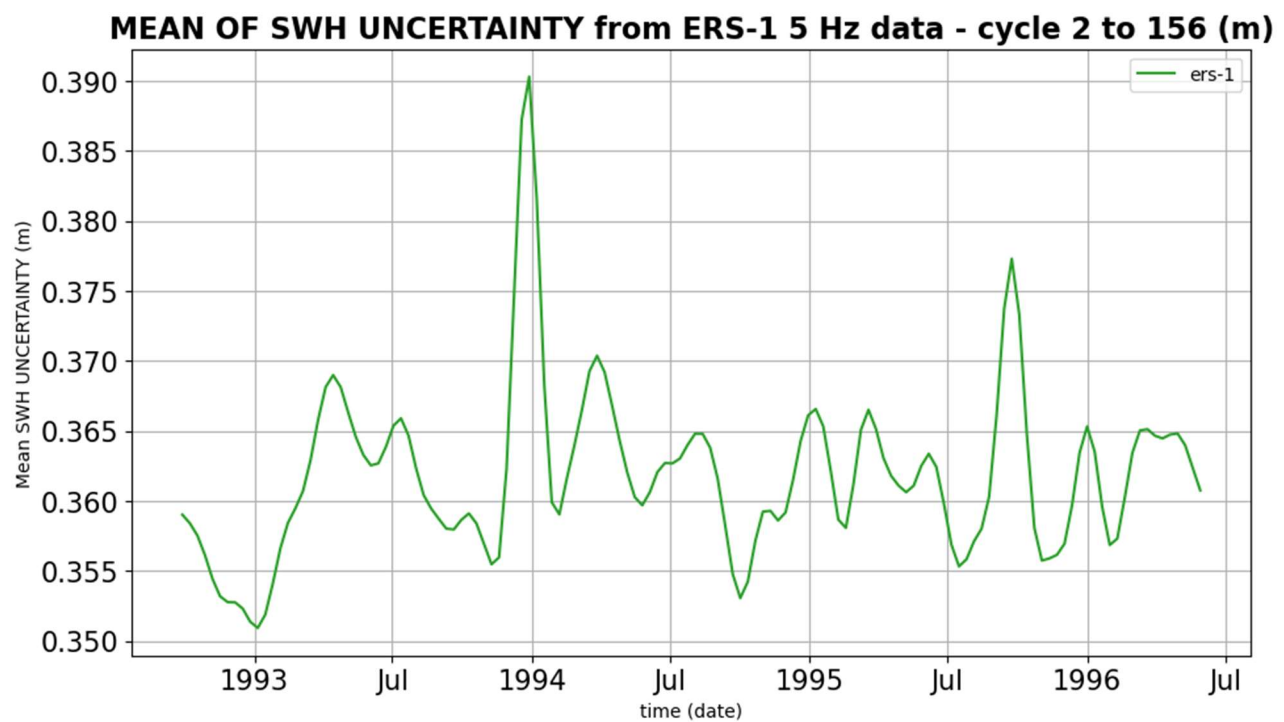


*Figure 4-23 : Long term monitoring of the SWH Uncertainty from ERS-1 5 Hz data (cycles 2 to 156)*

Long term monitoring associated with all three missions:
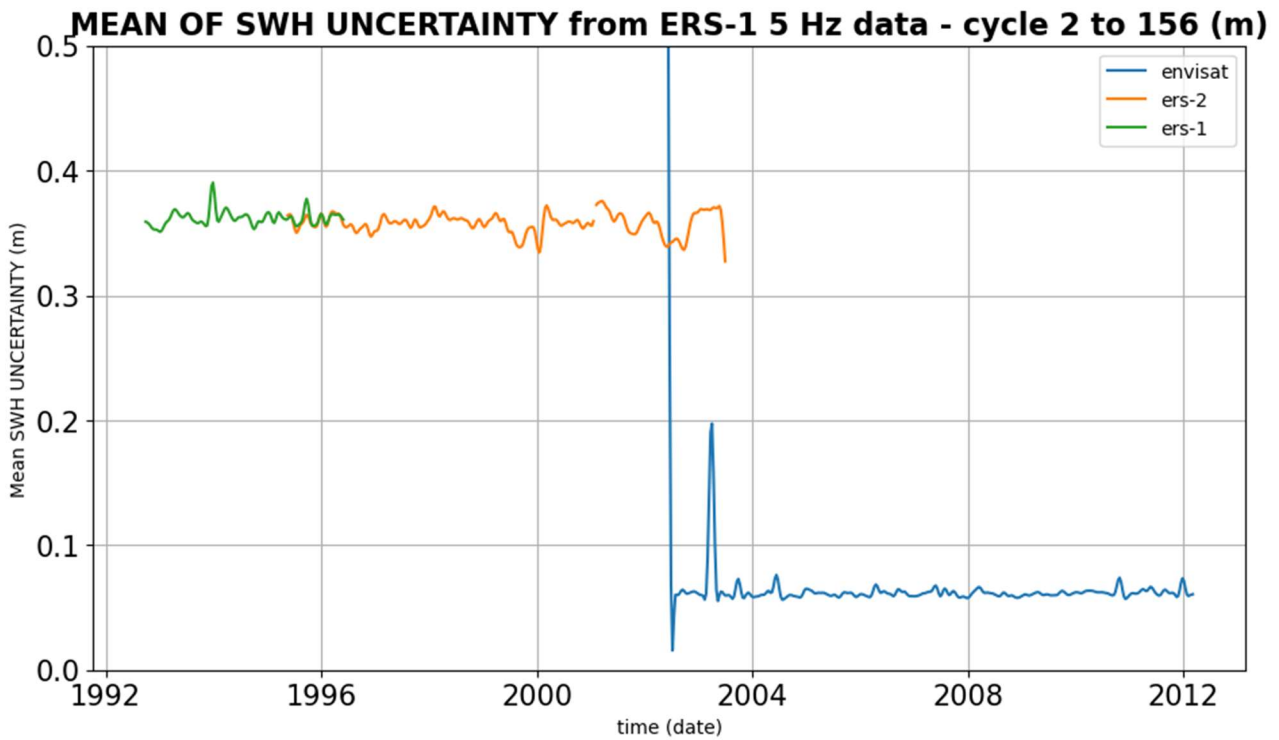
*Figure 4-24 : Long term monitoring of the SWH Uncertainty from all ENVISAT, ERS-2 and ERS-1 5 Hz data*

As shown in this last figure, uncertainties associated with SWH measures from ERS-1/2 are much higher than uncertainties associated with SWH measures from ENVISAT.

It is explained by the fact that this uncertainty contains the information of the speckle noise and the spectral bump at 10 km within the along track SWH signal.

For ENVISAT data, a numerical retracking (Adaptive) was used to compute geophysical parameters, and the resulting noise is lower than the one obtained with a MLE4 retracking. Moreover, a High Frequency Adjustment (HFA) processing was computed on data before the computation the EMD filter to obtain L3 products. This post processing reduces the speckle noise level of SWH data, and the spectral bump is the only component removed by the EMD filtering.

For ERS-1/2 data, the numerical retracking was not used and no HFA processing was computed. Thus, the speckle noise level is much higher than the one in ENVISAT data. This speckle noise level is so high that the EMD filter, dedicated to remove correlated along track errors, does not work as well as for ENVISAT data (see a residual spectral bump in the spectral analysis in the Product Validation Report [D-4-02]) (the separation of speckle random effect and correlated errors are more difficult to sort out).

The residual between filtered and non-filtered data contains more variability within ERS-1/2 data than within ENVISAT data. As the uncertainty associated with SWH data is defined by the variability of this residual in a 50 km window, it explains the great differences between uncertainties in ERS-1/2 and ENVISAT data.

## 4.4.3 Uncertainty provided

### 4.4.3.1 How uncertainty information is provided in the product

The uncertainty information is given as a field in each NetCDF file.

Each value of *swh_adjusted_filtered* has an associated uncertainty given in the field *swh_uncertainty* (more information can be found in FDR4ALT Products Requirements and Format Specifications [D-1-01]).

Here is an example of the header of a product:

short swh_uncertainty(time) ;

      swh_uncertainty:_FillValue = 32767s ;

      swh_uncertainty:long_name = "Uncertainty on top-of-Significant Wave Height" ;

      swh_uncertainty:units = "m" ;

      swh_uncertainty:scale_factor = 0.001 ;

      swh_uncertainty:add_offset = 0. ;

      swh_uncertainty:valid_min = 0s ;

      swh_uncertainty:valid_max = 32767s ;

      swh_uncertainty:coordinates = "longitude latitude" ;

      swh_uncertainty:comments = "This uncertainty is based on the residual between the filtered and the non-filtered signal." ;

### 4.4.3.2 How the uncertainty information should be used

These uncertainties should be used as an uncertainty bar on the filtered swh field (swh_adjusted_filtered) only.

### 4.4.3.3 Roadmap for further uncertainty analysis

To provide a more precise uncertainty field, it could be interesting not to limit the computation at the standard deviation of a moving window, but to use the Student law.

This way, it would be necessary to evaluate the number of independent measures in the considered moving window.

If a number N of independent measures is to be computed in a moving along track window, the new uncertainty would be given by a new formula obtained with the Student law:

$$uncertainty = k * \frac{STD}{\sqrt{N-1}}$$

Where k is a factor depending on the number N of independent measures and the confidence level wanted (typically 90%). This number of independent along track measure could be a subject to study on its own and this study was not carried out during this project.

This method would give a more precise idea of the real uncertainty associated to wave groups structures with the same idea of comparison between filtered and non-filtered data.

A second source of uncertainty that could be considered is the uncertainty associated with the calibration between mission. A possible approach would be to use the dispersion of the delta of SWH between missions at crossover points and apply the Student Law to this distribution to obtain a 90% confidence level interval.

Unfortunately, it was not possible to take the time to evaluate this number N of independent measures in the frame of this project, but it could be interesting to do so.

## 4.4.4 Reference documents

| RD 15 | https://www.frontiersin.org/articles/10.3389/fmars.2019.00124/full |
|---|---|
| RD 16 | De Carlo Marine, Fabrice Ardhuin, Annabelle Ollivier, et al. Wave groups and small scale variability of wave heights observed by altimeters. Authorea. February 27, 2023. |
| RD 17 | FDR4ALT: Product Requirements & Format Specifications |
| RD 18 | Queffeulou P. and Croizé-Fillon D. (2017): Global Altimeter SWH Data Set, version 11.4, February 2017. Technical report Ifremer. ftp://ftp.ifremer.fr/ifremer/cersat/products/swath/altimeters/waves/documentation/altimeter_wave_merge__11.4.pdf |
| RD 19 | Quilfen, Y. and Chapron, B.: On denoising satellite altimeter measurements for high-resolution geophysical signal analysis, Adv. Space Res., https://doi.org/10.1016/j.asr.2020.01.005, online first, 2020 |

## 4.5  Inland Water Thematic Data Products

### 4.5.1 Overview of the uncertainty analysis

The uncertainty for inland water targets is based on a bottom-up approach. The uncertainties of the Inland Water Thematic Data Product (IW TDP) are estimated by summing all uncertainties from each component of water surface height: atmospheric and geophysical corrections and orbit-range component.

The measurement function used for inland water level estimation is very similar to the function for open ocean except that there are no corrections for ocean tide, load tide or sea state bias as they are either non-existent or negligible in inland waters:

$$\text{Water Height} = (\text{Orbit} - \text{Range}) - (\text{DTC} + \text{WTC} + \text{IC} + \text{ET} + \text{PT})$$

*Equation 1*

where, the terms are:

Orbit          Orbital altitude of the satellite with respect to the ellipsoid
Range          Retracked Range (retracker dependant)
DTC            Dry Tropospheric Correction
WTC            Wet Tropospheric Correction
IC             Ionospheric Correction
ET             Earth Tide
PT             Pole Tide

### 4.5.2 Uncertainty evaluation

For inland water products it is not suitable to use the MWR to provide the tropospheric corrections as these products are mainly intended for open-ocean studies [**RD 20**]. In particular, the WTC is affected by land contamination in the radiometer and can be used only in the central parts of large lakes. Instead, it is preferable to use corrections that come from a model.  Thus, the uncertainties of these corrections are based on values reported in the literature.

However, the most significant source of uncertainty for the water height estimation over inland waters is given by the (orbit-range) component. The reason of estimating the uncertainty of the component (orbit-range) instead of making a separate calculation, is the implementation of an empirical method, described in 4.5.2.2, under the hypothesis that that the value of this component for consecutive measurements in time must be substantially equivalent because the satellite observes the same inland water target. . Atmospheric corrections uncertainties

Dry and wet tropospheric corrections come from ERA Interim model [**RD 21**], a global atmospheric reanalysis that is available from January 1979 to August 2019. The dry tropospheric correction depends on the atmospheric pressure at the target surface height above geoid and the latitude ([**RD 22**], [**RD 23**],[). The wet tropospheric correction depends on the presence of water in the atmosphere and its absolute value is less than 50 cm.

The dry tropospheric correction (DTC) needs to be applied to the ranges in order to account for the delay in propagation through the atmosphere. The ERA Interim reanalysis product, provided at 1.5° longitude and latitude, allows the estimation of the hydrostatic component of the tropospheric delay with an accuracy of 1 mm to 3 mm at the global scale, provided an adequate model for the height dependence of atmospheric pressure ([**RD 23**],[**RD 24**]). Concerning the wet tropospheric correction, [**RD 25**] has shown that the accuracy of the model over inland waters is about 3 cm.

The GIM model [**RD 26**], used for the ionospheric correction is generated on a daily basis at CODE using data from about 400 GPS/GLONASS sites of the IGS and other institutions. The average error of this model is about 2 cm over inland water [**RD 25**]). Before 1998, in ERS1 and ERS2 data, the NIC09 [**RD 27**] model is used. The RMS difference between the climatology and the GIM maps is about 0.57 cm path delay on Ku band altimeters [**RD 28**]. It can be assumed that the uncertainty is very similar in both models.

## 4.5.2.1 Tides

The corrections from earth and pole tides, as for the atmospheric corrections, are based on models as described in section 4.5.2. In the absence of inland water specific uncertainties values, the ocean uncertainty values are used: 3 mm [**RD 29**], [**RD 30**]).

## 4.5.2.2 Retracker

The (orbit – range) uncertainty was estimated empirically. As indicated previously, consecutive measurements estimate water surface height in the same target and the values should be similar. We estimated as the median (less impacted by outliers that he mean) of the difference between consecutive points per cycle belonging to a certain group depending on the waveform classification and the surface type. The surface type is based on the Global Lakes and Wetlands Database (GLWD3) as indicated in Table 4-5:

The choice of a cycle estimate is motivated by the fact that, on the one hand, it includes targets with different land surroundings, size and shape and, on the other hand, it also takes into account the impact of the season on terrestrial targets, as the presence of ice or snow affects the signal reflected from the target. For this last reason, there is also a separation between water bodies at high latitudes (40 degrees north limit) and targets south of this limit that are less impacted by the seasons.

A limitation of this method, especially for rivers, is that it is only based on measurements over wide rivers, with at least two measurements per satellite pass, and it does not consider the slope between the two measurements.

| GLWD3 cell value | Surface type |
|---|---|
| 1, 2 | Lake/Reservoir |
| 3 | River |
| 4 | Floodplain |
| 10, 11 | Wetlands (50-100% and 25-50%) |
| 5,6,7,8,9, 12 | Others: Swamp forest, Coastal wetland, Saline Wetland, Bog, Intermittent Wetland/Lake, wetland (0-25%) |

*Table 4-5 : Surface types based on GLWD3.*

The waveforms reflected by inland water bodies are very different depending on the target: ocean like for big lakes or very peaky for narrow rivers. Moreover, the waveforms can be contaminated by the land surrounding the water body. To account for this, the different values were first grouped by the waveform class, separated in 3 groups, following the type of the waveform representing the backscatter from the water body (Figure 4-25). The first group contains the waveforms classes clearly identified as the backscatter from one water body (lake, reservoir, river, ...) The second group contains waveform classes that may be contaminated by some land surroundings, but it is very probable that the signal comes from an off nadir hydrological target. In the last group, the classes show clearly a contaminated backscatter, and these measurements cannot be trusted. For example, in the case multi-peak waveforms (Waveform class 3), it is impossible to determine the peak corresponding to the off-nadir target. Therefore, the quality flag (good, medium, or bad) is associated with groups 1, 2 or 3.
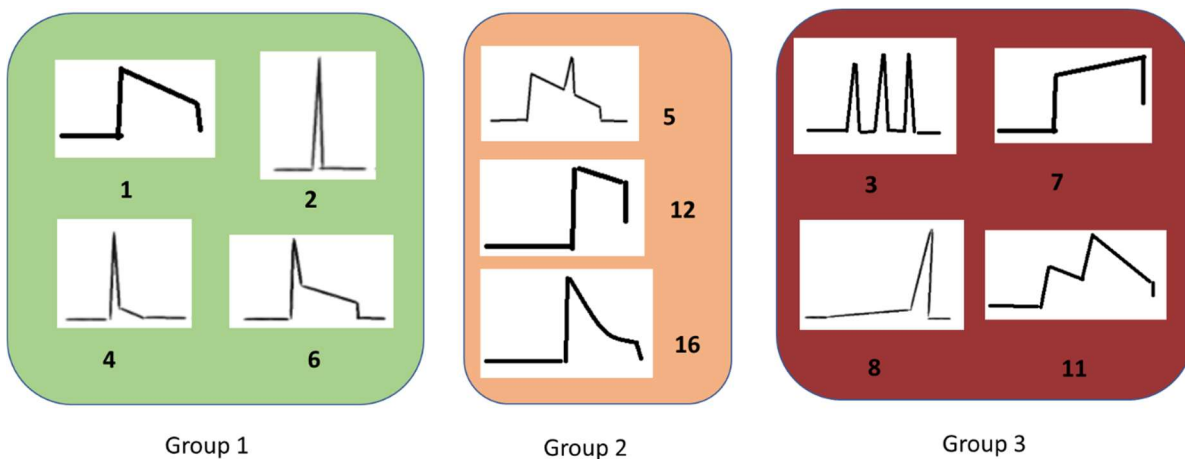


*Figure 4-25. Groups as a function of the waveform classification*

In addition, the uncertainty observed for targets located at high latitudes is highly dependent on the season. Indeed, measurements made during winter are strongly affected by the presence of ice and snow. A differentiation has also been taken into account for measurements above 40 degrees north.

## 4.5.3 Uncertainty provided

### 4.5.3.1 How uncertainty information is provided in the product

The uncertainty, provided along track in the inland water products, is given by the quadratic sum of the uncertainties from each component of water surface height. Table 4-6 lists the uncertainty values for the atmospheric and geophysical corrections as discussed in previous sections.

*Table 4-6. Geophysical uncertainties for inland water*

| Correction | Uncertainty (cm) |
|---|---|
| DTC | 0.3 |
| WTC | 3 |
| IC | 2 |
| ET | 0.3 |
| PT | 0.3 |

Concerning the (orbit-range) component, the estimation was performed per surface (lake, river, wetland, floodplain and other surfaces), per quality flag (good, medium, bad) and for high/low latitudes. The evolution of the uncertainties in centimetres over cycles and surfaces is shown in Figure 4-26 to Figure 4-30 where the impact of the seasons is clearly visible in high latitudes. Those values correspond to ice1, the retracker selected after the round robin process.
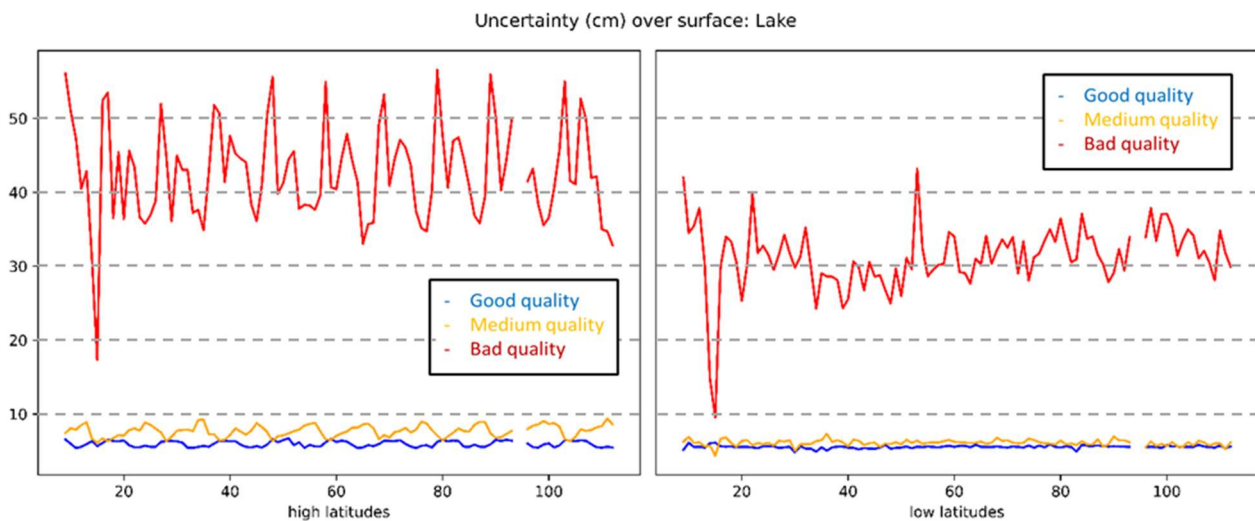


*Figure 4-26. (Orbit-Range) uncertainty per cycle over lakes and reservoirs.  Left: North of 40 degrees. Right. South of 40 degrees. Blue: good quality measurements, yellow: medium quality measurements and red: bad quality measurements.*
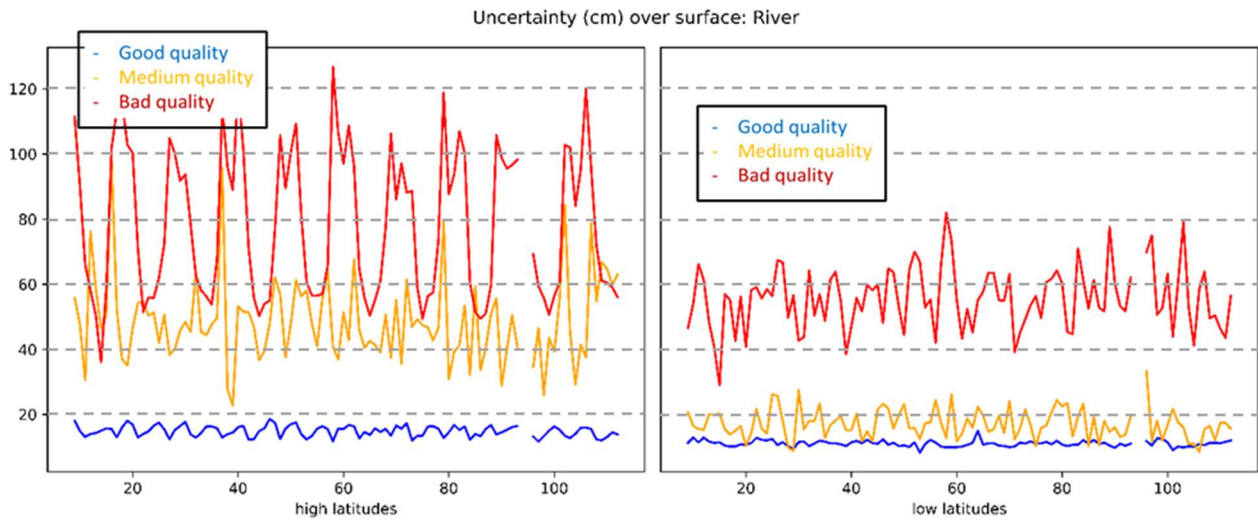
*Figure 4-27. (Orbit-Range) uncertainty per cycle over rivers. Left: North of 40 degrees. Right. South of 40 degrees. Blue: good quality measurements, yellow: medium quality measurements and red: bad quality measurements.*
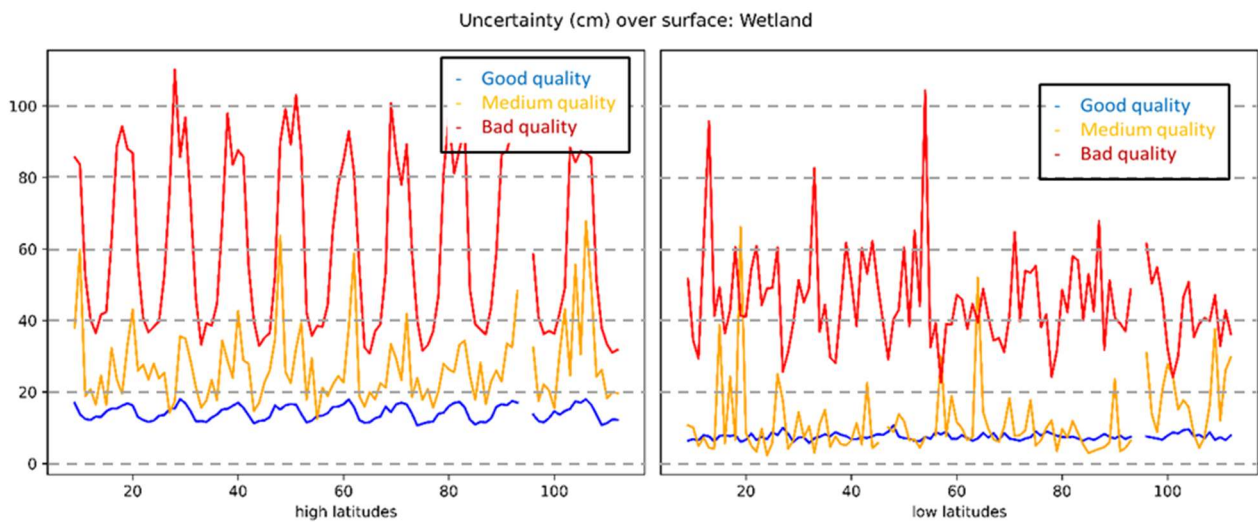


*Figure 4-28. (Orbit-Range) uncertainty per cycle over wetlands. Left: North of 40 degrees. Right. South of 40 degrees. Blue: good quality measurements, yellow: medium quality measurements and red: bad quality measurements. An outlier on cycle 55 was detected due to the small number of measurements available for the estimation (9 measurements).*
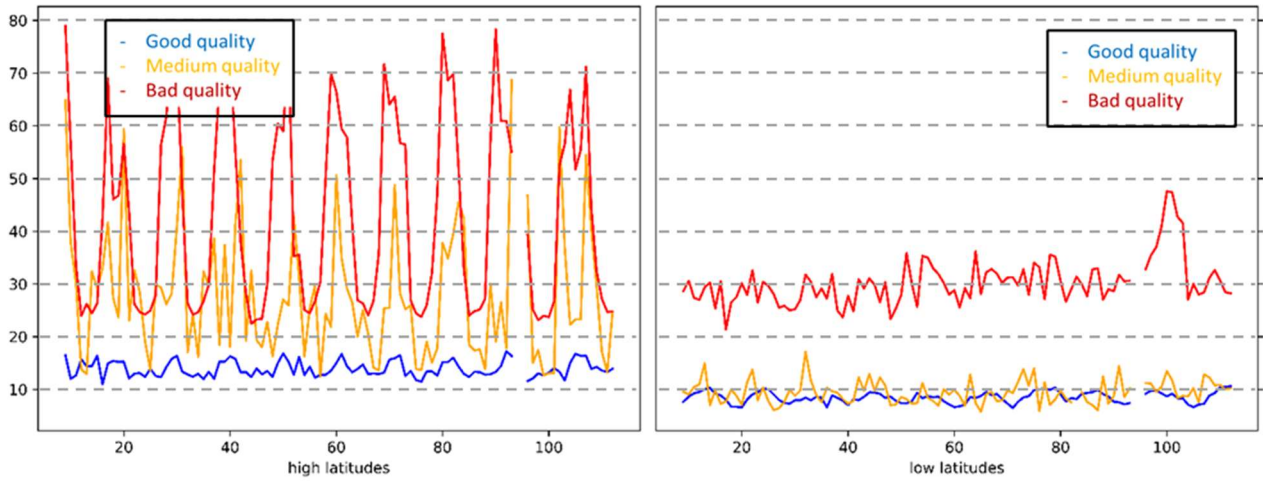
Figure 4-29 . (Orbit-Range) uncertainty per cycle over floodplains.  Left: North of 40 degrees. Right. South of 40 degrees. Blue: good quality measurements, yellow: medium quality measurements and red: bad quality measurements.
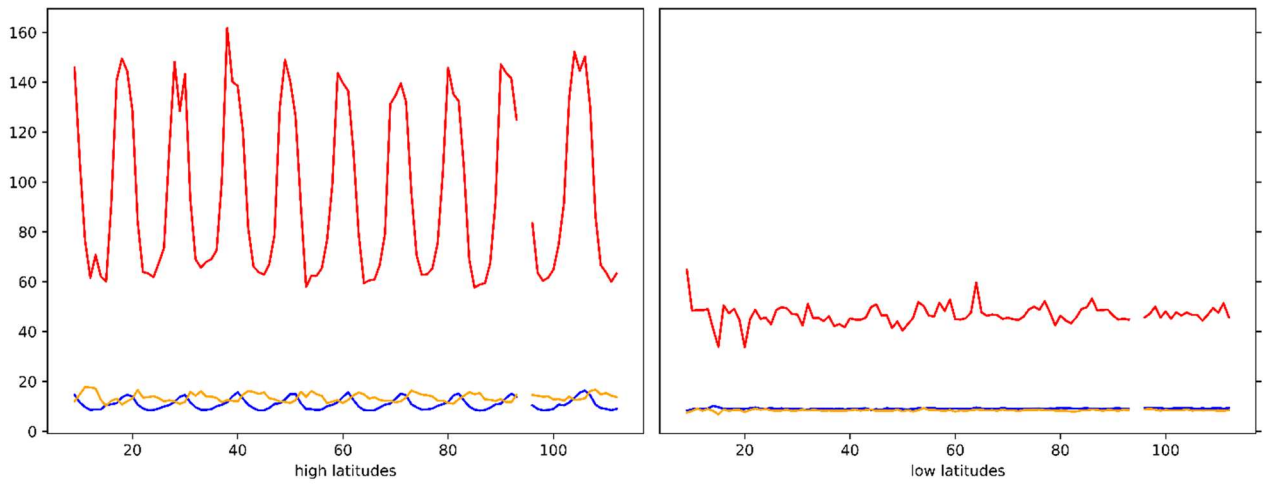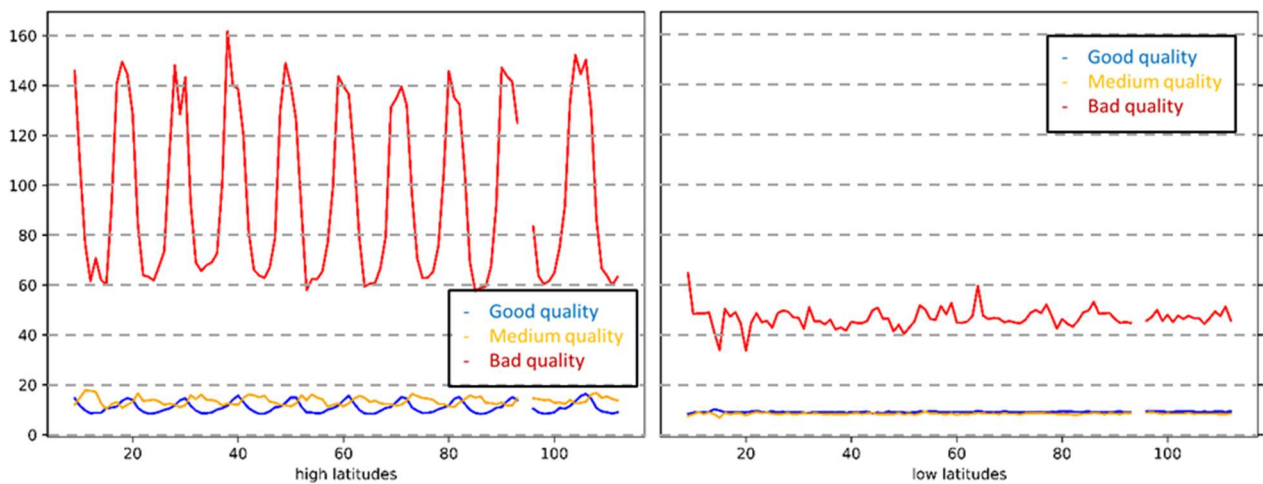
*Figure 4-30 . (Orbit-Range) uncertainty per cycle over other surfaces.  Left: North of 40 degrees. Right. South of 40 degrees. Blue: good quality measurements, yellow: medium quality measurements and red: bad quality measurements.*

## 4.5.3.2 How the uncertainty information should be used

The uncertainties values are the uncertainties associated with individual measurements of the water surface height values. As the uncertainty is estimated based on statistical methods, it is highly dependent on the number of measurements available (and used) per cycle/surface/quality flag. They reflect an overall performance of the mission, but they may be too coarse for a very local analysis.

## 4.5.3.3 Roadmap for further uncertainty analysis

The uncertainty is provided at Level 2.  The interpretation of those values at different spatial scales, for example to estimate the value along a transect over the same surface, needs further analysis.

## 4.5.4 Reference documents

| RD 20 | Lazaro, C., M.J. Fernandes, A.L. Nunes, N. Pires , Contributions to the improvement of the wet tropospheric corrections for SARAL/AltiKa, New frontiers of altimetry – AltiKa Workshop, 28-31 October 2014, Konstanz, Germany, 2014 |
|---|---|
| RD 21 | Berrisford, P, Dee, DP, Poli, P, Brugge, R, Fielding, M, Fuentes, M, Kållberg, PW, Kobayashi, S, Uppala, S, Simmons, A. The ERA-Interim archive Version 2.0, 2011 |
| RD 22 | Saastamoinen, J. Atmospheric correction for the troposphere and stratosphere in radio ranginf of satellites. In Geophys. Monogr. 15, Washington, DC: American Geophysical Union, 1972 |
| RD 23 | Fernandes, M. J.; Lázaro, Clara; Nunes, Alexandra L.; Scharroo, Remko. 2014. "Atmospheric Corrections for Altimetry Studies over Inland Water" Remote Sens. 6, no. 6: 4952-4997. https://doi.org/10.3390/rs6064952 |
| RD 24 | Crétaux, JF., Calmant, S., Romanovski, V. et al. An absolute calibration site for radar altimeters in the continental domain: Lake Issykkul in Central Asia. J Geod 83, 723–735 (2009). https://doi.org/10.1007/s00190-008-0289-7 |
| RD 25 | Birkett, C.M. and Beckley, B. (2010) Investigating the Performance of the Jason-2/ OSTM Radar Altimeter over Lakes and Reservoirs. Marine Geodesy, 33, 204-238. https://doi.org/10.1080/01490419.2010.488983 |
| RD 26 | Y. Béniguel, "Global ionospheric propagation model (GIM): A propagation model for scintillations of transmitted signals," in *Radio Science*, vol. 37, no. 3, pp. 1-14, June 2002, doi: 10.1029/2000RS002393 |
| RD 27 | Schmidt, A. R.: Analysis of stage-discharge relations for open channel flow and their associated uncertainties, Urbana, University of Illinois, 328 pp., 2002. |
| RD 28 | Scharroo, R., and W. H. F. Smith (2010), A global positioning system–based climatology for the total electron content in the ionosphere, J. Geophys. Res., 115, A10318, doi:10.1029/2009JA014719. |
| RD 29 | Desai, S., Wahr, J. & Beckley, B. Revisiting the pole tide for and from satellite altimetry. *J Geod* **89**, 1233–1243 (2015). https://doi.org/10.1007/s00190-015-0848-7 |
| RD 30 | D. E. Cartwright, Anne C. Edden. Corrected Tables of Tidal Harmonics. Geophysical Journal of the Royal Astronomical Society https://doi.org/10.1111/j.1365-246X.1973.tb03420x |

# 4.6 Atmosphere Thematic Data Products

## 4.6.1 ANN retrieval (main product)

### 4.6.1.1 Overview of the uncertainty analysis

An artificial Neural Network is a nonlinear mapping used to map a set of input variables $x=(x1,...x_{Ni})$ to set of output variables yj, provided a set of targets $t_j (j = 1..No)$. Such processors are organised in layers (Figure 4.31): the first layer is the input layer, the last layer is called the output layer, intermediate layers are the hidden layers.

For the retrieval of geophysical parameters, a very simple Multilayer Perceptron is used: only one hidden layer is considered with 8 or 12 neurons.
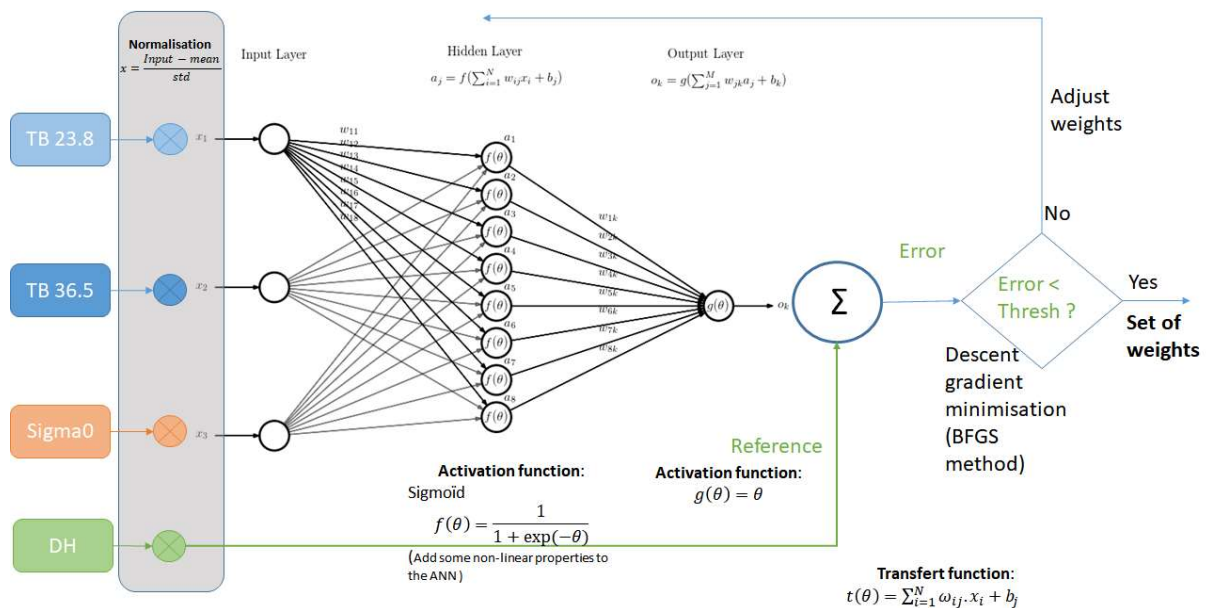


*Figure 4.31: Neural Network architecture. Parameters of the ANN are estimated by descent gradient minimisation of a loss function. For the hidden layer, the activation function is a sigmoid, and the identity function for the output layer.*

Neural networks have been used for a long time now to retrieve geophysical quantities. They have proven to be reliable techniques, even preferable in some cases to variational retrievals. However, the uncertainty estimation is not as straightforward as for variational retrievals. It is not often implemented in spatial observation retrievals as there exist very few comparative studies of confidence estimation techniques relevant to neural networks in the literature. [**RD-31**] has developed a procedure to compute uncertainties associated with the outputs by treating the sources of errors independently. The study presented in their paper is quite similar to our study. They are using a neural network to retrieve water vapor and liquid water path from MWR and G-band vapor radiometer. The training data set consists of brightness temperature simulated with a forward radiative transfer model and radiosonde profiles.

The authors estimate that the methodology might slightly underestimate some of the uncertainties, but the estimated values were in good agreement with the physical algorithm used for comparison. They partially follow [**RD-32**] and assume that the total retrieval variance $u^2(T)$ for the target parameter T is the sum of

three independent variances: the data target variance $u(t)^2$, the model variance $u(m)^2$, and the instrument noise $u(N)^2$.

The data target variance is the largest contributor. It includes radiative transfer model uncertainties.

Model uncertainties represent the errors associated with the determination of the optimal weights. This contributor was found out to be a small part of the overall error. It is estimated by computing the covariance matrix of the weights.

The instrument noise error is estimated by perturbing the input measurements and computing the resulting change in the network output.

## 4.6.1.2 Uncertainty evaluation

Uncertainties for ANN retrieval is not provided in the FDR4ALT product. During this study, a lot of work has been done on the FDR: the L1B processing has been improved but also the brightness temperatures uncertainties have been estimated for the first time for ERS and ENVISAT missions. Unfortunately, we did not have the time to pursue the effort up to the Level 2.

## 4.6.1.3 Uncertainty provided

### 4.6.1.3.1 How uncertainty information is provided in the product
Uncertainties for ANN retrieval is not provided in the FDR4ALT product.

### 4.6.1.3.2 How the uncertainty information should be used
Uncertainties for ANN retrieval is not provided in the FDR4ALT product.

### 4.6.1.3.3 Roadmap for further uncertainty analysis
The roadmap is obviously to pursue the work on ANN uncertainties estimation started in the FDR4ALT project, using as inputs the uncertainties estimated for the FDR.

There are also some interesting analyses to be performed by comparing ANN and 1DVAR uncertainties. 1DVAR uncertainties estimation being more mature than ANN, it will be very informative.

### 4.6.1.3.4 Reference documents

| RD-31 | M. P. Cadeddu, D. D. Turner, and J. C. Liljegren, "A neural network for real-time retrievals of PWV and LWP from arctic millimeter-wave ground-based observations," IEEE Trans. Geosci. Remote Sens., vol. 47, no. 7, pp. 1887–1900, 2009. |
|-------|------------------------------------------------------------------------------------------------------------------------|
| RD-32 | G. Papadopoulos, P. J. Edwards, and A. F. Murray, "Confidence Estimation Methods for Neural Networks," ESANN'2000 - Eur. Symp. Artif. Neural Networks, pp. 75–80, 2000. |

# 4.6.2 1DVAR retrieval (expert group)

## 4.6.2.1 Overview of the uncertainty analysis

The Atmospheric TDPs produced in the context of the FDR4ALT project comprise *Total Column Water Vapour* (TCWV), *Cloud Liquid Water Path* (LWP), and *Wet Tropospheric Correction* (WTC), and are retrieved from Microwave Radiometer (MWR) observations on-board ERS-1, ERS-2, and ENVISAT.

The underlying retrieval follows an optimal estimation 1D-VAR retrieval strategy [**RD-33**] [**RD-34**]. The 1D-VAR retrieval used herein combines an iterative approach to calculate the optimal estimate of TCWV and LWP, given the observed brightness temperatures and other information, as specified and discussed below. Speaking in general terms, 1D-VAR finds an optimal solution for a vector of variables, **x**, termed "state

vector", given the observations, **y**, and a set of other parameters that describe (amongst other things) the prior knowledge of the state of the parameters before the observations are incorporated. This prior knowledge is broadly termed "background knowledge", or "*a priori*" knowledge [**RD-33**].

One of the advantages of the 1D-VAR approach is that it explicitly distinguishes between different types of other input data, depending on their role in the retrieval process. This sets 1D-VAR approaches apart from other methods such as statistical inversion and provides (in principle) better control over how input is handled, and more insights into the behaviour of the system and its uncertainty characteristics.

Generally, uncertainties associated with the retrieval of the atmospheric TDPs (*i.e.*, uncertainties associated with **x**) result from three different types of uncertainty:

- Uncertainties associated with the observations **y**, for example due to calibration uncertainties or noise,
- Uncertainties associated with the ancillary background data **b** required for the retrieval,
- Uncertainties associated with the simplifications of the implemented forward model *h*.

Some further remarks on the current implementation of the retrieval scheme:

- Observations are assumed uncorrelated; therefore, only the diagonal elements of the uncertainty covariance matrix differ from zero. <u>These assumptions could potentially be extended if inter-channel error correlations</u> are known.
- "Reasonable" uncertainties for the individual brightness temperature observations are assumed (e.g., u(TB) = 1 K). See discussion further down regarding contributions to the observational uncertainties.
- The uncertainty correlations of the background data are captured in the uncertainty covariance matrix (see **RD-33**) and applied in a Bayesian approach.

In practical applications, a number of noise sources are typically not known well enough to describe the retrieval uncertainty in sufficient detail. Independent validation is therefore key to understand retrieval quality.

## 4.6.2.2 Uncertainty evaluation

The real-world relations between observations and the state of the observed system be characterized as follows:

$$\mathbf{y} = h^*(\mathbf{x}^*) + \mathbf{e_y}$$

| | | |
|---|---|---|
| **y** | : | Observations |
| $\mathbf{x}^*$ | : | Full, true state of the observed system in real world |
| $h^*(\mathbf{x}^*)$ | : | True relation between observations and system in real world |
| $\mathbf{e_y}$ | : | Sensor noise |

(1)

For any retrieval, the above Equation must be approximated by:

$$\mathbf{y} = h(\mathbf{x}, \mathbf{b})$$

    **y**     :   Observations

    **x**     :   State vector (variables to be retrieved from **y**)     (2)

    **b**     :   Variables not retrieved, but influencing forward model

    $h(\mathbf{x}, \mathbf{b})$   :   Forward model

At the most fundamental level, a 1D-VAR retrieval thus works by inverting Equation (2) under appropriate constraints:

$$\hat{\mathbf{x}} = h^{-1}(\mathbf{y}, \mathbf{b})$$

    $\hat{\mathbf{x}}$   :   Estimate of $\mathbf{x}$, given $\mathbf{y}$ and $\mathbf{b}$     (3)

The vector **b** is of crucial importance. It contains components of the observed system that affect **y** but are not directly retrieved. For example, in the context of WTC retrievals the vector **b** could include sea surface temperature and wind speed, amongst others.

The estimates of **b** must come from some source other than the observations and will inevitably also be associated with uncertainties. For example, a certain estimate of surface wind speed e.g., from altimeter or from a numerical weather prediction model will not be perfectly accurate. Rather it will have its own associated uncertainty. We therefore define another uncertainty matrix **F** that encompasses all uncertainties associated with **b** together with their covariances, expressed in kelvin. The term **F** can be arbitrarily complicated and often entails significant cross-correlations between different variables.

Defining the matrix **E** = *diag (e$_y$)*, where **e$_y$** represents sensor noise and other sensor related error sources such as calibration uncertainty or temporal stability, the derivation of Equation (3) and uncertainty propagation yields straight forward estimates of the *a-posteriori* uncertainty for the retrieved state:

$$\mathbf{E}_p = \left( \mathbf{K}(\mathbf{E}+\mathbf{F})^{-1}\mathbf{K}^{\mathsf{T}} \right)^{-1}$$

    (4)

    $K_{i,j}$   :   $\dfrac{\partial h_i(\mathbf{x}, \mathbf{b})}{\partial x_j}$

Here, the **K**-matrix is the Jacobian of *h*, holding the derivates of *h* with respect to **x**, while **E** and **F** represent instrumental uncertainties and representativeness uncertainties, respectively. The diagonal elements of the *a posteriori* uncertainty covariance matrix **E$_p$** hold the uncertainty of the retrieved variables $\hat{x}$. We note here that the *a posteriori* uncertainty can be reduced by properly including background knowledge and associated background uncertainty covariances if optimal estimation methods such as 1D-VAR are used [**RD-34**]. This, however, comes at the cost of including background information in the retrieval, which is not desirable in all instances. In any case, WTC retrievals are heavily constrained by the observations alone and therefore, the inclusion of background data affects the retrieval only weakly [**RD-35**]*.

The above formulation however highlights the important point that beyond sensor noise, other parameters also affect the retrieval.

## 4.6.2.3 Uncertainty provided

### 4.6.2.3.1   How uncertainty information is provided in the product

Uncertainties of primary retrieved quantities (TCWV, LWP) are derived using optimal estimation [**RD-33**, **RD-34**, **RD-35**].

Uncertainties of parameters calculated from primary retrieved parameters (WTC, attenuation) are derived using uncertainty propagation.

Uncertainties are provided for each Atmospheric TDP through a single value for each single observation. The following fields are provided:

*Table 4-7: Uncertainties provided for 1DVAR-retrieved atmospheric parameters.*

| Variable name in NetCDF file | Description | Units |
|---|---|---|
| **rad_water_vapor_uncertainty_1DVAR** | A posteriori uncertainty of 1DVAR TCWV retrieval | kg/m^2 |
| **rad_liquid_water_uncertainty_1DVAR** | A posteriori uncertainty of 1DVAR LWP retrieval | kg/m^2 |
| **rad_wet_tropo_corr_uncertainty_1DVAR** | A posteriori uncertainty of 1DVAR Wet Tropospheric Correction retrieval | m |
| **rad_attenuation_ku_uncertainty_1DVAR** | A posteriori uncertainty of 1DVAR Attenuation Ku retrieval | dB |

### 4.6.2.3.2   How the uncertainty information should be used

While information on uncertainty can obviously be used to assess the quality of individual retrievals, it also allows information to be deduced on the retrieval method in general and can thus contribute to pointing towards potential ways to improve the retrieval method.
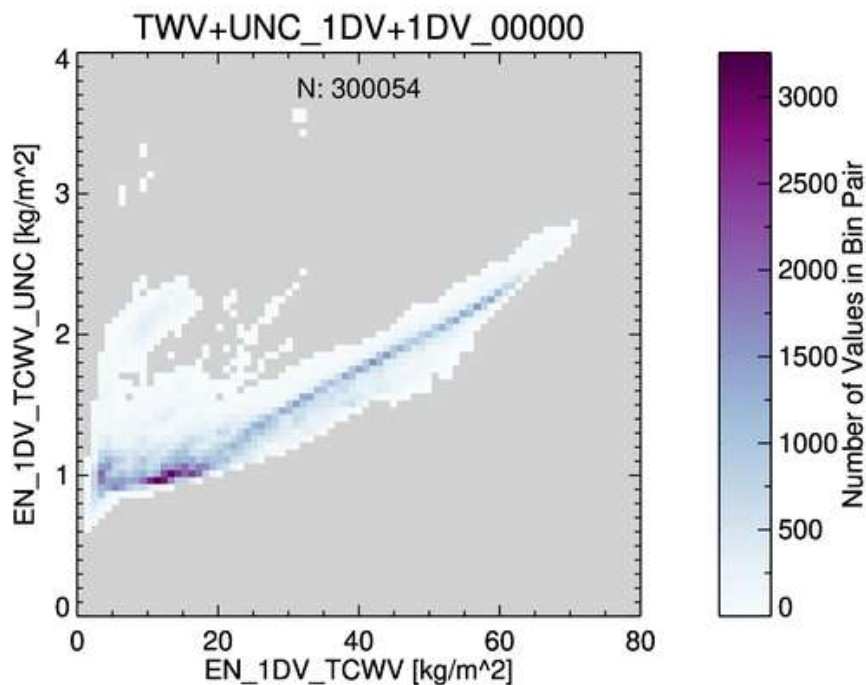


*Figure 4-32 : Two-dimensional histogram of TCWV (x-axis) vs. TCWV uncertainty (y-axis) for a one-day period (2002/07/29) of 1D-VAR TCWV retrievals derived from ENVISAT observations.*

Figure 4-32 shows the relationship between 1D-VAR retrieved TCWV and the corresponding uncertainty for >300 000 retrievals derived from ENVISAT observations on 29 July 2002. For TCWV values up to ca. 20 kg/m², TCWV retrieval uncertainty is on the order of 1 kg/m² translating into a range uncertainty (i.e., the uncertainty in the calculated distance between the observing instrument and the sea surface) of ca. 0.64 cm (rule of thumb), the actual value also depending on the atmospheric vertical profiles of temperature and humidity. For TCWV values between ca. 20 and 50 kg/m², the uncertainty increases rather linearly to adopt values of about 2 kg/m² for TCWV values of ~50 kg/m². For TCWV values >50 kg/m², the uncertainty appears to increase over-proportionately, resulting in the slightly non-linear shape observed in Figure 4-32. This over-proportionate increase of uncertainty is likely due to the onset of saturation effects at high atmospheric water vapour concentrations.

## 4.6.2.4 Reference documents

| RD-33 | Bennartz, R., Höschen, H., Picard, B., Schröder, M., Stengel, M., Sus, O., Bojkov, B., Casadio, S., Diedrich, H., Eliasson, S., Fell, F., Fischer, J., Hollmann, R., Preusker, R., and Willén, U.: An intercalibrated dataset of total column water vapour and wet tropospheric correction based on MWR on board ERS-1, ERS-2, and ENVISAT, Atmospheric Measurement Techniques, 10, 1387-1402, 10.5194/amt-10-1387-2017, 2017. |
|---|---|
| RD-34 | Deblonde, G., 2001: NWP SAF user's guide: Standalone 1D-VAR scheme for the SSM/I, SSMIS and AMSU, NWPSAF-MO-UD-001 Version 1.0, 22 August 2001. |
| RD-35 | Rodgers, C. D.: Inverse Methods for Atmospheric Sounding: Theory and Practice, World Scientific, Singapore [River Edge, N.J.], 2000. |

# Appendix A - FDR4ALT deliverables

The table below lists all FDR4ALT deliverables with their respective ID number and confidentiality level.

| Document | ID | Confidentiality Level |
|---|---|---|
| Products Requirements & Format Specifications Document | [D-1-01] [D-2-02] | Public |
| Roadmap & Product Summary Document | [D-1-02] | Project Internal |
| Data Requirements Document | [D-1-03] | Project Internal |
| System Maturity Matrix | [D-1-04] | Project Internal |
| Examples of products | [D-1-05] | Project Internal |
| Review Procedure Document | [D-1-06] | Project Internal |
| Review Data Package | [D-1-07] | Project Internal |
| Phase 1 Review Report Document | [D-1-08] | Project Internal |
| Detailed Processing Model Document | [D-2-01] | Public |
| Round Robin Assessment Report Document | [D-2-03] | Public |
| Data Production Status Report | [D-3-01] | Project Internal |
| Final Output Dataset | [D-3-01] | Public |
| Product Validation Plan | [D-4-01] | Project Internal |
| Product Validation Report | [D-4-02] | Public |
| Uncertainty Characterization Definition Document | [D-5-01] | Public |
| Uncertainty Characterization Report | [D-5-02] | Public |
| Product User Guide | [D-5-03] | Public |
| Completeness Report: FDR ALT | [D-6-01] | Public |
| Completeness Report: FDR MWR | [D-6-02] | Public |

*Table 4-8 : List of FDR4ALT deliverables*

# Appendix B - Acronyms

| | |
|---|---|
| **AATSR** | Advanced Along-Track Scanning Radiometer |
| **AEM** | Airborne electromagnetic |
| **AIR** | AIRWAVES2 |
| **AVISO** | Archivage, Validation et Interprétation des données des Satellites Océanographiques |
| **AMSR-E** | Advanced Microwave Scanning Radiometer - Earth Observing System sensor |
| **AMSU-A** | Advanced Microwave Sounding Unit-A |
| **ALT** | Altimetry |
| **ASSIST** | Arctic Shipborne Sea Ice Standardization Too |
| **ATM** | Airborne Topographic Mapper |
| **BDHI** | Base de datos Hidrologica integrada |
| **BGEP** | Beaufort Gyre Exploration Project |
| **CAL** | Calibration |
| **CCI** | Climate Change Initiative |
| **CFOSAT** | Chinese-French Oceanic SATellite |
| **CDS** | Copernicus Data Service |
| **CLS** | Collecte Localisation Satellite |
| **CMEMS** | Copernicus Marine Environment Monitoring Service |
| **CMSAF** | Climate Monitoring Satellite Application Facility |
| **CNES** | Centre National des Etudes Spatiales |
| **CRREL** | Cold Regions Research and Engineering Laboratory |
| **DAHITI** | Database for Hydrological Time Series of Inland Waters |
| **DGA** | Direccion General de Aguas |
| **ENVISAT** | ENVIronment SATellite |
| **EMD** | Empirical mode decomposition |
| **EO** | Earth Observation |
| **EPS** | European Polar System |
| **ERA** | ECMWF Re-Analysis |
| **ERS** | European Remote-Sensing Satellite |
| **ESA** | European Space Agency |
| **ESTEC** | European Space Research and Technology Centre |
| **FCDR** | Fundamental Climate Data Record |
| **FDR** | Fundamental Data Records |
| **FIDUCEO** | Fidelity and uncertainty in climate data records from Earth Observations |
| **FMR** | Full Mission Reprocessing |
| **FYI** | First Year Ice |
| **GEWEX** | Global Energy and Water Exchanges |
| **GFO** | Geosat Follow-On |
| **GIEMS** | Global Inundation Extent from Multi-Satellites |
| **GMSL** | Global Mean Sea Level |
| **GNSS** | Global Navigation Satellite System |
| **GPM** | Global Precipitation Measurement |
| **GRDC** | Global Runoff Data Centre |
| **G-REALM** | Global Reservoir And Lake Monitor |
| **G-VAP** | GEWEX Water Vapour Assessment |
| **HYBAM** | HYdro-géochimie du Bassin Amazonien |
| **ICARE** | |
| **IGM** | Instituto Geografico Militar |
| **IGN** | Instituto Geografico Nacional |

| | |
|---|---|
| **IMB** | Ice Mass Balance |
| **INA** | Instituto Nacional de Agua |
| **ISRO** | Indian Space Research Organisation |
| **IRPI** | Istituto di Ricerca per la Protezione Idrogeologia |
| **IWMI** | International Water Management Institute |
| **LEGOS** | Laboratoire d'Etudes en Géophysique et Océanographie Spatiales |
| **LIDAR** | Ligth Detection And Ranging |
| **LTAN** | Local time of the ascending node |
| **LWP** | Liquid Water Path |
| **MAC** | Multisensor Advanced Climatology |
| **MEAS-SIM** | Measure-Simulation |
| **MQE** | Mean Quadratic Error |
| **MSSH** | Mean Sea Surface Height |
| **MWR** | Microwave Radiometer |
| **NASA** | National Aeronautics and Space Administration |
| **NE** | North East |
| **NN** | Neural Network |
| **NPI** | Norwegian Polar institute |
| **NWP** | Numerical Weather Prediction |
| **NOAA** | National Oceanic and Atmospheric Administration |
| **OIB** | Operation Ice Bridge |
| **OLC** | Open Loop Calibration |
| **OSTST** | Oceanography Surface Topography Science Team |
| **POSTEL** | Pôle d'Observation des Surfaces continentales par TELEdétection |
| **PTR** | Point Target Response |
| **RD** | Reference Document |
| **PRT** | Platinium Resistance Thermometers |
| **REAPER** | Reprocessing of Altimeter Products for ERS |
| **RM** | Review Meeting |
| **RSS** | Remote Sensing System |
| **SALP** | Service d'Altimétrie et de Localisation Précise |
| **SARAL** | Satellite with Argos and Altika |
| **SLA** | Sea Level Anomaly |
| **SCICEX** | Submarine Arctic Science Program |
| **SGDR** | Sensor Geophysical Data Record |
| **SHOA** | Servicio Hidrografico y Oceanografico de la Armada |
| **SSB** | Sea State Bias |
| **SSH** | Sea Surface Height |
| **SSM/I** | Special sensor microwave/imager |
| **SST** | Sea Surface Temperature |
| **SWH** | Significant Wave Height |
| **SWIM** | Surface Waves Investigation and Monitoring instrument |
| **TAC** | Thematic Assembly Center |
| **TB** | Température de Brillance (Brightness Temperature) |
| **TDP** | Thematic Data Products |
| **TDS** | Test Data Set |
| **TFMRA** | Threshold First-Maximum Retracker Algorithm |
| **TMR** | Topex Microwave Radiometer |
| **TP** | Topex/Poseidon |
| **TCWV** | Total column water vapour |
| **VCC** | Vicarious calibration |
| **VS** | Virtual Station |

| **ULS** | Upward Looking Sonar |
|---------|---------------------|
| **USA** | United States of America |
| **USDA** | United States Department of Agriculture |
| **WHALES** | Wave Height Adaptive Leading Edge Subwaveform |
| **WTC** | Wet Tropospheric Correction |